MECHANISTIC MODELING, SIMULATION AND OPTIMIZATION OF WET GRANULATION PROCESSES

BY ANWESHA CHAUDHURY

A dissertation submitted to the

Graduate School—New Brunswick

Rutgers, The State University of New Jersey

in partial fulfillment of the requirements

for the degree of

Doctor of Philosophy

Graduate Program in Chemical and Biochemical Engineering

Written under the direction of

Dr. Rohit Ramachandran

and approved by

_____

_____

_____

_____

_____

New Brunswick, New Jersey

January, 2015

ABSTRACT OF THE DISSERTATION

MECHANISTIC MODELING, SIMULATION AND OPTIMIZATION OF WET GRANULATION PROCESSES

by ANWESHA CHAUDHURY
Dissertation Director: Dr. Rohit Ramachandran

Particulate processes involving handling of solids are ubiquitous in various industries and are typically operated inefficiently due to a lack of adequate mechanistic process understanding. A primary application of such processes is found in the pharmaceutical industry that involve manufacturing of solid dosage forms (e.g. tablets). Granulation is a critical particulate process that plays an important role in the overall manufacture of pharmaceutical drugs. This work focuses on improved mathematical modeling of granulation processes using the population balance framework. One of the primary objectives deals with model development for granulation followed by development of improved numerical techniques for reduced computational overheads associated with the solution techniques for solving population balance models. This study is also aimed at identifying the influence of various operating parameters on the final granule properties through the development of a novel semi-mechanistic kernel and an integrated mesoscale model framework that can effectively capture key granulation dynamics. A compartmentalized model has also been formulated for a high-shear wet granulator that can capture the inhomogeneities (with respect to liquid and particle velocity) within the vessel. This integrated, compartment-based model can be further extended for open

loop optimization and control of the granulation process, which can aid at obtaining an optimal recipe for the operation of the granulation process. This work will make a significant contribution towards improved understanding of the granulation process and is aimed at mitigating the current inefficient operation of the process.

Acknowledgements

The past four years of my life as a PhD student has been a rather wonderful and rewarding experience. Life is full of "ups and downs" and my journey as a PhD student is no exception to that theory. I believe I would not have completed this journey without the support from my mentors, family and my friends. They helped me enjoy and cherish every aspect of graduate school. First and foremost I would like to thank my PhD thesis advisor, Dr. Rohit Ramachandran, without whose support, this journey could not have been completed. He has always vested a lot of responsibilities on me, which really helped me evolve as a researcher and a human being. He has also let me travel abroad and experience various internship opportunities, which definitely led to an eye-opening experience. I would like to thank him for always believing in me and having faith in my abilities.

A big thank you also goes to my wonderful thesis committee-Prof. Marianthi Ierapetritou, Prof. Nina Shapley, Dr. Meenakshi Dutt and Dr. Preetanshu Pandey. Their advice, suggestions and feedback on my thesis really helped me objectify my goals and align my work accordingly. I have occassionally collaborated with Dr. Pandey during my PhD journey. His insightful thinking, sincerity and commitment has really inspired me. Prof. Ierapetritou has always inspired me with her accomplishments. Her expertise with systems engineering and involvement with her research (while also having other administrative responsibilities) make me really look up to her. Prof. Shapley is one of the nicest people I have ever met. She has supported me during my PhD and has also provided me with crucial feedback during my thesis proposal presentation that has helped me conclude the remaining part of my thesis work accordingly. I would also like to thank Dr. Meenakshi Dutt for providing me with feedback and raising the right questions that led me to think in the right direction.

problems that are faced in the pharmaceutical industry. I would also like to thank Dr. Debasish Sarkar and Dr. Saikat Chakraborty (my professors from undergraduate and masters) for amply motivating me and giving me directions on how to do research.

Along with having my friends within the department, I must say that my friends outside the department have also played a huge role with making my life better as a PhD student. They have always been by my side when I needed them and felt low. I will avoid taking names because I will inevitably forget some of them, although that does not make me any less grateful for their presence in my life. I have to specifically thank Akash Baid for being my best friend and always being by my side. He has always stuck with me through thick and thin and has made every attempt to cheer me up when I was frustrated or when I had some silly bug in my code which I could not fix. Thank you, Akash for being such a huge pillar of support all along.

Last but not the least, I would like to thank my family for being a huge support. My parents have gone through a lot and have fought with a lot of people to let me do what I wanted. I will be forever indebted to them for giving me the liberty to choose and do whatever I wanted. They have shown immense faith in me and I really appreciate their belief in me. My younger brother, Abir, is the sweetest person on earth and he has done a great job with being a younger brother and also taking great care of my family, while I have been thousands of miles away from home working on my PhD. I must also thank my aunts (mother's sisters), with whom I lived until I completed my undergraduate education. They took great care of me and taught me about the importance of discipline in life. My other family members have also played an important role in my life and I am grateful to them for being there in times of need. I miss my grandparents, who are not with us anymore and I wish they were around to see me defend my PhD thesis.

After thanking all mortals, I must thank "that eternal power" (some people call God) for looking after me and making sure I always chose the right path. This PhD thesis is a combined effort of many people/forces and I believe with the absence of any one of them, my journey might have turned out differently-just like the $Butterfly\ effect$ of chaos theory.

Table of Contents

List of Tables

List of Figures

xii

Chapter 1

Introduction and Objectives

Particulate processes are ubiquitous in various branches of engineering with crystallization, granulation, milling, polymerization and emulsification being examples of such processes. Such processes are pervasive in various industries involving food processing, pharmaceuticals, detergents etc. The pharmaceutical industry for instance is governed by tight regulations and strict quality criteria, thus emphasizing the need for improved manufacturing practices. The amendments to the laws dictated by the regulatory bodies suggest the production to be compliant with the good manufacturing practices (GMP) (Reklaitis et al., 2010). The rising overheads owing to research and development, manufacturing costs and expiration of patented drugs provide a lot of pressure on the pharmaceutical companies to adopt an economical manufacturing practice that would alleviate cost and generate profit. This motivates the implementation of predictive tools such as Quality by Design (QbD) and Process Analytical Tools (PAT) (Gernaey and Gani, 2010; Klatt and Marquardt, 2009) which have been recently launched by the Food and Drug Administration (FDA). QbD encourages a thorough understanding of the process and the product along with the knowledge of the risks involved in the manufacturing which could thereby be minimized utilizing detailed process knowledge. This necessitates the application of process systems engineering (PSE) approach to pharmaceutical manufacturing (Linniger et al., 2000) as it provides an impetus to such industries (that involve solids handling) to move to a more sustainable and process intensified position (Buccholz, 2010). Particulate processes involving granular materials are not very well understood and lack available fundamental knowledge. This results in the need for numerous assumptions while modeling or designing the system, which may result in various processing problems while carrying out the process for industrial

purposes (Boukouvala et al., 2010).

Granulation, a complex process involving the design of particle properties, is of immense importance to various industries that require handling of particulate matter. It is a process whereby primary powder particles adhere to each other (by creating liquid bridges and thereafter solid bridges upon drying between them through the use of a binding agent) to form larger, multi-particle entities called granules. Granulated particles exhibit better flow properties, increased bulk density, controlled dissolution and uniformity in the distribution of multiple solid components thereby facilitating further downstream operations such as tablet compaction (Sochon et al., 2010). Granulation can be carried out in batch or continuous mode using various equipments such as under high shear, using a fluid bed, in a twin screw granulator or in a drum. High-shear wet granulation is a complex process with several agglomeration and breakage mechanisms coming into play simultaneously: namely wetting and nucleation, aggregation and consolidation, breakage and attrition, and layering (Iveson et al., 2001a; Cameron et al., 2005).

The industrial operation of the granulation process is often associated with large recycle ratios and high batch rejection rate (Salman et al., 2007). This is highly undesirable due to the significant wastage of inventories. It is therefore advisable to use a model based systems approach in order to better control, predict and optimize the granulation process (Linniger et al., 2000). It can significantly aid in improved process understanding, supplement available knowledge with new data, reduce time and cost for process-product development. Numerous modeling approaches have surfaced over the past years that aim at alleviating the operation of the granulation process by providing apriori predictions.

In the following sections, a detailed description is provided which presents modeling work that would help circumvent the issues which are faced in the current operation of granulation process. Improved modeling frameworks exhibit better understanding of the process thus enabling the implementation of a systems engineering based approach for improved processing. Furthermore, numerical techniques have also been developed

such that the solution of the population balance models can be eased. Most models observed in the literature are empirical in nature. A more mechanistic understanding of the process is necessary in order to apply the approach of QbD into practice and also relate the various operating parameters to the final granule properties. A mechanistic model is also developed which can significantly alleviate the problems faced with empirical models/kernels and can enable predictions beyond the design space. A high-shear wet granulator is typically considered to be a well-mixed system and is commonly represented using a single equation describing the entire vessel. This is an oversimplification and is typically incapable of capturing the inhomogeneities within the system. A compartment based model is proposed for that purpose which can account for the system heterogeneities. Using the compartment model along with the mechanistic PBM for each individual compartment, an open loop optimization algorithm is run which can provide some insight on the optimal recipe that should be followed while operating granulation processes with a certain target output. With these intentions, the various aims of this dissertation can be detailed as

Specific Aim I: Model development for high shear and fluid bed wet granulation processes. Emphasizing on the importance of the various mechanisms influencing granulation and developing a heat and mass transport framework for drying during fluid bed granulation.

Specific Aim II: Development of numerical techniques for improved solution of population balance models (PBMs). Obtaining reduced order models for PBMs for alleviating the "curse of dimensionality" (i.e., reduce the simulation of time of high-dimensional PBMs) .

Specific Aim III: Developing a mechanistic framework for relating the effect of various operating parameters on the final outcome of the granulation process.

Specific Aim IV: Development of a generic compartment based model for high-shear wet granulation followed by optimization and open loop control of the process using a semi-mechanistic model.

Chapter 2

Specific Aim I: Population balance model development for high shear and fluid bed wet granulation

The details of the discussions provided in this section can be obtained in the publications:

- Chaudhury, A., Ramachandran, R., 2013, Integrated Population Balance Model Development and Validation of a Granulation Process. Particulate Science and Technology 31 (4), 407-418

- Chaudhury, A., Niziolek, A., Ramachandran, R., 2013, Multi-dimensional mechanistic modeling of fluid bed granulation processes: An integrated approach. Advanced Powder Technology 24 (1), 113-131

- Chaudhury, A., Barrasso, D., Pandey, P., Wu, H., Ramachandran, R., 2014,Population balance model development, validation, and prediction of CQAs of a high-shear wet granulation process: Towards QbD in drug product pharmaceutical manufacturing. Journal of Pharmaceutical Innovation 9 (1), 53-64

2.1   Granulation-Modeling and general overview

Granulation processes have been modeled using various approaches such as Discrete Element Modeling (DEM) (Gantt et al., 2006); hybrid models-DEM+PBM (Barrasso and Ramachandran, 2014), PBM+Volume of fluid (VoF) method (Stepanek et al., 2009); PBM+computational fluid dynamics (CFD) (Rajniak et al., 2009; Sen et al., 2014), PBM (Immanuel and Doyle III, 2005; Poon et al., 2009; Ramachandran and Chaudhury, 2012; Ramachandran et al., 2011; Chaudhury and Ramachandran, 2013), and so on. PBMs represent a mesoscopic framework wherein the microscopic information

in the form of kernels is utilized to predict the macroscopic properties (e.g size and porosity). Due to the inherent discrete nature of PBMs, it can efficiently describe particulate processes such as granulation. This dissertation is focussed on employing PBMs for effective modeling and optimization of granulation processes.

One dimensional PBMs have been widely studied for model-based analysis (Long et al., 2005) but they are often inadequate in explaining all the mechanisms governing the process (Iveson, 2002). Significant work has been done on the development of population balance models for granulation, but most of them emphasize on a single mechanism instead of studying the combined effect of all the sub-processes together (Rajniak et al., 2007). This suggests the need for using multidimensional models for improved and accurate modeling. It is not advisable to lump any of the multiple dimensions, since that may lead to modeling errors. Therefore, these three particle attributes are re-cast in terms of their individual volumes of solid *(s)*, liquid*(l)* and gas*(g)* as it enables decoupling of the integrated process with respect to the individual meso-scopic sub-processes (Verkoeijen et al., 2002).

Binder content, granule porosity and granule size are some of the most crucial characteristics that can be tracked using the PBM for a granulation process. Binder content has a significant role to play in the growth of granules, as, with higher amount of the binder, there is larger availability of surface-wet granules (Knight et al., 1993; Osborne et al., 2011). Studies have shown that the type and amount of binder fluid affect the type of coalescence/aggregation (Liu et al., 2000). Porosity is also very crucial while modeling granulation because with the granule porosity below a certain critical porosity, liquid is squeezed on the surface thus resulting in surface-wet granules which helps promote granule growth. Moreover, porous granules have a higher tendency to break initially and aggregate thereafter, leading to the formation of more dense granules (Annapragada and Neilly, 1996). Using these particle aspects, a multi-dimensional PBM can be formulated, which takes into account the key mechanisms that affect the final product properties.

Granulation processes have been widely investigated using regime-maps. Based on

various dimensionless numbers (e.g. spray flux, Stokes deformation number, viscous Stoke's number etc), the predominant mechanisms affecting the granulation process have been identified. Iveson et al. (2001b) have significantly worked on identifying the growth regimes for granulation based on the Stoke's deformation number and pore saturation. Iveson et al. (2001a); Litster et al. (2001); Emady et al. (2011, 2013) have also investigated the various regimes pertaining to the nucleation mechanism. Based on the operating conditions for the process, the granulation system has been categorized as droplet controlled or mechanical dispersion regime. These analysis provide meaningful insights towards the behavior of the system.

Traditionally, granulation has been performed in various equipment such as fluid bed, high shear, twin screw or in a drum. Significant work has been observed in literature that involve understanding the granulation behavior in these equipments. Previously, a detailed study has been conducted by Pandey et al. (2013) that focussed on the effect of the various operating parameters on the final granules formed in a high-shear granulator using a full factorial DOE (for liquid to solid ratio, impeller speed and the wet massing time). The study revealed a pronounced effect of wet massing time and impeller speed at higher liquid to solid ratios. The effect of the various binder addition modes have also been previously studied by Osborne et al. (2011). In a drum granulator, the effect of the formulation properties and the operating variables have been studied on the process dynamics and end-point granulation outcome in a lab-scale drum granulation process by Ramachandran et al. (2008). Glaser et al. (2009) had performed some initial control studies following which Ramachandran and Chaudhury (2012) used a compartment based model for conducting control studies on a drum granulator. In the latter work, a multiple input-multiple output (MIMO) control system was studied for the pairings followed by the assessment of a novel control configuration. Constrained optimization studies have also been performed on drum granulation for control purposes (Wang et al., 2006; Wang and Cameron, 2007). The operation of a fluid bed equipment is inherently complex and involves interconnected process variables that are available at the operator's disposal in obtaining a suitable recipe for achieving good granulation. Advantages of fluid bed granulation over other granulation methods are

usually indicated to be higher product density, and lower solvent and energy consumption (Boerefijn and Hounslow, 2005). In a fluid bed granulation aggregation occurs due to the combined effect of viscous and capillary forces by the binder (Reynolds et al., 2005). For the fluid bed operation, binder content and the particle/excipient solubility have an important role to play in the granulation process (Rajniak et al., 2007). Various other experimental studies have been carried out in order to link the process variables and various microscopic properties of the particles with the granulation process (Liu et al., 2000; Stepanek and Rajniak, 2006).

This work focuses on implementing the 3-D population balance model framework for the granulation process. The 3-D population balance equation can be written as

$$
\frac{\partial}{\partial t}F(s,l,g,t) + \frac{\partial}{\partial s}\left[F(s,l,g,t)\frac{ds}{dt}\right] + \frac{\partial}{\partial l}\left[F(s,l,g,t)\frac{dl}{dt}\right] + \frac{\partial}{\partial g}\left[F(s,l,g,t)\frac{dg}{dt}\right]
$$
$$
= \Re_{nuc} + \Re_{agg} + \Re_{break} \quad (2.1)
$$

where $F(s,l,g,t)$ represents the population density function such that $F(s,l,g,t)dsdldg$ is the moles of granules with solid volume between s and $s+ds$, liquid volume between l and $l+dl$ and gas volume between g and $g+dg$. The partial derivative term with respect to s accounts for the layering of fines onto the granule surface; the partial derivative term with respect to l accounts for the drying of the binder and the re-wetting of granules; the partial derivative with respect to g accounts for consolidation which, due to compaction of the granules, results in an increase of pore saturation and decrease in porosity.

2.2   Mechanisms included within the model

The key mechanisms that play a significant role in shaping the final characteristics of a granule are aggregation, breakage, nucleation, consolidation, layering and drying/re-wetting (Verkoeijen et al., 2002). In the integrated model considered in this work, all of the above mentioned mechanisms have been included except for nucleation, which can be easily incorporated in the developed framework given more advances and consensus in nucleation modeling. In literature, a mechanistic nucleation kernel has been proposed

by Poon et al. (2008) for the droplet-controlled regime. Intensive experimental studies have also been conducted on the nucleation of particles during granulation (Hapgood et al., 2003; Emady et al., 2011; Tan and Hapgood, 2011).

Aggregation is a sub-process in which two or more particles collide with each other and combine together to form larger particles. The overall net aggregation rate can be broken into the corresponding birth and death terms as

$$\Re_{agg}(s,l,g) = \Re_{agg}^{form} - \Re_{agg}^{dep} \tag{2.2}$$

such that,

$$\Re_{agg}^{form} = \frac{1}{2}\int_{s_{nuc}}^{s-s_{nuc}}\int_{0}^{l_{max}}\int_{0}^{g_{max}}\beta(s',s-s',l',l-l',g',g-g') \\ \times F(s',l',g',t)F(s-s',l-l',g-g',t)ds'dl'dg' \tag{2.3}$$

$$\Re_{agg}^{dep} = F(s,l,g,t)\int_{s_{nuc}}^{s-s_{nuc}}\int_{0}^{l_{max}}\int_{0}^{g_{max}}\beta(s',s-s',l',l-l',g',g-g') \\ \times F(s',l',g',t)ds'dl'dg' \tag{2.4}$$

where, s_{nuc} is the solid volume of nuclei (assumed zero in this study), $\beta(s',s-s',l',l-l',g',g-g')$ is the size-dependent aggregation kernel that signifies the rate constant for aggregation of two granules of internal coordinates *(s',l',g')* and *(s-s',l-l',g-g')*. The formation term accounts for the new particles that are formed after coalescence whereas the depletion term accounts for the particles that are lost when the smaller particles coalesce and aggregate.

An empirical kernel proposed by Madec et al. (2003) shown in Equation (2.5), that takes into account the various parameters such as the particle size and binder volume was considered to be more appropriate empirical kernel for the developed multi-dimensional PBM.

$$\beta = \beta_0(L_1^3 + L_2^3)\left((c_1+c_2)^{\alpha}\left(100 - \frac{c_1+c_2}{2}\right)^{\delta}\right)^{\alpha}, \tag{2.5}$$

where

$$c_i \equiv \frac{volume\ of\ liquid}{volume\ of\ agglomerate} \times 100 = \frac{l}{s+l+g} \times 100 \qquad (2.6)$$

and α and δ are empirical parameters. The length of the particles are L_1 and L_2. Breakage is the breakdown of a particle into two or more fragments and is mainly governed by attrition and impact. It plays a crucial role in controlling the final granule size distribution in high shear granulators. Many published breakage kernels have been observed in literature including an empirical kernel proposed by Pandya and Spielman (1983) and a semi-mechanistic kernel containing one tunable empirical parameter that was previously used by Soos et al. (2006). The semi-mechanistic kernel has also been utilized in this work. Mechanistic kernels have also been observed in literature, where the kernel has been expressed to be proportional to the ratio of the external stress to the intrinsic strength (Ramachandran et al., 2009). The breakage kernel used in this work is expressed as a function of the shear rate, G and empirical parameter, B as

$$K_{break}(s,l,g) = \left(\frac{4}{15\pi}\right)^{\frac{1}{2}} \times G \times exp\left(-\frac{B}{G^2 R(s,l,g)}\right) \qquad (2.7)$$

and the breakage function that has been used, is based on the work by Pinto et al. (2007). Using this information, the breakage term can be broken into its corresponding birth and death terms as

$$\Re_{break}(s,l,g) = \Re_{break}^{form} - \Re_{break}^{dep}, \qquad (2.8)$$

such that the birth and death terms can be explained using Equations (2.9) and (2.10)

$$\Re_{break}^{form} = \int_0^{s_{max}} \int_0^{l_{max}} \int_0^{g_{max}} K_{break}(s',l',g')b(s,s',l,l',g,g') \times F(s',l',g',t)ds'dl'dg' \qquad (2.9)$$

$$\Re_{break}^{dep} = K_{break}(s,l,g)F(s,l,g,t). \qquad (2.10)$$

Along with the various source terms-aggregation and breakage, various growth based

mechanisms also influence the granulation operation. These mechanisms include consolidation, drying/rewetting and layering. The consolidation model used in the works of Verkoeijen et al. (2002) was used to represent the negative growth with respect to the gas volume. For the growth rate with respect to the liquid dimension, a mass balance equation has been used to define the drying/rewetting. The layering of fines has been represented in the form of a Monod based growth model (Wang et al., 2006).

Consolidation

Consolidation is a negative growth process which represents the compacting of granules due to the escape of air from the pores. It can be modeled as an empirical exponential decay relation (Verkoeijen et al., 2002) given by

$$\frac{d\epsilon}{dt} = -c(\epsilon - \epsilon_{min}), \tag{2.11}$$

$$\frac{dg}{dt} = \frac{c(s + l + g)(1 - \epsilon_{min})}{s} \times [l - \frac{\epsilon_{min}s}{1 - \epsilon_{min}} + g] \tag{2.12}$$

where, the porosity ϵ is

$$\epsilon = \frac{l + g}{s + l + g} \tag{2.13}$$

Here ϵ_{min} is the minimum porosity of the granules and c is the compaction rate constant.

Layering

Layering of fines on the surface of particles is yet another crucial mechanism governing the growth rate of particles during granulation. It is strongly dependant on the fraction of powder/fines present in the system and the moisture content. The growth rate due to layering has been formulated (Wang et al., 2006) analogous to the Monod model as

$$\frac{ds}{dt} = G_{max} \frac{M_{powder}}{k_{layer} \sum M_i + M_{powder}} e^{[-\alpha_{layer}(x_w - x_{wc})^2]} \tag{2.14}$$

where G_{max} is the maximum growth rate, M_{powder} is the mass of fine powder (particles with a solid volume less than equal to that of the 7th bin is considered fines here and can be defined as $\rho_s \int_0^{s_7} \int_0^{l_{max}} \int_0^{g_{max}} F(s, l, g) ds dl dg$ with ρ_s being the density of solid), M_i is the mass of particles in the ith size class (based on the solid, liquid and gas volumes, x with respect to each internal coordinate), x_{wc} is the critical moisture content and considered a constant value of 0.1, k_{layer} and α_{layer} are fitting parameters.

Drying/Rewetting

Drying is associated with the gain or loss of liquid into or from the granulation system due to addition of more liquid or removal due to evaporation. As mentioned before, the inhomogeneities associated with binder distribution has not been considered in this work. Thus, we have assumed that all particles within the system receive equal amount of liquid. For a more accurate model that takes into account the various inhomogeneities, a multiscale approach is required which is beyond the scope of this work. The liquid rate can be obtained from mass balance as

$$\frac{dl}{dt} = \frac{\dot{m}_{spray}(1 - c_{binder}) - \dot{m}_{evap}}{F_{total} \times Na \times \rho_l}, \tag{2.15}$$

Here, $\dot{m}_{spray}$ is the spray rate of liquid, $\dot{m}_{evap}$ is the evaporation rate, Na is the Avogadro's number, c_{binder} is the concentration of the binder and F_{total} is the total particle distribution within the system. In the calculations for the drying/rewetting term, the evaporation rate is considered 0 for the high-shear case as the drying of particles is believed to exist in a separate unit operation altogether. In case of a fluid bed granulation process, the granules are dried simultaneously as they granulate. In the following discussions a heat and mass balance framework is also presented which illustrates the calculation of the evaporation term for a fluid bed operation.

2.3 Calculation of the evaporation term

The evaporation term in the liquid balance can be obtained by using a detailed mass and heat balance framework as presented in this section (Chaudhury et al., 2013b).

Drying/liquid distribution denotes the increase or decrease of liquid content into or from the granulation system due to addition of binder or removal due to evaporation. The liquid water balance can be written in (2.16) as

$$\frac{dx_{bed}}{dt} = \frac{\dot{m}_{spray}(1 - c_{binder}) - \dot{m}_{evap}}{M_{solid}}, \qquad (2.16)$$

where,

$$M_{solid} = M_{solid\ fraction} + \dot{m}_{spray}c_{binder}\Delta t, \qquad (2.17)$$

Here, x_{bed} is the moisture content of the fluid bed, $\dot{m}_{spray}$ is the spray rate of the liquid, c_{binder} is the concentration of the solid binder in the liquid added, $\dot{m}_{evap}$ is the rate of moisture evaporated and M_{solid} is the mass of initial solid particles.

The water vapor balance can be written in Equation (2.18) as

$$\frac{dx_{out}}{dt} = \frac{\dot{m}_{air}(x_{in} - x_{out}) + \dot{m}_{evap}}{M_{air}}, \qquad (2.18)$$

where,

$$\dot{m}_{evap} = \gamma A_{p,wet}k_{mass}\rho_{air}(x_{sat} - x_{out}), \qquad (2.19)$$

x_{out} is the moisture leaving the bed with the exiting air, $\dot{m}_{air}$ is the rate of air entering the bed, x_{in} is the moisture content of the entering air, γ is the experimental correction factor, $A_{p,wet}$ is the wet surface area of the particles, ρ_{air} is the density of air and x_{sat} is the saturated moisture content.

The wet surface area can be expressed as a fraction of the total surface area as $A_{p,wet} = \eta A_p$ and the mass transfer coefficient, k_{mass} can be expressed as a function of the diffusivity of water, D_{water} and particle diameter, D as

$$k_{mass} = \frac{2D_{water}}{D}, \qquad (2.20)$$

The surface area of granules can be approximated based on initial surface area as

$$A_pD = A_{p0}D_0. \qquad (2.21)$$

where D_0 is the initial diameter of a particle and $A_{p,0}$ is the initial surface of a particle. Combining equations (2.20), (2.21) and expressing the wetted area as a fraction of the overall surface area, we get

$$k_{mass}A_{p,wet} = 2D_{water}\eta A_{p0}\frac{D_0}{D^2} = 2D_{water}\eta\frac{A_{p0}}{D_0}\left(\frac{D_0}{D}\right)^2 \qquad (2.22)$$

The total heat balance for the granulator can be expressed as:

$$M_{air}\frac{dH_{out}}{dt} + M_{solid}\frac{dH_{bed}}{dt} = \dot{m}_{air}(H_{in} - H_{out}) - \dot{Q}_{evap} - \dot{Q}_{losses} \qquad (2.23)$$

with the assumption that the granulator is well-mixed, the reference temperature is the temperature of the liquid binder i.e., $T_{ref} = T_{spray}$, and the bed temperature is equivalent to the outlet air temperature i.e., $T_{bed} = T_{out}$. H_{in}, H_{out} and H_{bed} are the specific enthalpies of the inlet air, outlet air and the bed respectively. M_{air} is the mass of air in the granulator, Q_{evap} is the heat lost due to evaporation and Q_{losses} is an empirical correction quantity of heat used in the balance.

Making the necessary substitutions for Equation (2.23) and solving for $\frac{dT_{out}}{dt}$ gives:

$$\frac{dT_{out}}{dt} = \frac{g(1) - \dot{m}_{evap}\Delta H - \dot{Q}_{losses} - g(2)\frac{dx_{bed}}{dt} - g(3)\frac{dx_{out}}{dt}}{g(4)} \qquad (2.24)$$

where:

$$g(1) = \dot{m}_{air}[c_{p,air}(T_{in} - T_{out}) + c^g_{p,water}[x_{in}(T_{in} - T_{ref}) - x_{out}(T_{out} - T_{ref})]] \qquad (2.25)$$

$$g(2) = M_{solid}c^l_{p,water}(T_{out} - T_{ref}) \qquad (2.26)$$

$$g(3) = M_{air}c^g_{p,water}(T_{out} - T_{ref}) \qquad (2.27)$$

$$g(4) = M_{air}(c_{p,air} + x_{out}c^g_{p,water}) + M_{solid}(c_{p,solid} + x_{bed}c^l_{p,water}) \qquad (2.28)$$

and $c_{p,i}$ designates the specific heat capacity of the ith species.

Solving the above set of equations, the evaporation term, $\dot{m}_{evap}$ associated with the drying term can be obtained. Due to the fluidization, there is a decrease in the liquid

content of the particles from x_{liquid} to $x_{liquid} - \delta x_{liquid}$, as particles get dried while in the fluidized state. A mechanistic kernel has been utilized (for aggregation) in the simulations such that the effects can be captured more efficiently.
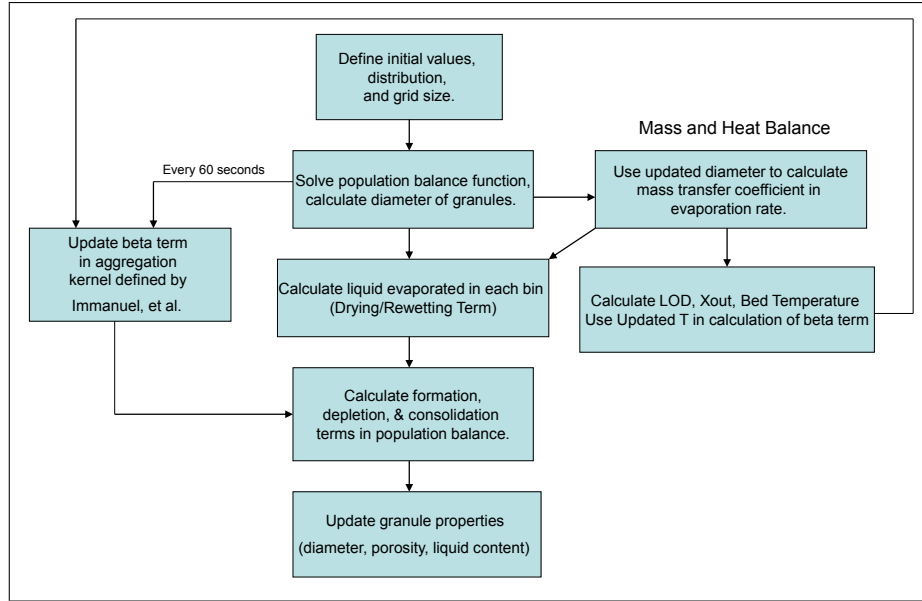
Figure 2.1: Schematic of the algorithm for solving the coupled heat/mass balance and PBM using a mechanistic kernel

2.4   Model calibration and Parameter estimation

The essence of developing sophisticated models to represent unit operations such as granulation is to be able to predict the outcome of the process in advance and abide by the principles of QbD. In order to obtain predictive models, it is important to calibrate the model by aligning the model outcome with the experimental results pertaining to a certain set of formulation and operating parameters. This suggests the need for employing optimization algorithms in order to minimize the error between the simulated property from the model and the experimental results obtained from real data. The objective function fed into the optimization algorithm is a simple least square error. In order to estimate the empirical parameters observed in the PBM, the error within the crucial measurable quantities are minimized. A multi-objective optimization (MOO) problem is formulated considering the particle size distribution (PSD) and the porosity

of the granules for a certain size class. The multi-objective optimization problem is formulated based on the principle of ε-constraint in order to obtain a pareto optima. The main objective function comprises of the error in the PSD while the error in the porosity is incorporated in the form of a constraint. The formulation is solved using the particle swarm algorithm (PSA) which is a well acceptable algorithm for solving MOO problems. The algorithm is forced to solve for parameters minimizing the PSD error under the restrictions that the porosity is less than the desired tolerance.

For the estimation, four experimental datasets were used (based on the DOE provided in Pandey et al. (2013)) and another three datasets were used for prediction purposes. Due to lack of mechanistic knowledge in terms of the influence of impeller speed to the different mechanisms, we have focussed on the datasets that were run at high RPM for estimation and predicted the datasets obtained at low RPM. The PSD and porosity measurements were used for the estimation.

To solve this optimization problem, the model was implemented in MATLAB. Since the formulation is in the form of a multi-objective optimization problem considering minimization of the error for both the PSD and the porosity, an attempt has been made to obtain the pareto optimal solution. A multiobjective optimization problem produces solutions which are not necessarily optimal with respect to any of the objectives considered separately, but are the best tradeoff solutions. The pareto solution provides a set of parameters which represents the best possible situation for both (simultaneously) the objective functions in focus. The multi-objective optimization problem has been implemented in the form of an $\varepsilon - constraint$ framework, where one of the objective functions is tracked for the overall minimization while the other objective function is incorporated in the form of a constraint which dictates the feasible domain for the search algorithm. The $\varepsilon - constraint$ restricts the optimization calculations such that the minimization of the PSD is brought about only for parameters that calculate the error in the porosity to be less than the tolerance. The overall multi-objective optimization (Equation (2.29)) framework was minimized using the particle swarm algorithm (PSA).

$$\Phi(\theta) = \min_{\theta} \sum_{k=1}^{N} (O_k - E_k(\theta))^2 \qquad (2.29)$$

$$\theta = [\beta_0 \ \alpha \ \delta \ B \ c \ x_{sat} \ \varepsilon_{min}] \qquad (2.30)$$

In this equation, θ is the set of adjustable parameters. O_k is the kth measurement value, and $E_k(\theta)$ is the simulated value of that measurement. N is the total number of measurements across all experiments used in parameter estimation. The measurements encompass the porosity values of a particular size class as well as the relative volume of each size class in the final PSD.

Particle swarm algorithm (PSA) that has been used for the minimization is a global optimization algorithm that mimics the flight of a flock of birds and was first proposed by Kennedy and Eberhart (1995). The algorithm is based on the synchrony of the flocking behavior and depends significantly on the inter-individual distances between the birds and their neighbors. The calculations using which the algorithm aims at obtaining the minima by scanning the entire domain in a smart way is shown in Equations (2.31)

$$v_b^{t+1} = w.v_b^t + c_1.rand_1.(b_{best} - x_b^t) + c_2.rand_2.(g_{best} - x_b^t) \qquad (2.31)$$

$$x_b^{t+1} = x_b^t + v_b^{t+1}.\Delta t \qquad (2.32)$$

Here b represents the bird, t is the number of iterations, v_b and x_b are the velocity and position of the birds respectively, c_1 and c_2 are called the cognitive and social parameters, w is the inertial weight which was an inclusion into the algorithm by Shi and Eberhart (1998), $rand_1$ and $rand_2$ are random numbers, b_{best} is the best known position x having the lowest objective function $\Phi(x)$ the bird itself and g_{best} is the best known position of the entire particle (bird) swarm. The cognitive and social parameters, c_1 and c_2 respectively were fixed at 0.3 for both in our PSA implementation. The inertial weight, w has been varied linearly with the iterations between a maximum (=1) and minimum value (=0.1). In Equation (2.31), the first term in the right hand side

represents the **inertial term**, the second term represents the **cognitive component** and the last term depicts the **social component**. Initially N birds were distributed randomly in the parameter space, with a random initial velocity using a maximum value of a fourth of the parameter spaces elongation. Birds leaving the parameter were updated according to the *mirroring* concept in which the bird is mapped back into the parameter space with a sign inversion of its velocity. After each iteration, the ability of each bird to improve its b_{best} or g_{best} is checked within the algorithm. In this approach, significant emphasis has been given to the fulfilment of the constraints and the feasibility of the problem. A schematic diagram showing the implementation of the PSA into our parameter estimation problem has been shown in Figure 2.2. The striking characteristic of this algorithm is its feature of having the birds spread all over in the search domain during the initial iterations and then have the birds more concentrated to the regions which seems more promising.
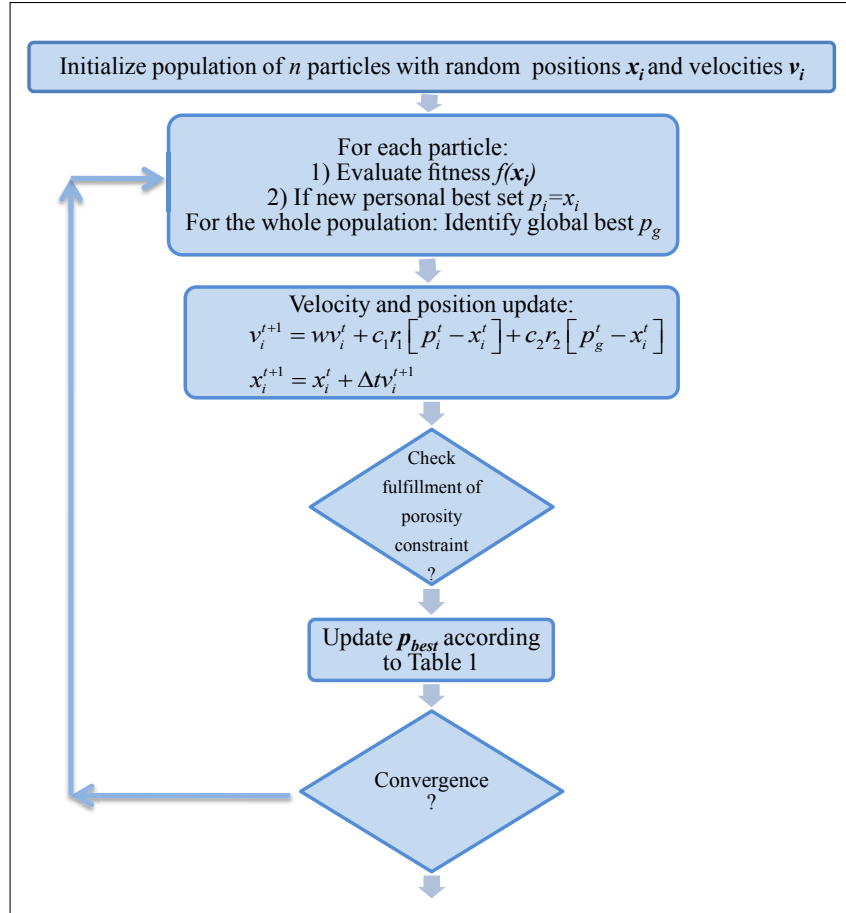
Figure 2.2: Schematic showing the algorithm employed for the parameter estimation using particle swarm algorithm

To evaluate the success of the estimation, R^2 values were calculated according to Equation 2.33, comparing the predicted values with the measurements.

$$R^2 = 1 - \frac{\sum\limits_{k}(E_k - O_k)^2}{\sum\limits_{k}(O_k - \bar{O}_k)^2} \tag{2.33}$$

$$\tag{2.34}$$

Here, $\bar{O}_k$ is the mean value of all measurements in k. R^2 values were determined separately for the porosity measurements and the relative volumes of each size class.

$$SSE = \sum_k (O_k - E_k)^2 \tag{2.35}$$

The SSE values for the three predicted porosity and PSDs were compared to those of the datasets used for parameter estimation. If the SSE of the predicted dataset is much greater than the SSE values of the fitted data, the predicted data is poor, indicating that the calibrated model fails to quantify the effects of the process conditions.

2.5   Calculation of output properties

After the multidimensional population balance equation is simulated, the various granule properties such as average diameter, average liquid and porosity are obtained from the simulation results in order to qualitatively and quantitatively analyse the macroscopic properties. The average particle diameter (Equation (2.37)) is obtained from the average volume with the assumption of the particle being spherical as

$$Average\ volume(t) = \frac{\sum_{i,j,k}[F(s_i, l_j, g_k, t) \times (s_i + l_j + g_k)]}{\sum_{s_i, l_j, g_k} F(s_i, l_j, g_k, t)} \tag{2.36}$$

$$Average\ diameter(t) = \frac{6}{\pi} \times (Average\ volume)^{\frac{1}{3}} \tag{2.37}$$

The average liquid content (Equation (2.38)) of the particles is obtained as a normalized quantity by dividing the total liquid with the total volume as

$$Average\ liquid(t) = \frac{\sum_{i,j,k}[F(s_i, l_j, g_k, t) \times \frac{l_i}{(s_i + l_j + g_k)}]}{\sum_{i,j,k} F(s_i, l_j, g_k, t)} \tag{2.38}$$

The average porosity (Equation (2.39)) of the granules is obtained as

$$Average\ porosity(t) = \frac{\sum_{i,j,k}[F(s_i, l_j, g_k, t) \times \frac{(l_j + g_k)}{(s_i + l_j + g_k)}]}{\sum_{i,j,k} F(s_i, l_j, g_k, t)} \tag{2.39}$$

Number $x_m(t)$ (Equation (2.40)) distribution were also obtained by converting the three

dimensional distribution function into a one-dimensional distribution. For better visualization purposes, the three dimensional distribution is converted into a 1-D granule size distribution by breaking the particle size span between the maximum and minimum diameter into a certain number of one dimensional grids and considering the cumulative distribution of the particles lying in each grid, as the overall distribution for the granule size range. D is the individual particle diameter at the i,j,k grid.

$$x_m(t) = \sum_{L_m \leq D_{ijk} < L_{m+1}} \left(\frac{F(s_i, l_j, g_k, t)}{\sum_{i=1}^{n_s} \sum_{j=1}^{n_l} \sum_{k=1}^{n_g} F(s_i, l_j, g_k, t)} \right) \tag{2.40}$$

2.6 Results and discussion

In this section, we will focus on obtaining a detailed analysis of the simulated PBM with respect to varying input conditions and describing the competing effects of the underlying mechanisms. We will also elucidate the effect of the various control variables towards the final granule properties for a fluid bed process. All model simulations were carried out on a 2.93 GHz Intel quad-core single processor desktop computer with 8GB RAM in Matlab. The key material, process, design and empirical parameters used for the simulations can be obtained from the paper (Chaudhury and Ramachandran, 2013). These simulations are representative of a high-shear system where the evaporation term is considered zero for the sake of simplicity.

2.6.1 Effect of various mechanisms on final product characteristics

Various cases have been considered as the basis to perform qualitative validation to conclude that the dynamics exhibited by a typical granulation process (e.g. high-shear) is best described by the consideration of multiple key granulation mechanisms as opposed to single mechanisms such as aggregation which are traditionally the only one considered. Moreover, the incorporation of a mass balance to account for liquid addition is key to discern the difference between the granulation and wet massing regime.

Table 2.1: Parametric values for the simulations used to study the effect of various mechanisms

Parameter name	Value
ρ_{solid}	2700 kgm^{-3}
ρ_{liquid}	1000 kgm^{-3}
ρ_{gas}	1.2 kgm^{-3}
Number of grids in solid, liquid and gas volume	22
Grid Width (same in each volume)	$1.79 \times 10^{-13} m^3$
Initial distribution: Mean	181.2μm
Initial distribution: Standard deviation	8.215μm
Binder Spray rate, u	$8 \times 10^{-5} m^3 s^{-1}$
Total volume of liquid added	0.048m^3
c_{binder}	0.1
ϵ_{min}	0.2
G_{max}	1×10^{-12}
Consolidation constant, c	1×10^{-4}
Aggregation Constant for the kernel, β_0	1×10^{19}
α for Madec kernel	1
δ for Madec kernel	1
Shear rate, G for the Breakage kernel	$64 s^{-1}$
Empirical parameter for Breakage	10

Table 2.2: Summary of the different cases used in PBM simulations

Case no.	Aggregation	Breakage	Consolidation	Liquid	Layering
1	$\checkmark$	$-$	$-$	$-$	$-$
2	$\checkmark$	$-$	$-$	$\checkmark$	$-$
3	$\checkmark$	$-$	$-$	$\checkmark$	$\checkmark$
4	$\checkmark$	$-$	$\checkmark$	$\checkmark$	$-$
5	$\checkmark$	$\checkmark$	$-$	$\checkmark$	$-$
6	$\checkmark$	$\checkmark$	$\checkmark$	$\checkmark$	$\checkmark$

Bulk Properties

Figure 2.3 depicts the evolution of the average granule diameter as a function of time for the different cases. Following the initial 200 seconds, the average diameter increases with time due to the addition of liquid which promotes granule growth (mainly through aggregation of particles). It can be seen that if the liquid addition is not accounted for, there is a smaller change in the rate of increase of average diameter from the granulation stage to the wet massing stage which is atypical of an industrial granulation process. Experimental studies have shown a predominant increase in average diameter at the granulation stage compared to the wet massing stage (Pandey et al., 2011). This can also be confirmed by the plots corresponding to cases 2-6. Within cases 2-6, the effect of other competing mechanisms such as breakage, consolidation and layering are investigated and results show their influence on bulk properties such as average diameter where breakage and consolidation demonstrate a reduction in average diameter and layering an increase in average diameter. The layering phenomenon does not result in significant increase in granule diameter compared to aggregation due to the assumption that the granulation takes place in the viscous regime where the viscous forces promote aggregation as compared to layering which predominantly occurs in the capillary regime (Ramachandran et al., 2008). Consolidation of particles lead to a reduction in the gas volume and hence Case 3 suggests less increase in the average particle diameter. Case 4, which considers aggregation, rewetting and breakage also indicate reduced increase in the average particle diameter, primarily because of the fragmentation of bigger particles into smaller bits.
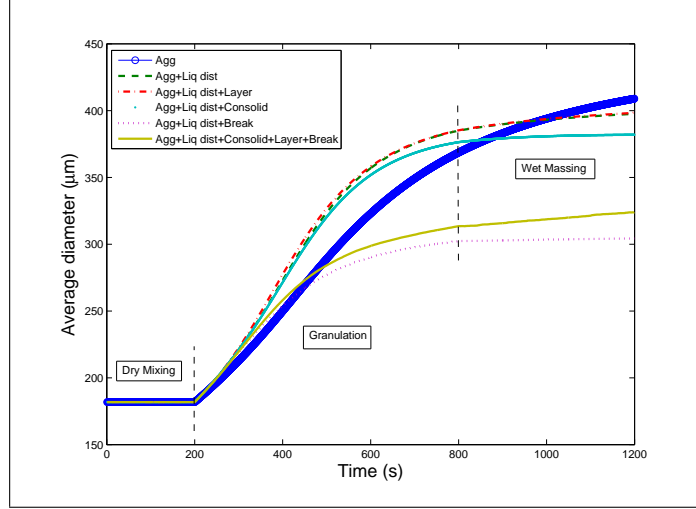
Figure 2.3: Effect of various mechanisms on particle diameter for liquid flowrate= 8×10^{-5} $m^3/sec, \rho_s = 2700$ $kg/m^3, \rho_l = 1000$ $kg/m^3, x_{w_c} = 0.04$, initial distribution of particles having a mean of $= 1.82 \times 10^{-4} m$
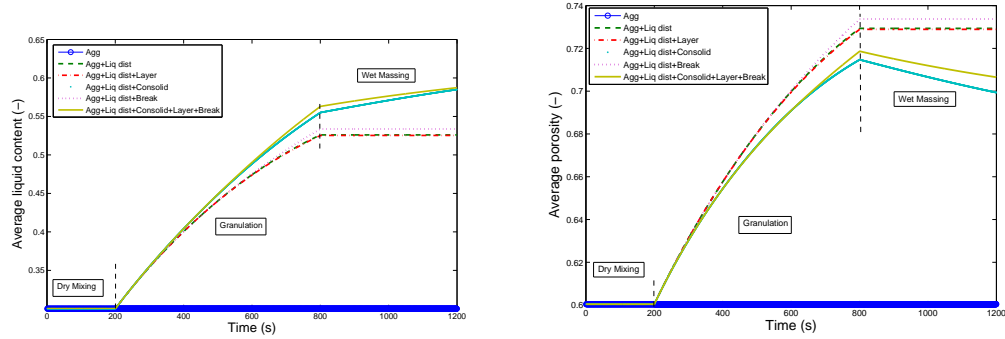
(a) Effect of various mechanisms on average liquid content

(b) Effect of various mechanisms on average porosity

Figure 2.4: Effect of various mechanisms on the bulk properties for liquid flowrate= 8×10^{-5} $m^3/sec, \rho_s = 2700$ $kg/m^3, \rho_l = 1000$ $kg/m^3, x_{w_c} = 0.04$, initial distribution of particles having a mean of $= 1.82 \times 10^{-4} m$

Figure 2.4 a shows the influence of each mechanism on the average liquid content of the population. Cases 4 and 6 show a rise in the average liquid content of the particles, primarily since the amount of liquid added is constant, but, due to consolidation, the gas volume is reduced and hence the denominator of the liquid content reduces thereby

leading to an increase in the liquid content term. Figure 2.4 b shows the effect of the various mechanisms on the average porosity of the granules. Overall, granulated particles are shown to have higher porosity and a similar trend is also observed in the figure. The average porosity of granules do not change when only aggregation is taken into consideration, since there is no change in the overall liquid or gas volume of the particles throughout the process. The figure suggests that the increase in porosity of the population is greater when there is breakage of granules. This outcome could be a result of the breakage kernel used which leads to particles with greater gas volume and thus increased porosity. The increase in porosity is less when consolidation comes into play since particles are compacted with the escape of gas from the granules. Both figures are qualitative indicators that an integrated model must be considered to demonstrate experimental observations in granulation processes (Ramachandran et al., 2008).

Distributed properties: Granule size distribution

Figure 2.5 shows the normalized mass frequency with respect to particle size classes of a batch of granules. The maximum distribution of particles can be observed to lie in the range of 180-500 μm. This suggests that particles tend to shift from smaller bins to the larger bins as granulation proceeds. The different cases illustrate the effect of competing mechanisms on the final GSD and results show that for integrated case (case 6) the GSD is in an intermediate range with the effects of liquid addition, aggregation and layering (positive growth mechanisms) striking a balance with breakage and consolidation (negative growth mechanisms). Case 2 and 3 exhibit highest number of large particles, since these two plots represent only the positive growth terms. Cases 4 and 5 have larger particles due to aggregation and liquid addition but there also exists negative growth and breakage terms which lead to a relative decrease in the particle size. Therefore, these cases have larger number of intermediate sized particles. The extent of shift (towards the left) of the distribution depends on the choice of parameters considered for the respective mechanisms.
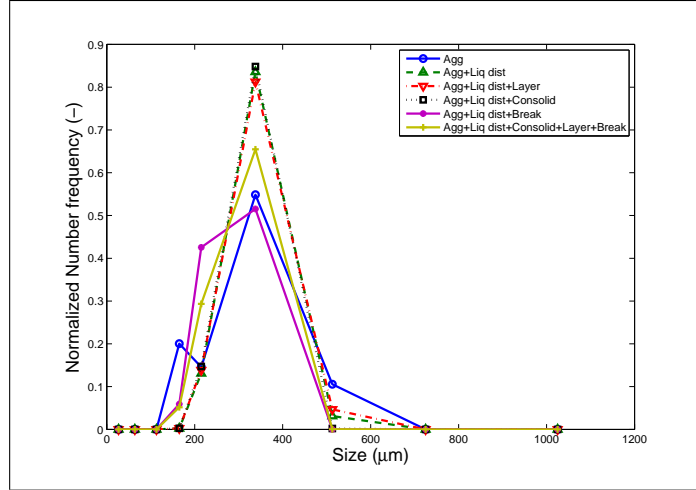
Figure 2.5: Mass frequency at final time for various mechanisms

Time evolution of granule size classes

Figure 2.6 suggests the variation in the number distribution for various mechanisms and under different regimes. We can see that as granulation proceeds, due to aggregation, smaller particles shift to larger bins as they agglomerate to form larger particles and hence there is a steady increase in the number distribution of larger particles with time and vice versa for smaller particles. With the addition of liquid, the number of smaller particles reduce with time due to an increase in the particle diameter, but with the onset of wet massing, the slope of the curve representing large particles decreases slightly and the reverse happens for smaller particles. This trend is more or less similar for all mechanisms, but as breakage comes into play, the decrease in the slope of larger particles becomes more due to the reduction in particle growth as breakage becomes dominant and leads to a decrease in the increase of larger particles.
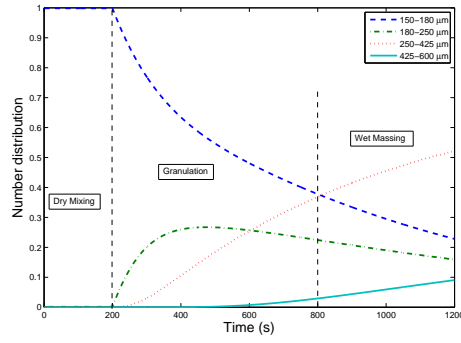
(a) Aggregation only
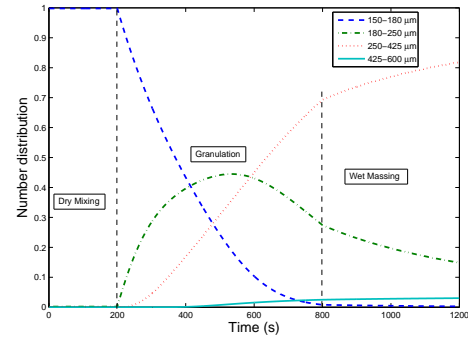
(b) Aggregation and liquid addition
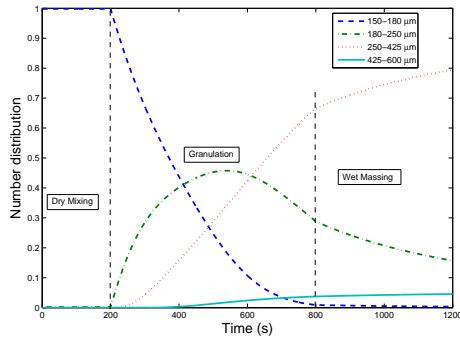
(c) Aggregation, liquid addition and layering
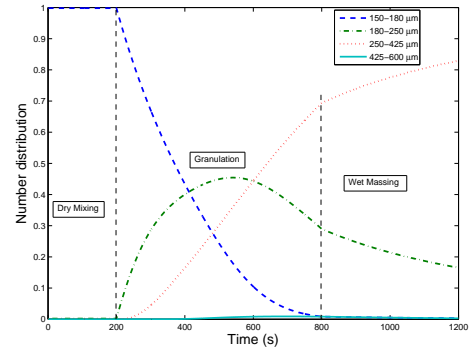
(d) Aggregation, liquid addition and consolidation
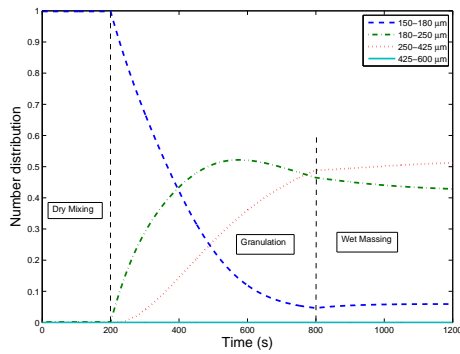
(e) Aggregation, liquid addition and breakage
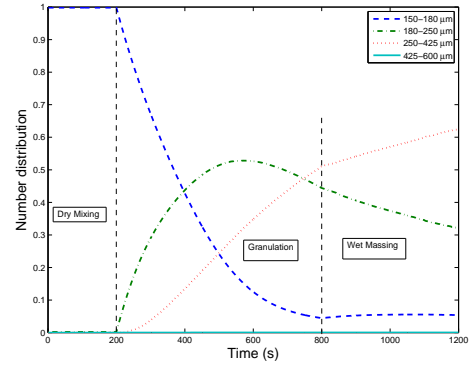
(f) Aggregation, liquid addition, layering, consolidation and breakage

Figure 2.6: Number density of particles under various mechanisms

The mode in which liquid is added also has a marginal effect on granule properties. In this simulation, the total volume of liquid added to the system was held constant

with the scheduling of liquid delivery varying. Three cases were considered which is 1) continuous addition (nominal case), 2) 3 pulse addition and 3) 7 pulse addition. Therefore with lower number of pulses for liquid addition, the rate of liquid addition in each pulse was raised. For the case considering liquid addition in 3 pulses, liquid was added at the time intervals 200-320, 440-560 and 680-800 seconds, whereas for the case considering 7 pulses, liquid was added at time intervals 200-246, 292-338, 384-430, 476-523, 569-615, 661-707 and 753-800 seconds. The total volume of liquid added was held constant at 0.6012 m^3. From Figure 2.7, it can be seen that for the continuous liquid addition mode, the plot for average diameter shows a smooth increase. With the addition of liquid in the form of semi-continuous pulses, the diameter is also observed to vary in a non-smooth fashion following the binder addition. Similar trend is observed for porosity, where porosity is observed to show a non-smooth variation at the intervals where binder is sprayed. From the number and porosity distributions, results show minimal variations in the variances of the distribution.

(a) Average Diameter

(b) Average Porosity

(c) Number frequency distribution
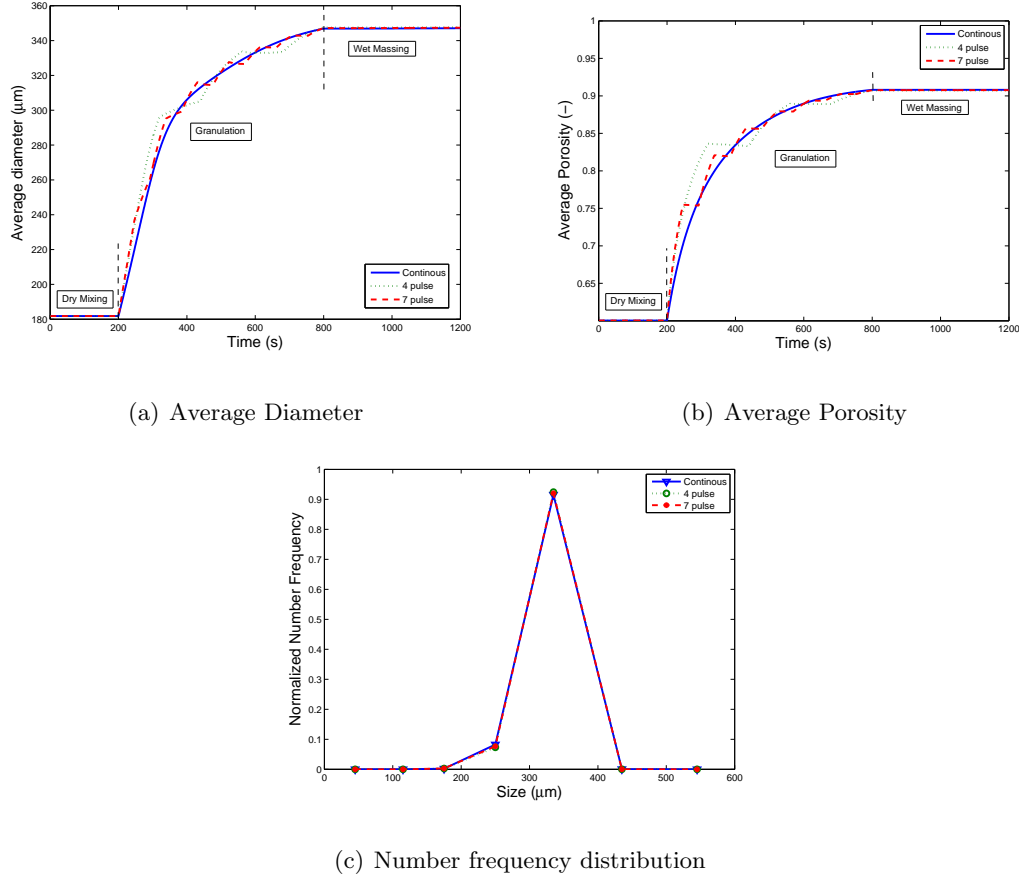
Figure 2.7: Bulk properties for different liquid addition modes, total liquid$=0.6012m^3$

2.6.2 Effect of initial primary particle size distribution on granule properties

The initial distribution also effects the final product characteristics. Figure 2.8 shows the average diameter, average porosity, number distribution and porosity distribution for various initial particle distributions. The initial particle population has same mean for all the three cases and only the standard deviation was different in each case. Batch 1 refers to the narrowest size distribution (6.665 σ), batch 2 refers to intermediate size distribution (8.215 σ), and batch 3 with the widest size distribution (12.72 σ). Results show that for average diameter versus time (Figure 2.8 a), batch 3 shows the largest increase in diameter during the granulation stage but batches 1 and 2 show a steeper increase during the wet massing stage. The dynamics of batch 1 can be attributed

to the fact that given the narrowest size distribution, there is less aggregation due to particles being more of the same size initially relative to batch 3, where there is preferential aggregation of bigger and smaller particles compared to particles of similar sizes. For average porosity (Figure 2.8 b), batch 1 shows the highest increase in porosity due to reduced consolidation for this case, as the initial particles were not very porous too begin with. The effect of variability is also captured in the number and porosity distributions (Figures 2.8 c and 2.8 d) where results show the difference in end-point variance due to the differences in initial primary particle size distributions. However the variability in primary particle size distribution demonstrates changes in the key granule properties demonstrating the propagation of disturbances through the process.

(a) Average Diameter

(b) Average Porosity

(c) Number frequency distribution
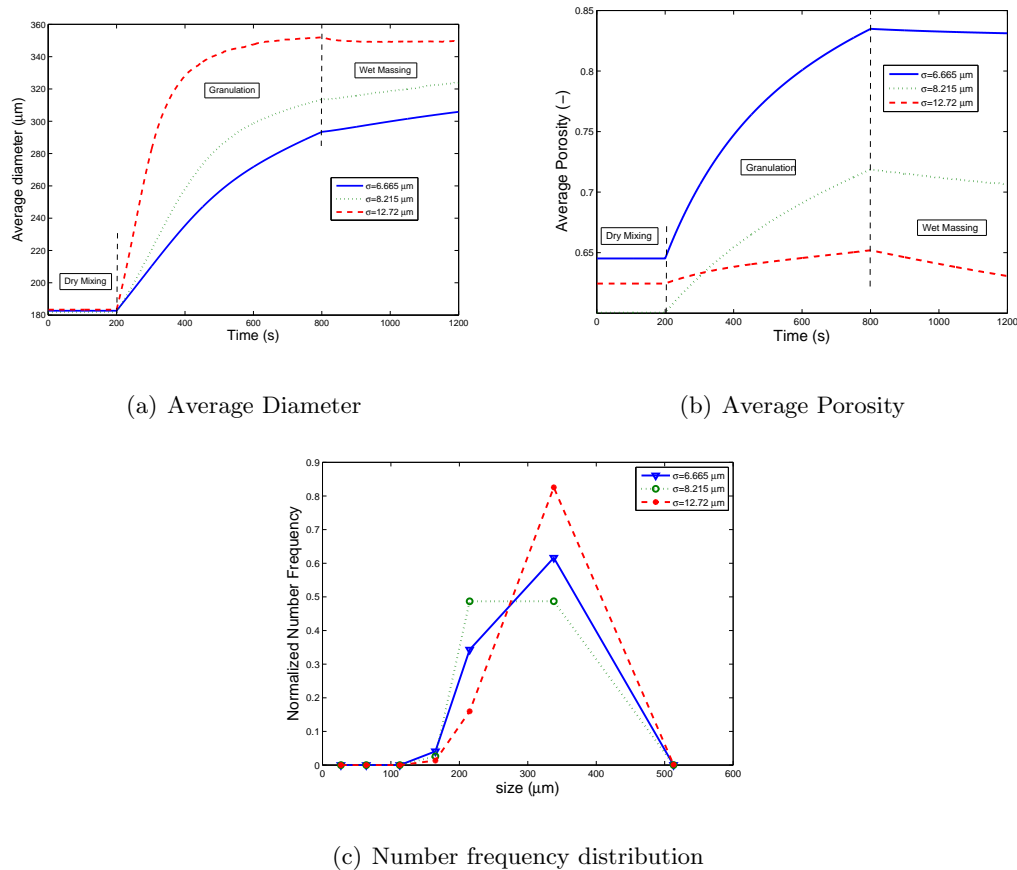
Figure 2.8: Bulk properties for initial particle distributions, Mean= $182.2 \mu m$

The effect of primary particle size distribution and the mode of binder addition also play a significant role in the final granule properties and a detailed discussion

can be found in Chaudhury and Ramachandran (2013). The previous results reflect the behavior and trends observed in a high-shear granulation system. The following subsection focuses at accounting for the evaporative term in the drying/rewetting term of the PBM. The effects of the multiple control parameters affecting a fluid bed system have been studied.

2.6.3 Effects of the evaporative term in case of a fluid bed process

The coupled model that has been developed considering the heat and mass balances with the PBM is applied and the different granulation process variables are simulated. In this work, the variables of interest are the spray rate of liquid binder, the inlet air temperature, the inlet dew point, and the flow rate of dry air. The values for the parameters used have been listed in Table 1 of Chaudhury et al. (2013b). The effects of these variables on the theoretical granule properties (loss on drying, particle size, porosity, etc.) have been discussed in the published paper (Chaudhury et al., 2013b) where the process variable of interest is varied, while all the other variables are held constant.

Effect of Spray Rate of Liquid Binder

Figure 2.9 (a) shows the effect of varying spray rate of liquid binder on the loss on drying (LOD) of the granules. From the figure, we see that as the spray rate of the liquid binder increases, the LOD increases. This is in accordance with the liquid water balance, Equation (2.16), as the spray rate directly affects the amount of moisture in the granulator and leads to an overall increase in the LOD. This trend is also in agreement with the experimental observations published previously (Rambali et al., 2001), (Hu et al., 2008).

Table 2.3: Parametric values for the fluid-bed simulations

Parameter name	Value
ρ_{solid}	2700 kg/m^3
ρ_{liquid}	1000 kg/m^3
ρ_{gas}	1 kg/m^3
Number of grids in solid, liquid and gas volume	6
Grid Width (same in each volume)	4.5×10^{-13} m^3
Initial mass charged to the granulation	2 kg
Initial LOD	0.018 $kg\ water/kg\ solid$
Temperature of inlet air	333 K
Volume of air in the granulator	0.009056
Mass of air in the granulator	0.0107 kg
Binder Spray rate, u	0.001 m^3/sec
x_{in}	0.00505
Specific heat capacity of air	1006 $J/kg - K$
Specific heat capacity of water vapor	1996 $J/kg - K$
Specific heat capacity of liquid water	4187 $J/kg - K$
Specific heat capacity of solid	1000 $J/kg - s$
Latent heat of vaporization	2270 kJ/kg
Q_{losses}	200 J/sec
Experimental correction factor, γ	0.002
c_{binder}	0.1
ϵ_{min}	0.2
Mass flowrate of inlet air	0.067 kg/sec
Consolidation constant, c	1×10^{-2}
Aggregation Constant for the kernel, β_0	2×10^{30}
Stokes deformation number, St_{def}	1
Yield Stress, Y_d	4.1×10^4 Pa
Y_d^*	0.01
Elastic modulus, E^*	$8.3 \times 10^4 Pa$
Granule saturation at which surface liquid first appears, s^*	0.2
Viscosity, μ	0.002 $kg/m - sec$
Simulation time	900 $secs$

(a) Loss on drying
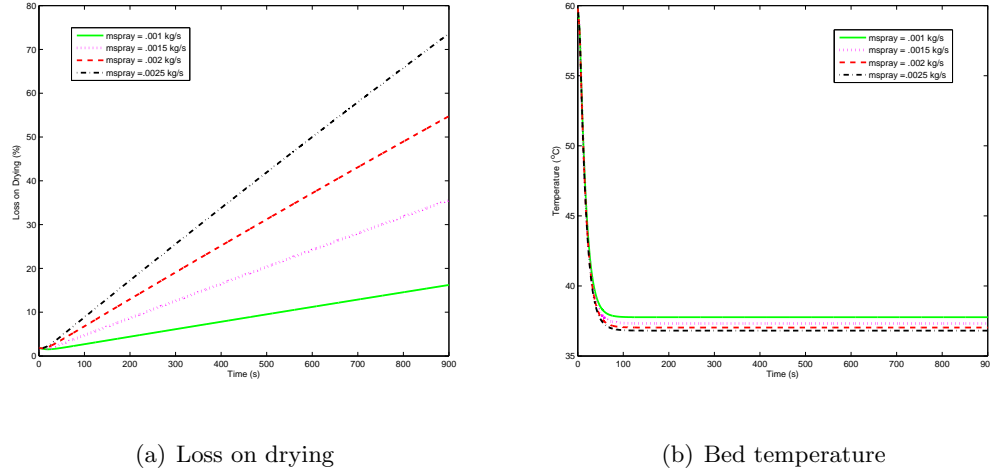
(b) Bed temperature

Figure 2.9: Effect of varying the mass spray rate of liquid binder on the output properties of the granules.

Figure 2.9 (b) illustrates the effect of varying spray rate on the bed temperature, which decreases as the spray rate increases. As mentioned previously, with increasing spray rate, the $\frac{dx_{bed}}{dt}$ term in Equation (2.16) increases, as does the LOD, or x_{bed}. These trends cause Equation (2.24) to decrease and therefore the resultant outcome is a decrease in the temperature of the bed.

Effect of Inlet Air Temperature

The effect of inlet air temperature on the loss of drying is shown in Figure 2.10 a. We see that as the inlet temperature increases, the LOD of the granules decreases. As mentioned in the previous section, at higher temperatures, x_{sat} increases. Therefore, from the model perspective, the evaporation rate increases. From Equation (2.16), the LOD decreases with an increased evaporation rate, consistent with the results shown in the figure and is in agreement with the observations found previously in Hu et al. (2008).

(a) Loss on drying

(b) Average particle diameter

(c) Bed temperature

(d) Outlet humidity
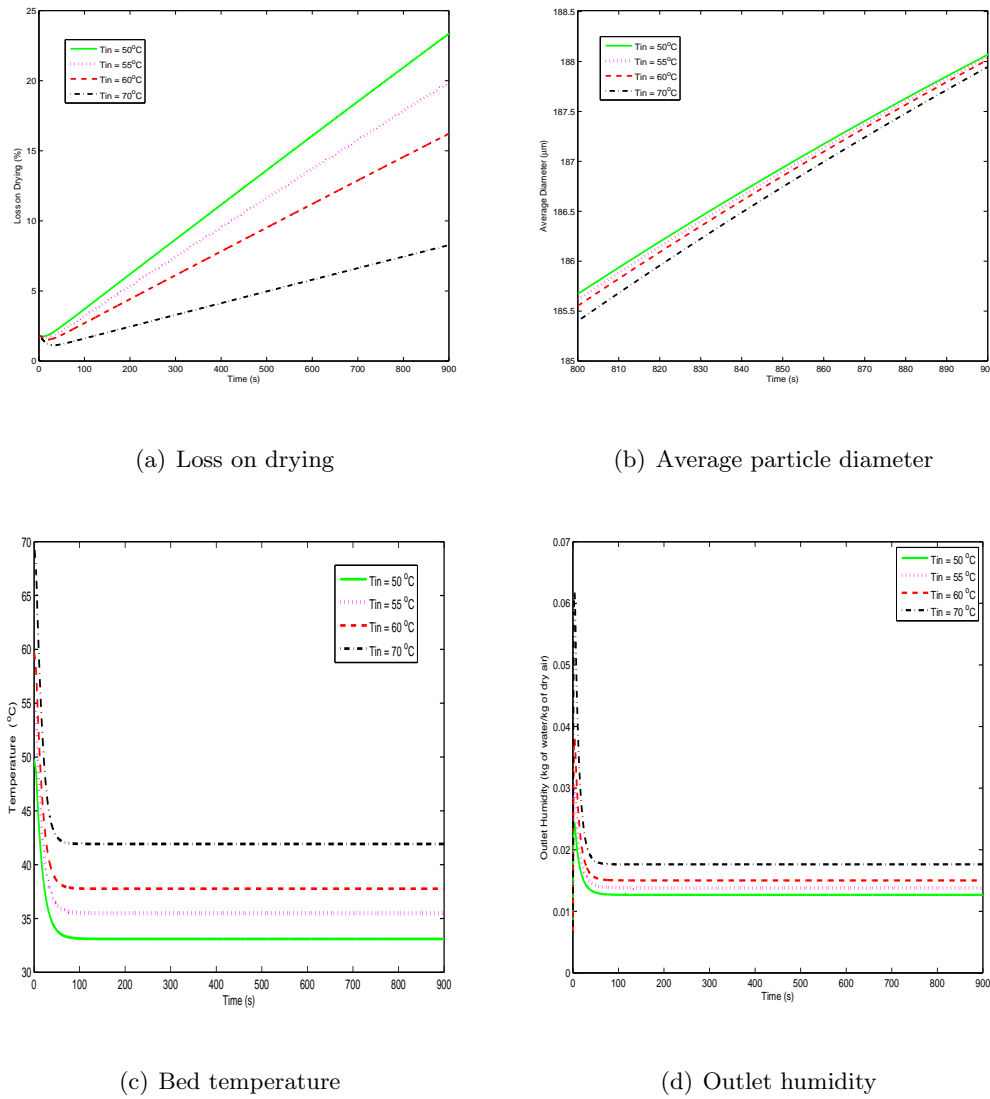
Figure 2.10: Effect of varying inlet air temperature on various output macroscopic properties

As the inlet air temperature increases, the average particle diameter decreases as also illustrated in Figure 2.10 b. With an increased inlet air temperature, there is a higher evaporation rate. Intuitively, the inlet temperature of air being higher, the overall bed temperature would rise, as also seen with reference to the model, the bed temperature is obtained by using the inlet air temperature as the initial conditions for Equation (2.24). From Figure 2.10 c it can be observed that as the inlet air temperature increases, the temperature of the bed of granules increases. This way the mechanistic kernel is reduced

as well, which results in lower agglomeration. These result in a smaller liquid volume and also a reduced particle diameter. The effect of inlet air temperature was investigated extensively by Rambali et al. (2001), Davies and Gloor (1971), and similar results were observed by the authors.

With increasing inlet air temperature, the evaporation rate increases and therefore the outlet humidity increases (Figure 2.10 d), which is consistent with the qualitative results from the mass balance for water vapor as shown in Equation (2.18). As the inlet humidity increases, the driving force for evaporation decreases as more moisture is supplied to the granulator. Thus the evaporation rate in the system decreases which leads to an increases in the loss on drying as also shown in Figure 2.11 a.

With an increased inlet humidity, the moisture content of the system increases and hence the bed temperature is reduced due to the removal of heat from the system. Moisture has a relatively high specific heat capacity and acts as a coolant. This trend has also been exhibited in Figure 2.11 b.

(a) Loss on drying

(b) Bed temperature
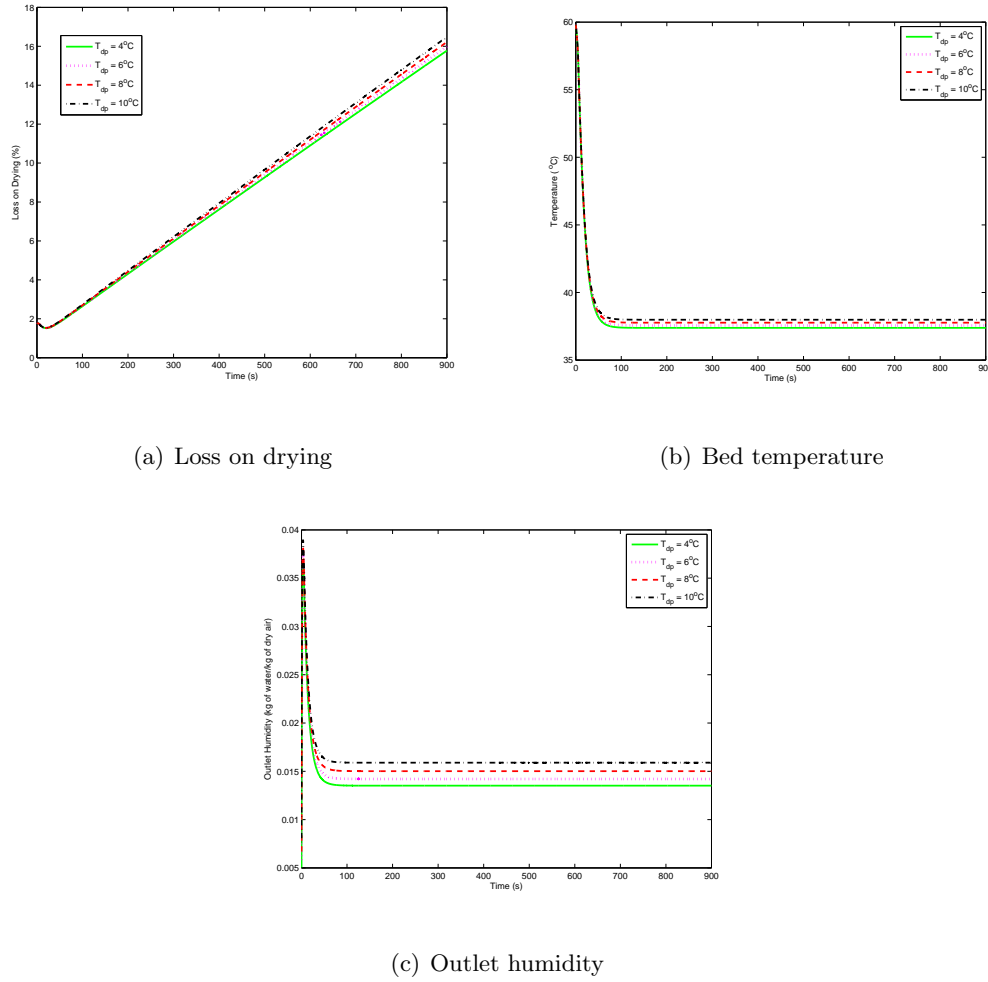
(c) Outlet humidity

Figure 2.11: Effect of varying inlet air humidity on various output macroscopic properties

As the inlet humidity of air increases, the outlet humidity increases as well Figure 2.11 c since the increased moisture content that enters the granulator, also leaves the granulator in the form of outlet humidity. Although, in this case, the increase in the outlet humidity imparted by the evaporation of existing moisture is reduced. From the model perspective, this is mainly because the initial conditions for Equation (2.18) are determined by the inlet air humidity.

Effects of Mass Flow Rate of Dry Air

It can be observed from Figure 2.12 a that as the flow rate of dry air increases, the LOD decreases. This trend is exhibited due to the increase in the evaporation rate due to increased air flow rate which leads to a decrease in the moisture content of the bed. This is in agreement with the observations found in Hu et al. (2008).

In Figure 2.12 b, the flow rate of air was varied to study the effect on the particle size. Due to increased evaporation with higher air flow rate, the liquid content of the particles decreases, which results in a reduction in the liquid volume of the particles and also a reduced aggregation kernel. Therefore, the particle size decreases slightly, which has also been reported previously by Rambali et al. (2001).

In Figure 2.12 c, we vary the flow rate of dry air and examine the effects this has on the temperature of the granules. From the figure, we observe that as we increase the flow rate, the bed temperature increases.

Figure 2.12 d shows the effects on the outlet humidity that is an outcome of varying the flow rate of dry air. With an increased air flow rate, the evaporation rate increases and therefore more water is expected to exit the system with the outlet air. Since the outlet humidity is expressed as the ratio between the mass of water and the mass of dry air, $\frac{kg\ of\ water}{kg\ of\ dry\ air}$, we see from the figure that the flow rate of dry air does indeed increase the amount of water leaving the system.
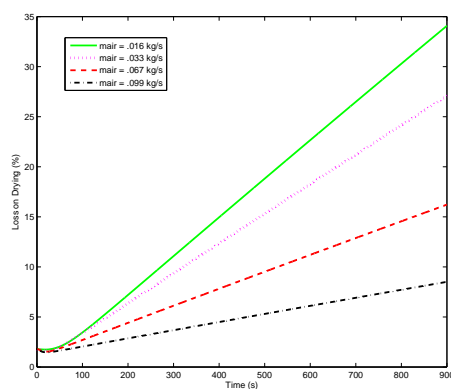
(a) Loss on drying
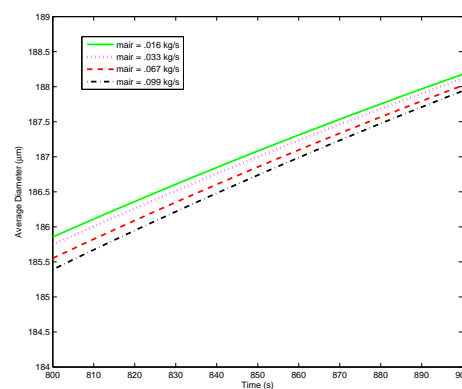
(b) Average particle diameter
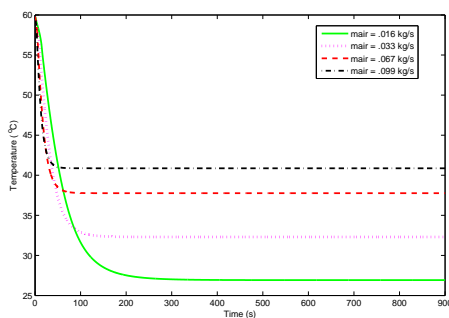
(c) Bed temperature
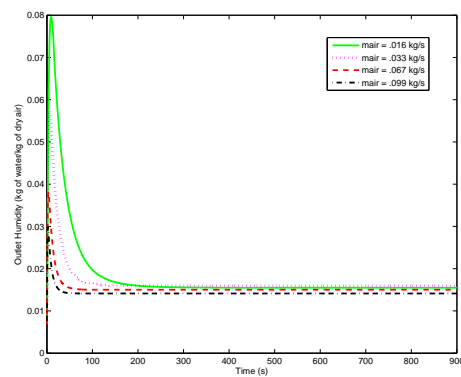
(d) Outlet humidity

Figure 2.12: Effect of varying flow rate of dry air on various output macroscopic properties

2.6.4 Parameter estimation and predictive modeling

The PBM that has been utilized in this work and has been described above consists of multiple empirical parameters. This necessitates the need for parameter estimation in order to calibrate the model for making effective predictions. This section describes the methodology utilized for the same. The DOE presented in Table 2.4 has been run in a high-shear 1-L $Diosna^{®}$ (16-cm diameter and 8-cm depth). The material used for the placebo formulation in this study comprised of microcrystalline cellulose and anhydrous lactose in a 2:1 ratio. Batches of 200 gms were mixed at an impeller speed of 5 m/s and a chopper speed of 2000 rpm. During the liquid addition time, the amount

of liquid and impeller speed were varied based on the DOE presented in Table 2.4. The wet massing time has also been varied based on the values outlined in the DOE. The resultant granules were characterized for size by sieve analysis using an Allen Bradley Sonic Sifter (Allen Bradley, Milwaukee, WI) equipped with six screens and a pan-US 30 (590 μm), 40 (420 μm), 60 (250 μm), 80 (180 μm), 140 (106 μm), and 270 mesh (53 μm). The details on the experimental results and the experimental procedure is presented in Pandey et al. (2013). The batches utilized for the estimation are 3, 4, 7 and 10 from the DOE shown in Table 2.4. If one solution is better than another with respect to one objective, while the second is better with respect to a different objective, then the two solutions are considered nondominated or equivalent, and are called pareto solutions. The pareto set of optimal solutions obtained from the estimation are such that an improvement in one objective function would lead to a deterioration in the other objective functions.

Table 2.4: Full Factorial DOE

Batch #	Liquid to Solid ratio (%)	Impeller speed (m/s)	Wet massing time (s)
1	40	4.0	30
2	30	4.75	60
3	20	5.5	90
4	20	5.5	30
5	20	4.0	30
6	30	4.75	60
7	40	5.5	90
8	40	4.0	90
9	30	4.75	60
10	40	5.5	30
11	20	4.0	90
12	30	4.75	60

The estimated parameters from the optimization algorithm has been listed in Table 2.5. The optimization algorithm not only fits the model to the experimental PSD but also the porosity. The fitted particle size distributions have been shown in Figure 2.13. The sum of square error, SSE between the simulated and the experimental distributions are significantly low. It can be seen that there is a fairly good agreement

between the experimental results and the simulated distribution from the estimated parameters. The median diameter, D_{50} values were calculated for the experimental and the simulated particle size distributions. Comparison between the median diameters for the experimentally measured PSD and the simulated PSD has been shown in Figure 2.14. The 45^0 line in the plot represents complete agreement between the experimental and simulated values. The simulated values are close to the 45^0 line and thus reveal good estimation of the median diameters using the parameter estimation technique.

The optimization technique employed in this estimation simultaneously considered the errors in both the PSD and porosity for adequate estimation of the empirical parameters. Figure 2.15 shows the porosity values from the experimental measurements and simulated parameters. The estimation could capture the porosity values reasonably close to the experimental measurements. The error in porosity, SSE is also significantly reduced, however there is some mismatch associated with the porosity fits. A vital causal link behind the mismatch in the porosity fits is the empirical and inadequate representation of the consolidation rate of the granules. Consolidation has been observed to be a function of the material cohesion (liquid to solid ratio) and the impeller speed (Iveson et al., 1996). However, a mechanistic representation has not yet been developed. It is expected that a mechanistic expression depicting the effect of moisture content and impeller speed on the consolidation rate can yield better predictive capability for the granule porosity. Iveson and Litster (1998) had proposed the consolidation rate as a function of the viscous Stoke's number, while Litster and Ennis (2004) had related the consolidation rate to the Stoke's deformation number. Future work can be proposed investigating the moisture content to the yield strength of particles so that the consolidation rate can be effectively correlated to the impeller speed and moisture content of the granulation system.

Table 2.5: Set of pareto optimal solutions from the parameter estimation technique

Parameter name	β_0	δ	α	**B**	**c**	ε_{min}	x_{sat}
Estimated value	$1.6362e^{22}$	0.0993	0.4538	4.6644	$1.865e^{-4}$	0.134	0.5013

(a) Batch 3   (b) Batch4
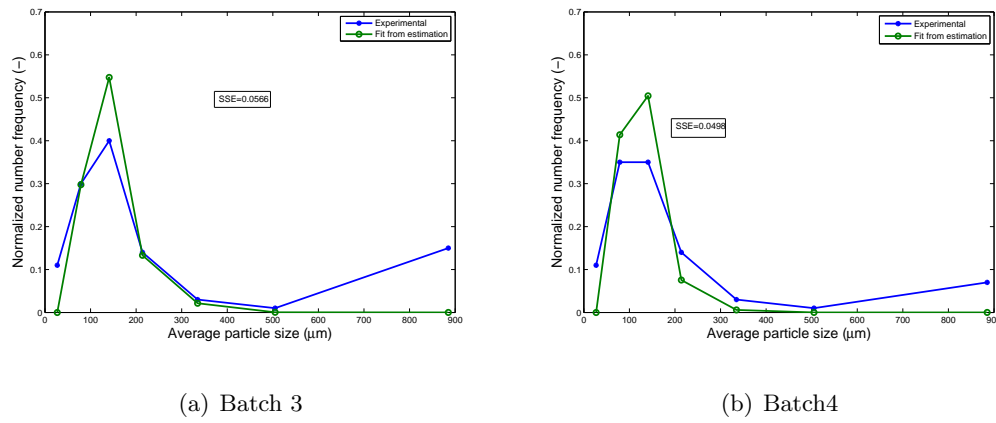
Figure 2.13: Selected experimental and estimated simulated particle size distributions from high shear granulator using multi-objective parameter estimation
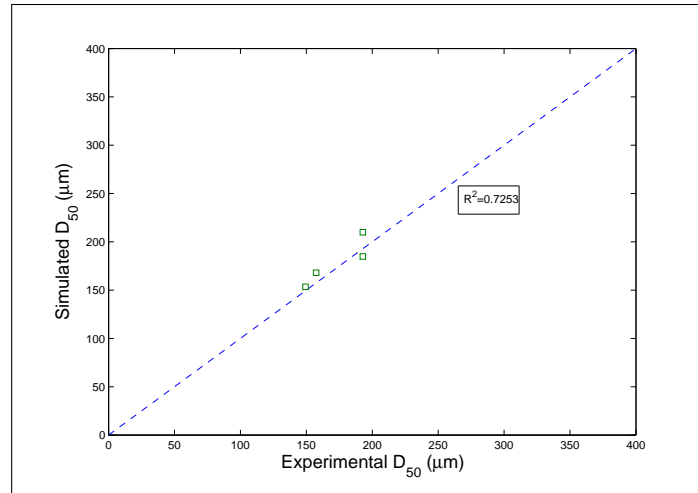
Figure 2.14: Experimental and estimated simulated D_{50} from high shear granulator using multi-objective parameter estimation
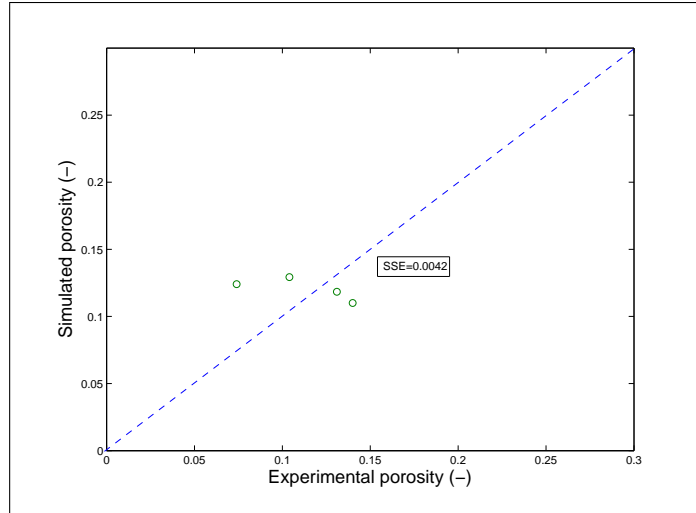
Figure 2.15: Experimental and estimated simulated porosity from high shear granulator using multi-objective parameter estimation

The batches utilized for the predictions are 1, 2 and 11 from Table 2.4. The model predictions have been shown in Figures 2.16-2.18. The predicted PSD shows low error between the simulated and the experimental distributions (Figure 2.16). The predicted median size has been shown in Figure 2.17 which also shows considerable agreement with the experimental measurements. The predicted porosity values for the desired size class has been shown in Figure 2.18 which shows predictions that are close to the actual experimental values.
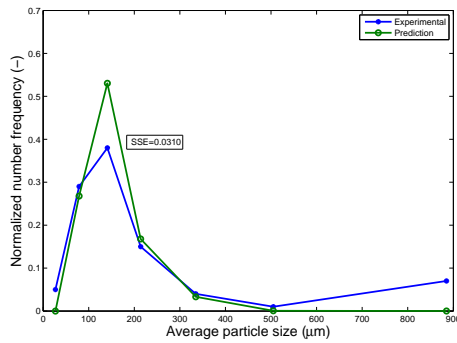
(a) Batch 2
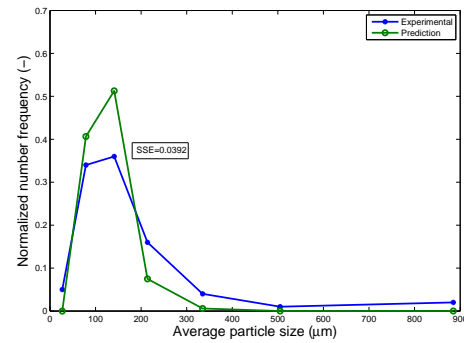
(b) Batch 11

Figure 2.16: Experimental and predicted simulated particle size distributions from high shear granulator from the calibrated model
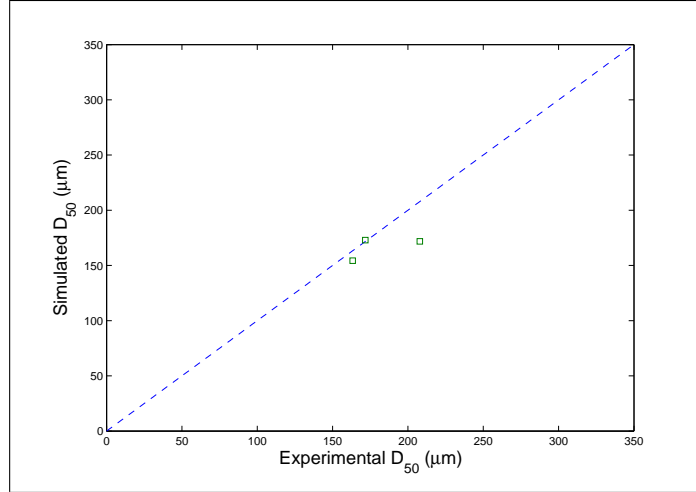
Figure 2.17: Experimental and predicted simulated D_{50} from high shear granulator from the calibrated model
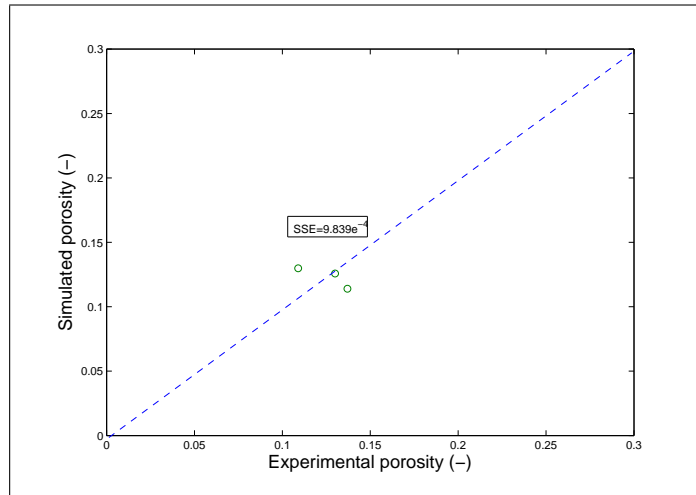
Figure 2.18: Experimental and predicted simulated porosity from high shear granulator from the calibrated model

2.7 Chapter Conclusions

In this study, an integrated 3-D population balance model is developed to describe the dynamics of granulation process. The model specifically incorporated liquid addition to demarcate the regimes of pre-mixing, granulation (liquid addition) and wet massing, showing qualitative agreement with profiles obtained in the literature (Pandey et al.,

2011). The mode of binder addition in the form of continuous addition or different pulses was simulated in the integrated model and results suggested the lack of sensitivity in current form but highlights the implementation of more mechanistic kernels to capture accurate sensitivities. The effect of variability in primary particle size distribution was also studied and results illustrated the effect of this variability on key granule properties. Results showed that the integration of all the different key granulation mechanisms need to be considered to ensure better validation and prediction of key granule properties. Without the consideration of all mechanisms within the PBM, the effect of all process conditions cannot be taken into account which might lead to poor predictive ability of the model.

Later, a mechanistic PBM has also been integrated with a coupled heat and mass model for a fluid bed granulator, in order to obtain a more mechanistic understanding of the granulation dynamics. The various quantities such as particle diameter, liquid content and temperature change in the system evolve as granulation proceeds. These updated quantities have been used after an interval of 60 seconds to modify the aggregation kernel used in the PBM simulation. With increasing computational power, this update can be performed more often to obtain a more refined coupling. Since, the kernel used is mechanistic in nature, it can effectively capture the behavioral changes introduced due to the varying quantities in the system. The detailed analysis performed provides a better insight on the outcome of the system that is associated with the changes in the various input parameters. The coupled heat and mass model is novel in nature and enables to track the various granule properties. This lends credence to the use of the overall model for predictive granulation process design in fluid bed systems.

The parameter estimation considering the PSD and the porosity simultaneously shows good calibration of the model. The simulated quantities during the estimation can very well capture the results observed experimentally. The predictions obtained from the calibrated model are in line with the experimental results. The porosity could not be tracked as accurately as the PSD due to the fact that the consolidation of granules is not mechanistically related to the liquid to solid ratio or the impeller speed as known from literature (Iveson and Litster, 1998). The current empirical kernel cannot capture

the system behavior accurately, however, in later chapters a more mechanistic approach is discussed for modeling granulation.

Chapter 3

Specific Aim II: Development of numerical techniques for the solution of PBMs

The details of the discussions provided in this section can be obtained in the publications:

- Chaudhury, A., Kapadia, A., Prakash, A. V., Barrasso, D., Ramachandran, R., 2013, An extended cell-average technique for a multi-dimensional population balance of granulation describing aggregation and breakage. Advanced Powder Technology, 24 (6), 962-971

- Chaudhury, A., Oseledets, I., Ramachandran, R., 2014, A computationally efficient technique for the solution of multi-dimensional PBMs of granulation via tensor decomposition. Computers and Chemical Engineering, 61, 234-244

3.1 Numerical solution techniques of PBMs

Population balance models are hyperbolic integro partial differential equations that describes the dynamic evolution of a discrete distribution with respect to a certain attribute. Population balance models are used in various fields of research such as crystallization, granulation, polymerization, extraction, milling, aerosol engineering and biological applications (considering cells). The discrete nature of the PBM is characteristic of its application to the various particulate processes. The numerical solution to such equations are complicated due to the presence of the advective growth terms that impart to the hyperbolic nature of the partial differential equation (PDE). However, the calculations involving the integral terms is associated with large simulation times. The

advective terms primarily attribute to stability issues and can lead to numerical diffusion (due to lack of optimal discretization of the spatial domain) while using explicit solution techniques. The consideration of a fine grid (with large number of grid points) makes the calculation of the integral terms highly expensive. The discretization scheme has to be thus chosen wisely, such that the Courant-Friedrich-Levy (CFL) criterion is fulfilled.

Many approaches have surfaced over the past few decades that illustrate the obtainment of the solution for this class of equations. The solution of a population balance equation can be obtained using various methods such as direct discretization, Monte Carlo and the method of moments. Direct discretization methods are a more deterministic approach, where the internal coordinate affecting the process is discretized over the entire domain using techniques such as finite difference method, finite volume method or finite element method (Marchal et al., 1988; Kumar and Ramkrishna, 1996a; Immanuel and Doyle III, 2003). Direct discretization is a more straightforward approach for obtaining an accurate estimate of the particle size distribution, but a disadvantage associated with such methods is the inaccuracy with tracking the moments. Monte Carlo methods are more stochastic in nature and can be used to obtain the solution of multi-component or poly-disperse population balance equations provided the probability of dynamic behavior in the system obeys the balance principle for system details, the time step for each successful event can be calculated accurately and all the events occurring in the system are mutually dependant (Fichthom and Weinberg, 1991; Marshall Jr. et al., 2011, 2013). Monte-Carlo methods can be broadly classified into time-driven and event-driven algorithms. Time driven algorithms were proposed by Liffman (1992) whereas approaches using the theory of Markov chains was proposed by Garcia et al. (1987). Event-driven approaches were proposed by Smith and Matsoukas (1998); Lin et al. (2002) which aimed at overcoming the shortcomings of the previous methods. A very crucial drawback of using the Monte Carlo methods is the presence of noise in the data and also the difficulty to couple it with other approaches such as CFD for multi-scale granulation modeling. The method of moments is yet another approach used for solving population balance equations since the initial days. Depending on the

value of k in Equation (3.1), the moments can be expressed as

$$m_k(t) = \int_0^\infty \xi^k f(\xi, t) d\xi \qquad (3.1)$$

Here, k=0 represents the number of particles, k=1 represents the total length of particles, k=2 leads to obtaining the total area and k=3 indicates the total volume of particles. Various approaches involving the method of moments were developed by Hulburt and Katz (1964); Marchisio et al. (2006); Lee (1983). Quadrature method of moments (QMOM) and discrete quadrature method of moments (DQMOM) are some of the more recent and commonly used methods for solving population balance equations. There have been many improvisions on these approaches in order to alleviate the previous existing problems. A lot of significant developments have been made by Wright et al. (2001); Marchisio et al. (2003b,a); Attarakih et al. (2006); Su et al. (2007, 2008, 2009) with regard to implementing the method of moments.

This work will focus on the solution of the PBM utilizing direct discretization methods. Batterham et al. (1981) had initially derived a numerical technique to address the aggregation of particles which was further extended to breakage by Vanni (2000). These techniques were associated with the inability to conserve the total number of particles. Hence Hounslow et al. (1988) developed a novel discretization technique for a geometric grid, which could conserve particles, but it was lacking in conserving the other moments and showed reduced accuracy when the grid was made coarser. This drawback was later overcome by the improved approach suggested by Litster et al. (1995) which could accommodate adjustable geometric discretizations involving a progression factor of $2^{\frac{1}{q}}$. The problem still persisted as Wynn (2004) showed that the method was only applicable to formulations where $q < 4$. Recently further advancements have been made with regard to the approach proposed by Hounslow et al. by Peglow et al. (2006). Qamar and Warnecke (2007) had proposed a second accurate finite volume discretization technique for one and two-component aggregation processes, using a semi-discrete upwind scheme for a geometric grid. A wavelet based approach was also proposed by Liu and

Cameron (2001, 2003) which was appropriate for multiple peak distributions. A significant development made by Kumar and Ramkrishna (1996b,a) led to the proposal of the fixed-pivot discretization technique (FPDM) and moving pivot discretization technique which could be used to allocate particles to the neighboring grids when the daughter particle did not exactly fall on the pivot in a non-linear grid. Chakraborty and Kumar (2007) extended this approach for higher dimensional formulations and also investigated the usage of triangular grids. This technique by Kumar and Ramkrishna (1996b) was quite efficient but was accompanied by over-prediction of particle property distribution. The shortcomings from this technique was alleviated to a great extent by the cell-average technique proposed by Kumar (2006); Kumar et al. (2008, 2011).

In our previous works, the PBM solution has also been tackled using parallel computing tools with the help of the Parallel Computing toolbox (PCT), JACKET (Prakash et al., 2013b) and the MATLAB distributed computing toolbox (Prakash et al., 2013a). Reduced order models have also been obtained by lumping the various internal coordinate dependencies (Barrasso and Ramachandran, 2012). This significantly speeds the computations, however the accuracy in the results is compromised.

Separation of variables are associated with low parameter representations of the high dimensional systems as

$$f(x_1, x_2, .., x_d) \approx \sum_{\alpha=1}^{r} f_\alpha^{(1)}(x_1) f_\alpha^{(2)}(x_2) .. f_\alpha^{(d)}(x_d) \tag{3.2}$$

Singular value decompositions can be implemented on such systems which can aid at obtaining faster computations of the system (Oseledets and Tyrtyshnikov, 2009). This representation can also be extended for the d-dimensional tensors using the canonical decomposition (Oseledets, 2011). Significant developments have been made by several groups aiming at using this approach of tensor representations and separation of variables for faster computations and reduced memory requirements of high dimensional systems. The application of such techniques have been found in areas which require immense data handling and have been compiled in the review by Kolda and Bader

(2009). Implementing the tensor decomposition approach for solving PBMs is however novel and has never been exploited before. The discretized PBMs lead to sparse systems. Bader and Kolda (2007) has presented, in his work, the fast computations for such sparse systems. This considers a combination of singular value decomposition (SVD) for multi-dimensional systems, lower rank, cross approximations and tensor representations for obtaining an overall ROM.

The inability of a complex model to solve due to the presence of high dimensions or larger number of grids in the discretized domain can be termed as *curse of dimensionality*. Such complex models not only take large computational times but can also be not be solved due to memory limitations. Sometimes, even though the ROM enables the calculation of some large sized problems, the computational times required are higher than the original model. Although this helps with being able to obtain the solution for some large sized problems, it is more desirable to have a ROM that also has savings in terms of the computational overheads. In this study, the particle population is first discretised into sub-populations and the population balance is formulated for each of these semi-lumped sub-populations. This is obtained by the integration of the population balance equation (see Equation 2.1) over the domain of the sub-populations and re-casting the population into finite volumes. In this finite volume scheme, Equation 2.1 may be re-written in a discrete form as shown in Equation 3.3.

$$
\begin{aligned}
\frac{dF'_{i,j,k}}{dt} &+ \frac{F'_{i,j,k}}{\triangle s_i}\frac{ds}{dt}\bigg|_{s_i} - \frac{F'_{i,j,k+1}}{\triangle s_{i+1}}\frac{ds}{dt}\bigg|_{s_{i+1}} + \frac{F'_{i,j,k}}{\triangle l_j}\frac{dl}{dt}\bigg|_{l_j} - \frac{F'_{i,j,j+1}}{\triangle l_{j+1}}\frac{dl}{dt}\bigg|_{l_{j+1}} \\
&+ \frac{F'_{i,j,k}}{\triangle g_k}\frac{dg}{dt}\bigg|_{g_k} - \frac{F'_{i,j,k+1}}{\triangle g_{k+1}}\frac{dg}{dt}\bigg|_{g_{k+1}} = \Re_{agg}(s_i, l_j, g_k) + \Re_{break}(s_i, l_j, g_k) \qquad (3.3)
\end{aligned}
$$

Here $F'_{i,j,k} = \int_{s_i}^{s_{i+1}} \int_{l_j}^{l_{j+1}} \int_{g_k}^{g_{k+1}} F(s, l, g)\, ds\, dl\, dg$. s_i, l_j and g_k are the values of the solid, liquid and gas volume at the upper end of the ith, j^{th} and k^{th} bins along the solid, liquid and gas volume axes respectively. $\triangle s_i$, $\triangle l_j$ and $\triangle g_k$ are. the sizes of the ith, j^{th} and k^{th} bins. The particle population is assumed to be uniform within each of the finite volumes. Thus, by this technique, the integro partial-differential equation

as represented by the population balance equation, is reduced to a system of ordinary differential equations in terms of the rates of aggregation ($\Re_{agg}(s_i, l_j, g_k)$) and breakage ($\Re_{break}(s_i, l_j, g_k)$).

The numerical solution to such a class of equations is however very time consuming and computationally complex. The solution technique for these equations therefore require improvision which can enable quick and accurate solutions. Obtaining reduced order models (ROMs) can help at alleviating the issues faced with large computational time and *out of memory* limitations. In order to break the *curse of dimensionality*, we have implemented the tensor decomposition technique to the PBM which can significantly reduce the memory requirements and speed the computations.

3.2   Reduced order model using tensor decomposition

The overall model reduction technique can be subdivided into two broad subprocesses. One of the aspects deal with the computation of the aggregation and breakage terms using convolution, while the other subprocess involves approximation of the 6-D aggregation kernel β which would aid in speeding up the overall computation.

3.2.1   Discretization of the problem

To compute the integrals (Equations (2.3, 2.4)), an appropriate discretization of the problem is required. Firstly, the integral is replaced by a summation using a suitable quadrature, followed by employing a fast summation technique in order to reduce the complexity. For the discretization, the product rectangular rule has been implemented. Uniform grids with n points have been introduced in the variables s, l, g, yielding in total n^3 quadrature points. The functions β and F have been replaced by their discrete counterparts β_h and F_h. β_h is a 6-dimensional array, and F_h is a 3-dimensional array. While describing our calculations, the indices for s, l and g have been represented as i, j and k.

The resulting summation has the form

$$\Re_{agg}^{form}(i,j,k)_h = \sum_{i_1=1}^{i-1} \sum_{j_1=1}^{j-1} \sum_{k_1=1}^{k-1} \beta_h(i_1,j_1,k_1,i-i_1,j-j_1,k-k_1)F_h(i_1,j_1,k_1)F_h(i-i_1,j-j_1,k-k_1)$$

$$(3.4)$$

$$\Re_{agg}^{dep}(i,j,k)_h = F_h(i,j,k) \sum_{i_1=1}^{i-1} \sum_{j_1=1}^{j-1} \sum_{k_1=1}^{k-1} \beta_h(i_1,j_1,k_1,i-i_1,j-j_1,k-k_1)F_h(i_1,j_1,k_1)$$

$$(3.5)$$

The computation of these terms is the most expensive part. The computation of the sum (Equation (3.4)) is considered first and the sum Equation ((3.5)) is treated analogously. The direct computation of Equation (3.4) has the complexity $\mathcal{O}(n^6)$, which is not acceptable even for very small n. In what follows, the procedure to obtain a reduction in this complexity to $\mathcal{O}(n^3 \log n)$ using the separation of variables, is shown.

3.2.2 Approximation of β

The main idea involves approximating β in the form

$$\beta(i_1,j_1,k_1,i-i_1,j-j_1,k-k_1) \approx \sum_{\alpha=1}^{r} \Phi_\alpha(i_1,j_1,k_1)\Phi_\alpha(i-i_1,j-j_1,k-k_1) \quad (3.6)$$

where r is the "so-called" separation rank. The aggregation kernel, β_h can be written as

$$c_h(i,j,k) = 100 \frac{x_2(j)}{x_1(i) + x_2(j) + x_3(k)}, \quad (3.7)$$

$$V_h(i,j,k) = x_1(i) + x_2(j) + x_3(k), \quad (3.8)$$

$$\beta_h(i,j,k,i_1,j_1,k_1) = \beta_0 \Big(V(i,j,k) + V(i_1,j_1,k_1)\Big)\Big(c(i,j,k) + c(i_1,j_1,k_1)\Big)^{\alpha^2} \quad (3.9)$$
$$\times \Big(100 - \Big(\frac{c(i,j,k) + c(i_1,j_1,k_1)}{2}\Big)\Big)^{\delta\alpha}.$$

To get the separation of (i,j,k) from (i_1,j_1,k_1), β can be reshaped into a $n^3 \times n^3$ matrix and its singular value decomposition (SVD) can thereby be computed. However, it is not the optimal path given the associated computational expense ($\mathcal{O}(n^9)$ operations).

β_h is represented as a product of three terms. The first term has a rank of 2, while the second and third terms have the form

$$A(S, S_1) = (d(S) + e(S_1))^\gamma, \tag{3.10}$$

where S is the multi-index (i, j, k), S_1 is the multi-index (i_1, j_1, k_1), and d, e are some vectors of length n^3. For matrices of the form given by Equation (3.10), it can be proven that there always exists a low-rank approximation (de Silva and Lim, 2008; Chen and Saad, 2009). The rank of the product is bounded by the product of the ranks of each terms; therefore, it is not difficult to prove the existence of the low-rank approximation for β with the rank, independent of n. To compute this low-rank approximation we used the cross approximation method from previous works Oseledets and Tyrtyshnikov (2010); Goreinov (2008). The computational complexity of this method is $\mathcal{O}(n^3 r)$ operations. The typical rank of β was about 10.

3.2.3   Computation of the aggregation terms via convolution

As mentioned earlier, the discretized form for Equation (2.3) can be represented by Equation (3.4). Substituting the low-rank approximation of β into Equation (3.4), the following could be written

$$\begin{aligned}
\Re_{agg}^{form}(i,j,k)_h &= \sum_{i_1=1}^{i-1}\sum_{j_1=1}^{j-1}\sum_{k_1=1}^{k-1} \beta_h(i_1,j_1,k_1,i-i_1,j-j_1,k-k_1)F_h(i_1,j_1,k_1)F_h(i-i_1,j-j_1,k-k_1) \\
&= \sum_{\alpha=1}^{r}\Big(\sum_{i_1=1}^{i-1}\sum_{j_1=1}^{j-1}\sum_{k_1=1}^{k-1}\Phi_\alpha(i_1,j_1,k_1)\Phi_\alpha(i-i_1,j-j_1,k-k_1) \\
&\quad \times F(i_1,j_1,k_1)F(i-i_1,j-j_1,k-k_1)\Big) \\
&= \sum_{\alpha=1}^{r}\phi_\alpha(i,j,k)
\end{aligned}$$

where,

$$\phi_\alpha(i,j,k) = \sum_{i_1=1}^{i-1}\sum_{j_1=1}^{j-1}\sum_{k_1=1}^{k-1}\Phi_\alpha(i_1,j_1,k_1)\Phi_\alpha(i-i_1,j-j_1,k-k_1)F(i_1,j_1,k_1)F(i-i_1,j-j_1,k-k_1).$$

$$\tag{3.11}$$

A new variable, $\widehat{F}_\alpha$ is now introduced as:

$$\widehat{F}_\alpha(i,j,k) = \Phi_\alpha(i,j,k)F(i,j,k). \tag{3.12}$$

The equation for ϕ_α can be thus written as

$$\phi_\alpha(i,j,k) = \sum_{i_1=1}^{i-1}\sum_{j_1=1}^{j-1}\sum_{k_1=1}^{k-1} \widehat{F}_\alpha(i_1,j_1,k_1)\widehat{F}_\alpha(i-i_1,j-j_1,k-k_1). \tag{3.13}$$

The computation of ϕ_α is just the convolution: it can be evaluated in $\mathcal{O}(n^3\log n)$ operations using the Fast Fourier Transform (FFT).

Applying a similar idea to $\Re_{agg}^{dep}$ we get

$$
\begin{aligned}
\Re_{agg}^{dep}(i,j,k)_h &= F_h(i,j,k)\sum_{i_1=1}^{n_1-i}\sum_{j_1=1}^{n_2-j}\sum_{k_1=1}^{n_3-k} \beta_h(i_1,j_1,k_1,i,j,k)F_h(i_1,j_1,k_1)\\
&= F_h(i,j,k)\sum_{\alpha=1}^{r}\left(\sum_{i_1=1}^{n_1-i}\sum_{j_1=1}^{n_2-j}\sum_{k_1=1}^{n_3-k} \Phi_\alpha(i_1,j_1,k_1)\Phi_\alpha(i,j,k)F_h(i_1,j_1,k_1)\right)\\
&= F_h(i,j,k)\sum_{\alpha=1}^{r}\psi_\alpha(i,j,k).
\end{aligned}
\tag{3.14}
$$

where

$$\psi_\alpha(i,j,k) = \sum_{i_1=1}^{n_1-i}\sum_{j_1=1}^{n_2-j}\sum_{k_1=1}^{n_3-k} \Phi_\alpha(i_1,j_1,k_1)\Phi_\alpha(i,j,k)F_h(i_1,j_1,k_1). \tag{3.15}$$

We introduce

$$\widehat{F}_\alpha(i_1,j_1,k_1) = F_h(i_1,j_1,k_1)\Phi_\alpha(i_1,j_1,k_1), \tag{3.16}$$

therefore

$$\psi_\alpha(i,j,k) = \sum_{i_1=1}^{n_1-i}\sum_{j_1=1}^{n_2-i}\sum_{k_1=1}^{n_3-i} \Phi_\alpha(i,j,k)\widehat{F}_\alpha(i_1,j_1,k_1), \tag{3.17}$$

which can be computed in $\mathcal{O}(n^3\log n)$ operations using the FFT.

It is reduced to

$$V(i,j,k) = \sum_{i_1=1}^{n_1-i}\sum_{j_1=1}^{n_2-j}\sum_{k_1=1}^{n_3-k} V_1(i_1,j_1,k_1) \tag{3.18}$$

where $V_1(i_1, j_1, k_1) = \Phi_\alpha(i, j, k)\widehat{F}_\alpha(i_1, j_1, k_1)$

$$V(i, j, k) = \sum_{i_1=1}^{n_1} \sum_{j_1=1}^{n_2} \sum_{k_1=1}^{n_3} V_1(i_1, j_1, k_1)|_{[i_1<=n_1-i][j_1<=n_2-j][k_1<=n_3-k]} \qquad (3.19)$$

$$= \sum_{i_1=1}^{n_1} \sum_{j_1=1}^{n_2} \sum_{k_1=1}^{n_3} \widehat{c}(i_1, i)\widehat{c}(j_1, j)\widehat{c}(k_1, k)V_1(i_1, j_1, k_1)$$

,

$$V(i, j, k) - V(i+1, j, k) = \sum_{j_1=1}^{n_2-j} \sum_{k_1=1}^{n_3-k} V_1(n_1 - i, j_1, k_1)$$

The total complexity of the evaluation of the sum is then $\mathcal{O}(n^3 \log nr)$, and the constant in $\mathcal{O}(\cdot)$ is not too high, around 5. The question thus posed is the extent of the rank r (how high it is), and how can we compute the decomposition of β.

3.2.4   Approximation of the breakage term

Similar to the aggregation terms, the breakage of particles can also be expressed as a function of the formation and depletion terms. The breakage term does not have multiple integrals, however, due to the existence of the 6-D breakage distribution, multiple loops (6 nested loops) are required for the calculations which adds to the computational overheads. For our simulations, a simple model for addressing the breakage distribution has been considered, such that as a particle breaks, all the grids where the fragments could fall into have an equal probability of receiving the fragmented daughter particle. For breakage, the formation of particles happen in the smaller bin, (s, l, g), while the bigger particle is represented by (s', l', g'). For our convenience, we would express the smaller particle (s, l, g) as (i, j, k) and the bigger particle as (i_1, j_1, k_1). In the original/unreduced problem, the breakage distribution function could be written as

$$b(i, j, k, i_1, j_1, k_1) = 1/N_{i,j,k,i_1,j_1,k_1} \qquad (3.20)$$

where N_{i,j,k,i_1,j_1,k_1} represents the number of instances in which a bigger particle represented by the grid (i_1, j_1, k_1) could break into a smaller bin, (i, j, k). This

function could be separated as a product of three variables of lower dimensions and could be expressed as

$$b(i, j, k, i_1, j_1, k_1) = c(i, i_1)c(j, j_1)c(k, k_1) \tag{3.21}$$

such that

$$c(i, i_1) = \begin{cases} 0 & \text{if } i >= i_1, \\ d(i) & \text{if } i < i_1 \end{cases} \tag{3.22}$$

where

$$d(i) = \frac{1}{i-1}, i = 2, \ldots, n \tag{3.23}$$

This could also be extended for the other dimensions $(j, \ k)$. After employing the separation of variables for the breakage distribution term, the formation term has been rewritten as

$$\Re_h^{break}(i_1, j_1, k_1) = \sum_{i,j,k} F_h(i, j, k)K_{break}(i, j, k)c(i, i_1)c(j, j_1)c(k, k_1) \tag{3.24}$$

We introduce a new variable $\widetilde{F}_h(i_1, j_1, k_1)$ as

$$\widetilde{F}_h(i, j, k) = F_h(i, j, k)K_{break}(i, j, k) \tag{3.25}$$

Substituting Eq. (3.25) into Eq. (3.26), we obtain

$$\Re_h^{break}(i_1, j_1, k_1) = \sum_{i,j,k} \widetilde{F}_h(i, j, k)c(i, i_1)c(j, j_1)c(k, k_1) \tag{3.26}$$

This simplifies the calculation and the breakage term can be evaluated in $\mathcal{O}(n^4)$ operations. The following steps show the method by which the sum is evaluated.

1. Summing over i, $F_h'(i_1, j, k) = \sum_i \widetilde{F}_h(i, j, k)c(i, i_1)$,

2. Summing over j, $F_h''(i_1, j_1, k) = \sum_j F_h'(i_1, j, k)c(j, j_1)$,

3. Summing over k, $F_h'''(i_1, j_1, k_1) = \sum_k F_h''(i_1, j_1, k)c(k, k_1)$,

This way a reduced order model has been obtained based on the principles of separation of variables, tensor representations, low rank approximation and fast fourier transforms. These techniques are individually applied or a combination of these methods are utilized to obtain the computationally fast, reduced memory requiring ROM.

Besides using a ROM for easing the calculation procedure, using a nonlinear grid for the discretization can also significantly aid at speeding the computation of the PBM. Using a nonlinear grid can span the entire particle size domain by using fewer grids in the discretized domain. This can significantly reduce the time required for the solution as the computational complexity increases polynomially with increasing grid size. Since we are considering a non linear grid to formulate the population balance equation, the new-born particle from aggregation might not exactly lie on the grid, therefore the need to use this technique comes into play. Similarly, for breakage, a larger particle fragments into two smaller particles. Of the two daughter particles, one is considered to lie on the grid point whereas the other is considered to lie anywhere which may or may not be coinciding with the representative point. Therefore, this particle needs to be reallocated, in certain fractions, to the neighboring grids.

3.3 Discretization of PBM using a nonlinear grid
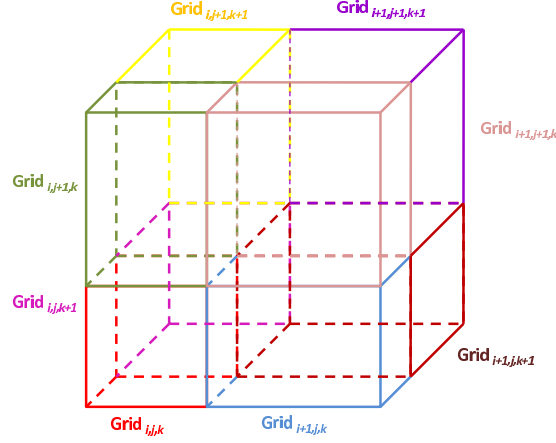
Figure 3.1: Three-dimensional non-linear grid showing bins of varying sizes in each dimension

The approach similar to that of Kumar (2006) has been utilized, where primarily the third moment, total volume/mass of particles is conserved. We have denoted each representative point of the grid as s_i, l_j, g_k and the upper and lower bounds for each grid with $s_{b,i}$ and $s_{b,i+1}$, $l_{b,j}$ and $l_{b,j+1}$, $g_{b,k}$ ans $g_{b,k+1}$. The representative point of each grid is the mid point between the upper and lower bounds. For n grid points with respect to each individual volume, there are n^3 ODE's representing the number of particles in each bin (i,j,k). The discrete number density N_{ijk} in a single cell, can be described as follows:

$$N_{ijk} = \int_{s_{b,i}}^{s_{b,i+1}} \int_{l_{b,j}}^{l_{b,j+1}} \int_{g_{b,k}}^{g_{b,k+1}} F(s,l,g,t)dsdldg \qquad (3.27)$$

Substituting $F(s,l,g,t)$ into the aggregation and breakage PBM, the following equation is obtained after differentiating with respect to time:

$$\frac{dN_{ijk}}{dt} = \frac{1}{2} \int_{s_{b,i}}^{s_{b,i+1}} \int_{l_{b,j}}^{l_{b,j+1}} \int_{g_{b,k}}^{g_{b,k+1}} \int_0^{s_{max}} \int_0^{l_{max}} \int_0^{g_{max}} \beta(s',l',g',s-s',l-l',g-g')F(s',l',g',t)$$

$$F(s-s',l-l',g-g',t)ds'dl'dg'dsdldg + \int_{s_{b,i}}^{s_{b,i+1}} \int_{l_{b,j}}^{l_{b,j+1}} \int_{g_{b,k}}^{g_{b,k+1}} \int_s^{s_{max}} \int_l^{l_{max}} \int_g^{g_{max}} K_{break}(s',l',g')$$

$$b(s',l',g',s-s',l-l',g-g')F(s',l',g',t)ds'dl'dg'dsdldg -$$

$$F(s,l,g,t) \int_{s_{b,i}}^{s_{b,i+1}} \int_{l_{b,j}}^{l_{b,j+1}} \int_{g_{b,k}}^{g_{b,k+1}} \int_0^{s_{max}} \int_0^{l_{max}} \int_0^{g_{max}} \beta(s',l',g',s,l,g)F(s,l,g,t)ds'dl'dg'dsdldg -$$

$$\int_{s_{b,i}}^{s_{b,i+1}} \int_{l_{b,j}}^{l_{b,j+1}} \int_{g_{b,k}}^{g_{b,k+1}} K_{break}(s,l,g)b(s',l',g',s-s',l-l',g-g')F(s,l,g,t)dsdldg \qquad (3.28)$$

Essentially, this equation shows that the change in number density per time is equal to:

$$N_{ijk} = B_{ijk} - D_{ijk} \qquad (3.29)$$

where B_{ijk} is particle birth and D_{ijk} is particle death. Furthermore, a discretized expression for $F(s,l,g,t)$ can be written in terms of the dirac delta function, assuming all the particles in a single cell are concentrated at the representative node as

$$F(s,l,g,t) = \sum_{i=1}^{I_s} \sum_{j=1}^{I_l} \sum_{k=1}^{I_g} N_{ijk}\delta(s-s_i)\delta(l-l_j)\delta(g-g_k) \qquad (3.30)$$

Here, I_s, I_l, and I_g represent the total number of cells in the s, l and g directions, respectively. For aggregation, this technique can be employed to reassign only the one new-born particle formed from the coalescence of two particles. In case of breakage, two daughter particles are formed, out of which, we have assumed one particle to lie exactly on the representative point, hence allocating it is straightforward. The other new-born particle from breakage, was then reassigned to the adjoining bins using this technique of local averaging followed by fractionation. The birth and death terms can be rewritten in discrete form, using the dirac delta function to discretize the aggregation birth term, as follows:

$$B_{ijk} = \sum_{a,b=1}^{i} \sum_{c,d=1}^{j} \sum_{e,f=1}^{k} \left[(1 - 0.5\delta_{a,b}\delta_{c,d}\delta_{e,f})\beta_{abcdef}N_{ace}N_{bdf} \right]|_{(s_a+s_b)\in s_i, \ (l_c+l_d)\in l_j, \ (g_e+g_f)\in g_k}$$

$$+ \sum_{i'=i}^{I_s} \sum_{j'=j}^{I_l} \sum_{k'=k}^{I_g} N_{i'j'k'} K_{break-i',j',k'} \int_{s_{b,i}}^{p_l'^i} \int_{l_{b,j}}^{p_m'^j} \int_{g_{b,k}}^{p_n'^k} b(s, s_{l'}, l, l_{m'}, g, g_{n'}) ds dl dg$$

$$(3.31)$$

and

$$D_{ijk} = \sum_{p=1}^{I_s} \sum_{q=1}^{I_l} \sum_{r=1}^{I_g} \beta_{ipjqkr} N_{ijk} N_{pqr} + K_{break-i,j,k} N_{ijk} \tag{3.32}$$

The limits $p_{l'}^i$ is defined as

$$p_l^i = \begin{cases} s_i & \text{if } l = i, \\ \\ s_{b,i+1} & \text{otherwise} \end{cases} \tag{3.33}$$

$$p_m^j = \begin{cases} l_j & \text{if } m = j, \\ \\ l_{b,j+1} & \text{otherwise} \end{cases} \tag{3.34}$$

$$p_n^k = \begin{cases} g_k & \text{if } n = k, \\ \\ g_{b,k+1} & \text{otherwise} \end{cases} \tag{3.35}$$

AB is the set of agglomerates for which $s_{b,i} < (s_a + s_b) < s_{b,i+1}$. CD is the set of agglomerates for which $l_{b,j} < (l_c + l_d) < l_{b,j+1}$. EF is the set of agglomerates for which $g_{b,k} < (g_e + g_f) < g_{b,k+1}$. $b(s, s_l, l, l_m, g, g_n)$ is the breakage distribution function (Pinto et al., 2007). The flux of the properties s,l and g ($V_{s,i,j,k}$, $V_{l,i,j,k}$ and $V_{g,i,j,k}$) into each representative cell has been shown in the published paper (Chaudhury et al., 2013a). From this information, the average value of each property in cell C_{ijk} can be calculated, as follows:

$$V_{s,i,j,k} = \sum_{a,b=1}^{i} \sum_{c,d=1}^{j} \sum_{e,f=1}^{k} (1 - 0.5\delta_{a,b}\delta_{c,d}\delta_{e,f})\beta_{abcdef}N_{ace}N_{bdf}(s_a + s_b)|_{(s_a+s_b)\in AB,(l_c+l_d)\in CD,(g_e+g_f)\in EF}$$

$$+ \sum\sum\sum N_{i,j,k}K_{break-i,j,k} \int_{s_{b,i}}^{p_l^i} \int_{l_{b,j}}^{p_m^j} \int_{g_{b,k}}^{p_n^k} (s_{a1} - s_{b1})b(s, s_l, l, l_m, g, g_n)dsdldg$$

$$(3.36)$$

$$V_{l,i,j,k} = \sum_{a,b=1}^{i} \sum_{c,d=1}^{j} \sum_{e,f=1}^{k} (1 - 0.5\delta_{a,b}\delta_{c,d}\delta_{e,f})\beta_{abcdef}N_{ace}N_{bdf}(l_c + l_d)|_{(s_a+s_b)\in AB,(l_c+l_d)\in CD,(g_e+g_f)\in EF}$$

$$+ \sum\sum\sum N_{i,j,k}K_{break-i,j,k} \int_{s_{b,i}}^{p_l^i} \int_{l_{b,j}}^{p_m^j} \int_{g_{b,k}}^{p_n^k} (l_{c1} - l_{d1})b(s, s_l, l, l_m, g, g_n)dsdldg$$

$$(3.37)$$

$$V_{g,i,j,k} = \sum_{a,b=1}^{i} \sum_{c,d=1}^{j} \sum_{e,f=1}^{k} (1 - 0.5\delta_{a,b}\delta_{c,d}\delta_{e,f})\beta_{abcdef}N_{ace}N_{bdf}(s_a + s_b)|_{(g_e+g_f)\in AB,(l_c+l_d)\in CD,(g_e+g_f)\in EF}$$

$$+ \sum\sum\sum N_{i,j,k}K_{break-i,j,k} \int_{s_{b,i}}^{p_l^i} \int_{l_{b,j}}^{p_m^j} \int_{g_{b,k}}^{p_n^k} (g_{e1} - g_{f1})b(s, s_l, l, l_m, g, g_n)dsdldg$$

$$(3.38)$$

Here, s_a, l_c, g_e and s_b, l_d, g_f are the two aggregating particles, whereas, s_{a1}, l_{c1}, g_{e1} is the bigger particle that breaks and s_{b1}, l_{d1}, g_{f1} is the daughter particle from breakage that falls exactly on the representative point of the grid.

$$\bar{s}_{i,j,k} = \frac{V_{s,i,j,k}}{B_{ijk}} \tag{3.39}$$

$$\bar{l}_{i,j,k} = \frac{V_{l,i,j,k}}{B_{ijk}} \tag{3.40}$$

$$\bar{g}_{i,j,k} = \frac{V_{g,i,j,k}}{B_{ijk}} \tag{3.41}$$

These average values, in each cell, represent the total birth due to aggregation and breakage. For sake of conciseness, $s_{i,j,k}$, $l_{i,j,k}$ and $g_{i,j,k}$ is expressed as s_i, l_j and g_k.

This is the birth which is distributed to the neighboring nodes when the birth does not fall exactly on a representative node (the usual case). The number of nodes to which birth is distributed depends on the number of moments being preserved and the number of dimensions present. In this study, we seek to preserve the two moments, particle number and mass (or volume, since particle density is constant). Hence, with a three-dimensional grid, distribution would occur to eight neighboring nodes. Let us suppose that the particle fractions $a_1, a_2, a_3, a_4, a_5, a_6, a_7$, and a_8 are distributed to the neighbouring nodes $P_{i,j,k}, P_{i+1,j,k}, P_{i+1,j+1,k}, P_{i,j+1,k}, P_{i,j,k+1}, P_{i+1,j,k+1}, P_{i+1,j+1,k+1}, and P_{i,j+1,k+1}$, respectively. Then, the particle fractions must satisfy the thirteen conservation equations (can be found in the paper (Chaudhury et al., 2013a)), to conserve the total volume as well as the particle number.

$$B_{ijk} = a_1 + a_2 + a_3 + a_4 + a_5 + a_6 + a_7 + a_8 \tag{3.42}$$

$$a_1 s_i + a_2 s_{i+1} = (a_1 + a_2)\bar{s}_i \tag{3.43}$$

$$a_3 s_{i+1} + a_4 s_i = (a_3 + a_4)\bar{s}_i \tag{3.44}$$

$$a_5 s_i + a_6 s_{i+1} = (a_5 + a_6)\bar{s}_i \tag{3.45}$$

$$a_7 s_{i+1} + a_8 s_i = (a_7 + a_8)\bar{s}_i \tag{3.46}$$

$$a_1 l_j + a_4 l_{j+1} = (a_1 + a_4)\bar{l}_j \tag{3.47}$$

$$a_2 l_j + a_3 l_{j+1} = (a_2 + a_3)\bar{l}_j \tag{3.48}$$

$$a_5 l_j + a_8 l_{j+1} = (a_5 + a_8)\bar{l}_j \tag{3.49}$$

$$a_6 l_j + a_7 l_{j+1} = (a_6 + a_7)\bar{l}_j \tag{3.50}$$

$$a_1 g_k + a_5 g_{k+1} = (a_1 + a_5)\bar{g}_k \tag{3.51}$$

$$a_2 g_k + a_6 g_{k+1} = (a_2 + a_6)\bar{g}_k \tag{3.52}$$

$$a_3 g_k + a_7 g_{k+1} = (a_3 + a_7)\bar{g}_k \tag{3.53}$$

$$a_4 g_k + a_8 g_{k+1} = (a_4 + a_8)\bar{g}_k \tag{3.54}$$

This system of equations has eight unknowns and thirteen equations and has a unique solution. Similarly, in Kumar (2006), a system of five equations with four unknowns had a unique solution. The fractions for the three-dimensional case are given in details in the paper (Chaudhury et al., 2013a).

$$a_1 = \frac{(s_{i+1} - \bar{s}_i)(l_{j+1} - \bar{l}_j)(g_{k+1} - \bar{g}_k)}{(s_{i+1} - s_i)(l_{j+1} - l_j)(g_{k+1} - g_k)} B_{ijk} \tag{3.55}$$

$$a_2 = \frac{(\bar{s}_i - s_i)(l_{j+1} - \bar{l}_j)(g_{k+1} - \bar{g}_k)}{(s_{i+1} - s_i)(l_{j+1} - l_j)(g_{k+1} - g_k)} B_{ijk} \tag{3.56}$$

$$a_3 = \frac{(\bar{s}_i - s_i)(\bar{l}_j - l_j)(g_{k+1} - \bar{g}_k)}{(s_{i+1} - s_i)(l_{j+1} - l_j)(g_{k+1} - g_k)} B_{ijk} \tag{3.57}$$

$$a_4 = \frac{(s_{i+1} - \bar{s}_i)(\bar{l}_j - l_j)(g_{k+1} - \bar{g}_k)}{(s_{i+1} - s_i)(l_{j+1} - l_j)(g_{k+1} - g_k)} B_{ijk} \tag{3.58}$$

$$a_5 = \frac{(s_{i+1} - \bar{s}_i)(l_{j+1} - \bar{l}_j)(\bar{g}_k - g_k)}{(s_{i+1} - s_i)(l_{j+1} - l_j)(g_{k+1} - g_k)} B_{ijk} \tag{3.59}$$

$$a_6 = \frac{(\bar{s}_i - s_i)(l_{j+1} - \bar{l}_j)(\bar{g}_k - g_k)}{(s_{i+1} - s_i)(l_{j+1} - l_j)(g_{k+1} - g_k)} B_{ijk} \tag{3.60}$$

$$a_7 = \frac{(\bar{s}_i - s_i)(\bar{l}_j - l_j)(\bar{g}_k - g_k)}{(s_{i+1} - s_i)(l_{j+1} - l_j)(g_{k+1} - g_k)} B_{ijk} \tag{3.61}$$

$$a_8 = \frac{(s_{i+1} - \bar{s}_i)(\bar{l}_j - l_j)(\bar{g}_k - g_k)}{(s_{i+1} - s_i)(l_{j+1} - l_j)(g_{k+1} - g_k)} B_{ijk} \tag{3.62}$$

This fractionation can cause many births to occur on a single representative point. These births need to be added together, as follows, to obtain the cell average birth. This cell average birth is used in lieu of the birth term in the PBM. No redistribution occurs to obtain a death term, as death is just the disappearance of particles from a representative point. From the method of mathematical induction, it can be noted that for an N-dimensional population balance equation, a particle would distribute into 2^N fractions into its adjacent grid points. The 2^N fractions corresponding to the 2^N neighboring grids can be obtained in a similar way as the 2^3 fractions for the 3-dimensional population balance was obtained.

3.4 Results and discussion

The ROM can improve the solution of the PBM by not only overcoming memory limitations but also speeding the calculations and providing an accurate representation of the original model. It can capture the shape of the various bulk and distributed properties as per the original model. However, the computational savings and accuracy of the reduced framework are showcased in the following paragraphs.

Reduced order models (ROMs) help in alleviating the issues faced due to the *curse of dimensionality*. Using the tensor decomposition approach for model reduction, there is not only the

scope of using larger number of grids but also there is a significant savings in the computational time. A comparison between the computational times between the original and reduced models have been reported in Table 3.1. It can be seen that the time required by the reduced framework is much less (as also shown in Table 3.1). It should also be noted that for larger number of grids in the discretized domain, the tensor decomposition approach is significantly beneficial.

Table 3.1: Computational time of the original and the reduced model for 500 seconds (simulation)

Number of grids	Original model (secs)	Reduced model (secs)
6	22.617	3.8
9	96.772	13
12	299	30
16	1274	58
19	2414	77
22	4756	130
26	9959	200

Table 3.2: Computational time (in seconds) for the individual terms within the original model for one time step calculation

| Grids | Original model | | | | Reduced model | | | |
| | β | Agg | Breakage | | β | Agg | Breakage | |
			form+dep	break dist			form+dep	break dist
6	0.67	$2.5e^{-2}$	$7e^{-5}$	0.0484	0.26	$2.1e^{-3}$	$5.2e^{-4}$	0.002548
9	6.4	$9e^{-2}$	$9.5e^{-5}$	0.3505	0.29	$7.7e^{-3}$	$1.5e^{-3}$	0.002393
12	36	0.25	$1e^{-4}$	1.944	0.31	$2.2e^{-2}$	$3.8e^{-3}$	0.002447
16	200	0.91	$1.6e^{-4}$	13.181	0.34	$3.3e^{-2}$	$1.5e^{-2}$	0.002496
19	570	1.9	$1.6e^{-4}$	36.023	0.34	$5.2e^{-2}$	$2e^{-2}$	0.002571
22	1300	3.5	$1.8e^{-4}$	96.462	0.35	$7.8e^{-2}$	$2.2e^{-2}$	0.002583
26	4200	9.3	$3e^{-4}$	278.2950	0.46	$1.1e^{-1}$	$5.8e^{-2}$	0.002573

Table 3.2 shows the time required for calculation of the individual aggregation and breakage terms for 1 time step. It can be seen that the computation of the aggregation kernel and the breakage distribution (calculated offline) can be significantly reduced

using the reduced framework. The time recorded during the calculation of the breakage distribution indicates almost no influence with respect to the increasing grid size. The variations in the computational times could be interpreted as an artifact of time reproducibility with MATLAB. The computation of the aggregation (formation+depletion) terms have a huge improvement using the reduced framework, considering the fact that these calculations repeat and occur dynamically over the time domain. The calculation of the breakage (formation+depletion) terms indicate lower computational time requirement for the original 3-D PBM. However, combining the calculation of the breakage distribution and the formation+depletion terms might add up to higher computational load for larger grid sizes. Thus, for larger grid sizes, the reduced framework will prove to be more efficient compared to the original multi-dimensional model even for the computation of breakage.

3.4.1   Error analysis

The ROM enables us to overcome the limitations faced with solving large sized problems. Not only does it allow the solution to the PBM with large number of grids, but also requires much less time for the calculations. The optimal scenario would require the ROM to also be as accurate as the original PBM. The partial differential equation (PDE) representing the PBM has been solved using the hierarchical two tier technique proposed by Immanuel et al (Immanuel and Doyle III, 2003) and utilized in our previous works (Chaudhury and Ramachandran, 2013). The various terms that have been approximated in the calculations are the 6-D aggregation kernel (β), the formation of particles due to aggregation $(\Re_{agg}^{form})$, the depletion/loss of particles due to aggregation $(\Re_{agg}^{dep})$ and the formation of particles due to breakage $(\Re_{break}^{form})$. The terms directly affect the number density of particles, $F(s, l, g, t)$ and hence influence the bulk and distributed properties of the granules.
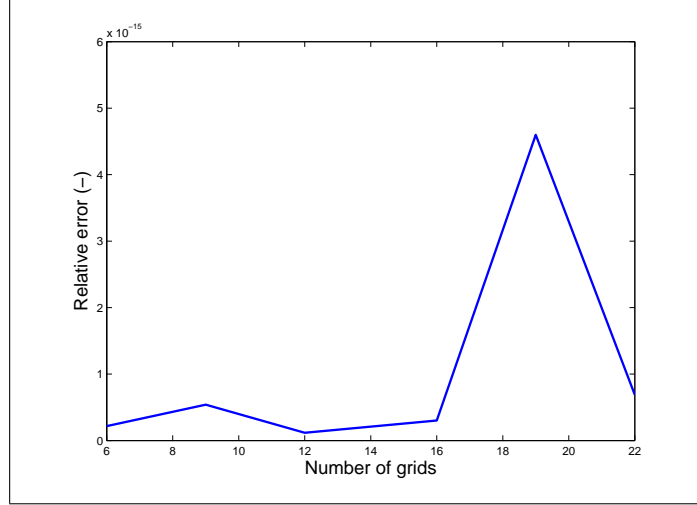
Figure 3.2: Relative error for the aggregation kernel obtained from lower rank approximation and the original model

The error between the original and the reduced model can be obtained using Equation (3.64). Although the simulation could be run in the reduced and the original form for 26 grids with respect to each individual internal coordinate, the results could not be saved for the original model (memory limitations) thus disabling us from comparing the errors.

The aggregation kernel, β is reduced using a lower order approximation. Thus, while comparing the reduced and the original β, it is required that the lower rank tensor approximation is converted to the full size 6-D array (using the *full* command in MAT-LAB that is available with the tensor transform toolbox) for the purpose of correct error calculation. The error in the β obtained from the lower rank approximation and the original model can be expressed as in Equation (3.63) and has been shown in Figure 3.2.

$$Relative\ error_\beta = \frac{||\ \beta_{original\ model}(:)\ || - ||\ full(\beta_{reduced\ model})(:)\ ||}{||\ \beta_{original\ model}(:)\ ||} \qquad (3.63)$$

$$Relative\ error_{variable} = \frac{\parallel Variable_{original\ model} \parallel - \parallel Variable_{reduced\ model} \parallel}{\parallel Variable_{original\ model} \parallel} \quad (3.64)$$
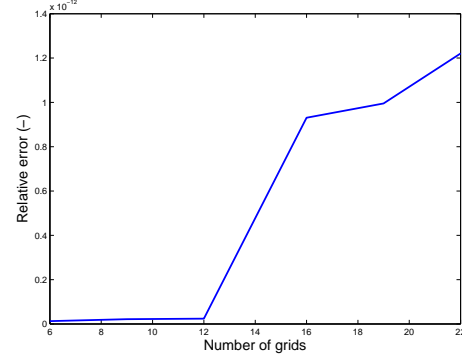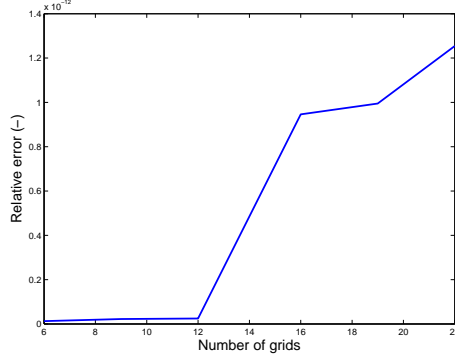
(a) Relative error of formation due to aggregation (b) Relative error of depletion due to aggregation
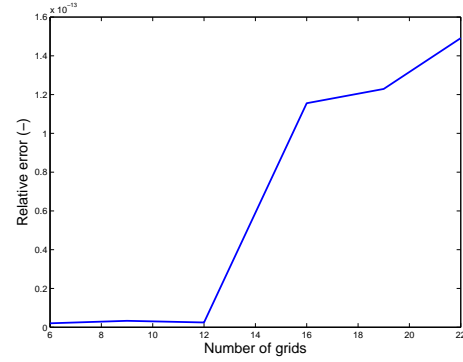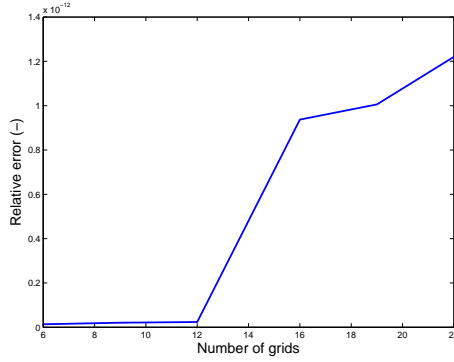
(c) Relative error of formation due to breakage (d) Relative error of the overall number density

Figure 3.3: Variation of relative errors for the various terms averaged over time with respect to number of grids

The relative error is calculated for the various terms involved in aggregation and breakage and the overall number density using Equation (3.64). Figures 3.4 a,b,c reveal that the error reduces over time, however for the overall number density, the error seems higher as time proceeds. This could be a by product of the varying signs for the individual terms. Even though the individual mechanisms have smaller error (absolute value) at a later stage, the error could get cancelled or added up thus revealing this

disparity. It should be noted that the error increases or decreases with the progression of time but the values are so small, that the ROM can be considered to be a very good approximation of the original model with minimal compromise in accuracy.
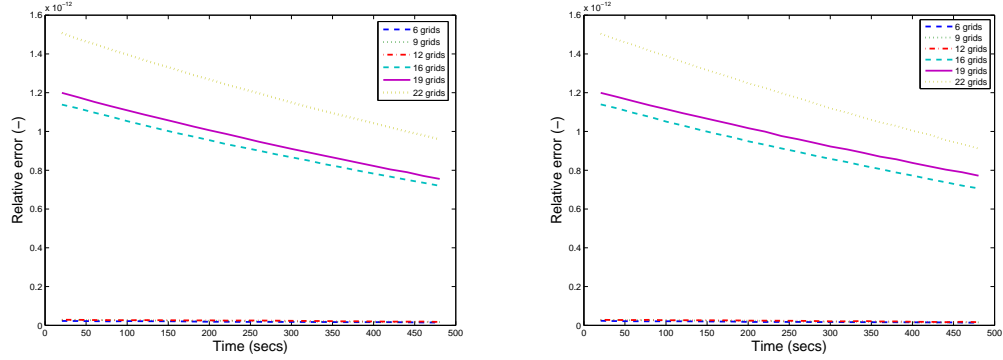
(a) Relative error of formation due to aggregation (b) Relative error of depletion due to aggregation
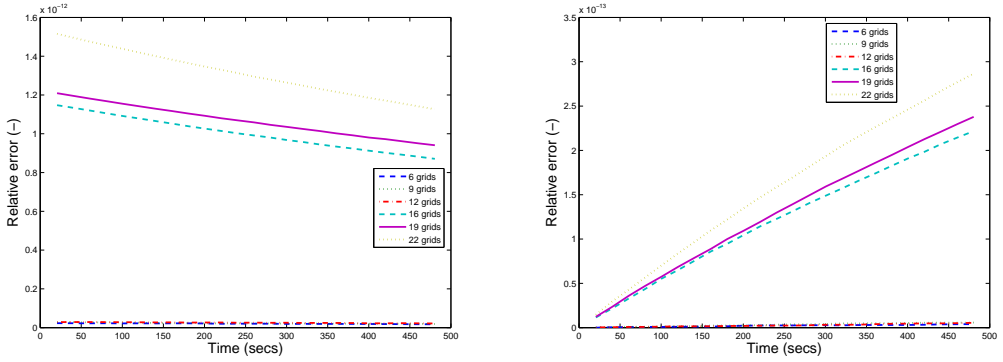
(c) Relative error of formation due to breakage   (d) Relative error of the overall number density

Figure 3.4: Variation of the evolution of relative errors over time for the various terms

Using larger number of finer grids (without violating the CFL conditions) for spanning the overall domain show more accurate results for the PBM. The discretization error which is a function of the discretization width (h) typically increases with increasing h. In this work, the bulk and distributed properties could not be analysed for the discretization error since varying the width of the discretized grid would result in changing the start and end span of the domain and the comparison would be erroneous due to the fact that the systems would be different. The original model without the reduction could not be run for greater than 29 grids with respect to each individual

internal coordinate. The model in the TT format could however accommodate 250 grids with respect to each internal coordinate.

It can clearly be seen that the ROM significantly alleviates the issues with the large computational time required for the solution of PBMs. As mentioned before, discretizing the grid using a nonlinear grid can also aid in fast computation of the PBM as it can span the entire particle property domain with fewer grids. The simulations were ran using the parameters mentioned in the paper (Chaudhury et al., 2013a).

Table 3.3: Parametric values for the simulations

Parameter name	Value
Simulation time	$900secs$
Number of grids in solid, liquid and gas volume	8
Width of ith Grid (same in each volume)	$10^{-13} \times 4^{(i-1)}m^3$
Initial distribution	1×10^{-12} in $(s, l, g) = (1, 1, 1)$
Binder Spray rate, u	$5 \times 10^{-3}m^3/sec$
c_{binder}	0.1
ϵ_{min}	0.2
Consolidation constant, c	1×10^{-9}
Aggregation Constant for the kernel, β_0	2×10^{19}
α for Madec's aggregation kernel	1
δ for Madec's aggregation kernel	1
P_1 for breakage	0.7
G_{shear} for Pandya's breakage kernel	6×10^{-7}
P_2 for Pandya's breakage kernel	1.3

The results from the extended cell average technique, reveal conservation in terms of particle number and total volume (Figure 2 and 3 in (Chaudhury et al., 2013a).
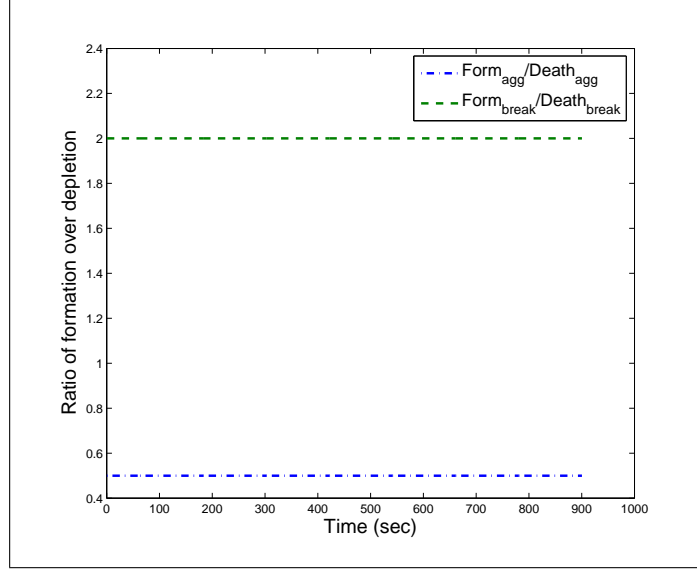
Figure 3.5: Ratio of the rate of birth by death for aggregation and breakage, where, Ratio $\equiv \frac{\Re_{birth}}{\Re_{death}}$

(a) No growth

(b) Liquid addition stops at t=500 seconds
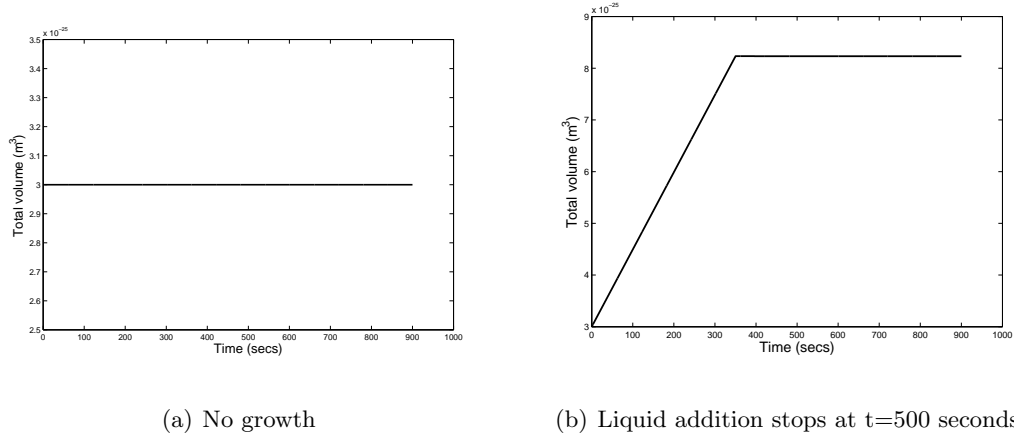
Figure 3.6: Conservation of total volume: (a) No growth term considered, hence volume held constant, (b)Source terms and liquid addition considered till time=500 secs, thereafter liquid addition stopped

The primary advantage of using the nonlinear grid for simulating granulation process is the reduced computational expense. The range for the discretization has been kept constant, but the discretization was performed using a linear and a nonlinear grid (which used the CAT for reassignment). Thus, the property can be tracked exactly using a nonlinear grid as a linear grid. The grid sizes and the initial distribution have

been kept same as mentioned in the parametric table in the paper (Chaudhury et al., 2013a).
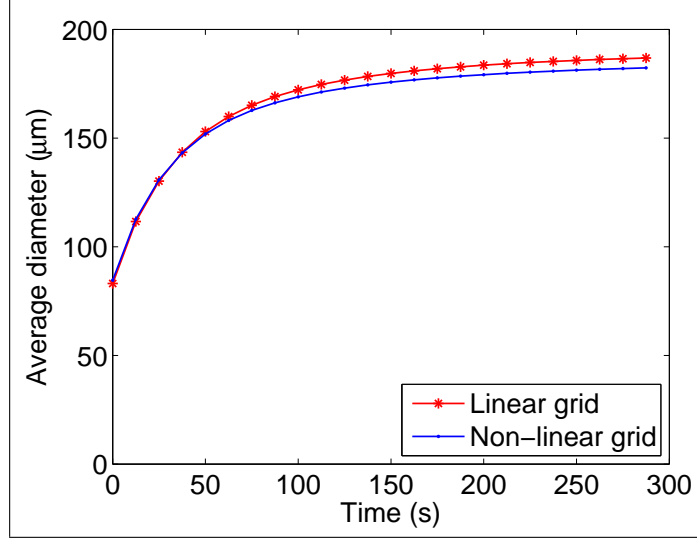
Figure 3.7: Comparison between the predicted average diameter of particles from a linear grid, and a nonlinear grid using the cell average technique

It was observed that the linear grid requires much more time as compared to the nonlinear grid in order to cover the same range (Chaudhury et al., 2013a). For covering a certain range of particle size, the linear grid required 15 number of grids in each individual volume coordinate whereas the non-linear grid spanned the same range using only 8 grids in each volume coordinate thus reducing the computational expense to a great extent. The simulations were carried out for 300 seconds (model time). Both simulations were run on the same computer and the time recorded for the simulation to finish running using the nonlinear grid was 45.0 seconds whereas the simulation using a linear grid took 551 seconds to run. Thus, we can see that a speed-up of around 12 times can be observed. Thus, an increase in grid size would result in a greater difference in computation time between the linear and nonlinear grids.

3.5 Chapter conclusions

Two approaches have been presented in order to speed up and ease the computations for obtaining a solution to the PBMs. The ROM developed using tensor decompositions and separation of variables enable us to overcome the obstacles faced due to memory limitations. The accuracy obtained from the ROM solution shows promising results. The nonlinear grid also enables the realization of wide size distributions (as seen in the industry) with minimal number of grids. The need to capture the process using accurate models is a crucial task, however the effective solution of the equation cannot be overlooked, either. There have been multiple solution techniques proposed by multiple research groups in the past, however there is a dearth of solution techniques that can accommodate the solution for high-dimensional PBMs. There is a continuing need for developing efficient numerical techniques that can preserve the accuracy while also requiring minimal computational overheads. PBMs are almost inevitably utilized for parameter estimation techniques, which requires multiple iterations of solving the model. In order to obtain results within reasonable time frames and also obtain a solution for varying parametric values, there is a need for stable reduced order modeling techniques which can not only solve the model quickly, but is also independent of the parametric values that are considered within the model.

The application of tensor decomposition for obtain an ROM is a very powerful tool, which if extended further, can mitigate a lot of issues associated with computational limitations. The tensor-decomposition enables the minimization of discretization error (by accommodating large number of grids) while also preserving the accuracy of the solution. The non-linear discretization approach can significantly reduce the computation overheads by reducing the need for large number of grids in order to span a size domain. The solution framework can be and has been further sped up by introducing the concepts of parallel computing. Parallel computing can prove to be a very powerful tool when running the simulations on a multi-core computer.

Chapter 4

Specific Aim III: Mechanistic modeling of granulation process

The details of the discussions provided in this section can be obtained in the publication:

- Chaudhury, A., Wu, H., Khan, M., Ramachandran, R., 2014, A mechanistic population balance model for granulation processes: Effect of process and formulation parameters, Chemical Engineering Science, 107, 76-92

In the previous sections, a detailed discussion has been provided on the current state of developments that have emerged in the broad field of modeling granulation processes and its numerical solution. It is important to model and solve granulation processes with more predictive approaches, however the employment of non-empirical kernels/rates to describe the various mechanisms is yet another crucial task for obtaining predictive models that can be furthered for control and optimization. It is very common to implement size dependant, empirical aggregation kernels for the description of the aggregation process. A review has been provided by Cameron et al. (2005) on the various aggregation and breakage kernels while describing granulation. Initially, constant kernels were used for describing aggregation, which was then replaced by more size dependant kernels. The EKE (equipartition of kinetic energy) kernel based on the kinetic theory of granular flow was proposed by Hounslow (1998). Later, Madec et al. (2003) proposed an empirical aggregation kernel which also takes into account the liquid fraction (volume based) in the agglomerating particles. This kernel, although empirical in nature, takes into account the presence/amount of liquid in the particles. Eventually a mechanistic kernel was proposed by Immanuel and Doyle III (2005) which was based on the physics of the problem. The aggregation kernel is represented as a Fuch stability ratio, W for the two types of coalescence mechanisms outlined by Liu et al. (2000); Liu

and Litster (2002) earlier. The calculations are very intensive and require large time for computing the mechanistic kernel. The mechanistic aggregation kernel observed in literature (Immanuel and Doyle III, 2005) does not demarcate the liquid volume that exists on the surface as opposed to the volume that percolates into the pore volume. The consideration of the contact angle of the liquid binder is also missing in the existing mechanistic kernel. This suggests the need for a semi-mechanistic kernel which adequately relates the granule properties with the microscopic/processing attributes, yet requires relatively simpler calculations. The semi-mechanistic kernel proposed in this work tactfully demarcates the internal vs external liquid and also accommodates the effect of contact angle on the kernel describing the aggregation event.

The description of the breakage mechanism has similar shortcomings as the aggregation of particles. Researchers mostly use empirical kernels to quantify the breakage mechanism. Earlier, Pandya and Spielman (1983) had proposed an empirical kernel which quantified breakage as a function of the shear and particle size. However, Soos et al. (2006) proposed a semi-empirical breakage kernel that expressed the breakage of particles as an exponential function of the shear and the particle size.

4.1 Aggregation kernel development
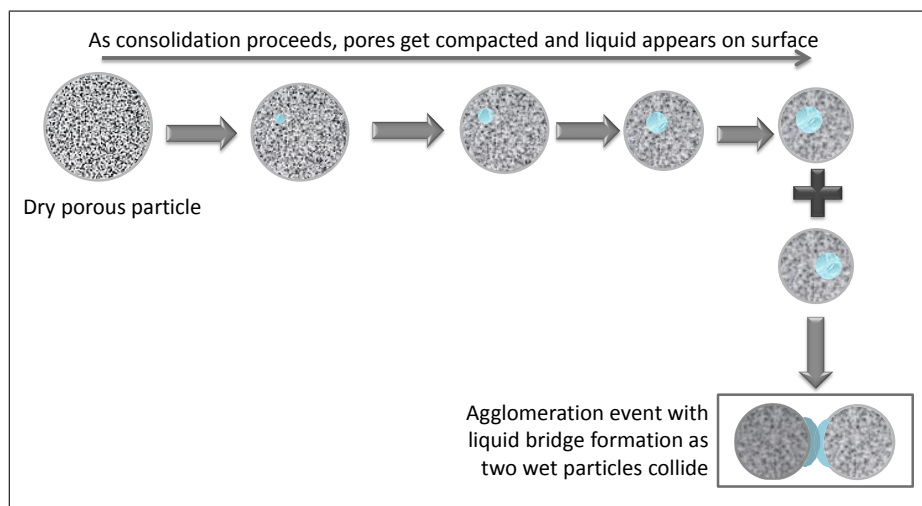
Figure 4.1: Schematic showing the effect of consolidation on agglomeration event

Figure 4.1 shows a schematic of how the agglomeration mechanism proceeds as a coupled effect of consolidation and aggregation. From literature, it has been observed that some of the crucial parameters affecting aggregation are the impeller speed (Nursin, 2010), binder viscosity (Iveson et al., 2001a), contact angle and the amount of surface liquid (Immanuel and Doyle III, 2005). The impeller speed and binder viscosity influences the Stoke's criterion that has been previously used for various works that has studied the aggregation of powder (Stepanek et al., 2009). The contact angle of the binder liquid influences the wetting of the particle surface by the liquid and hence gives an idea about the amount of wetted area and liquid depth available on the particle surface. The wetted area and the liquid depth are crucial parameters that affect the aggregation of particles.

The amount of liquid on the surface of the particle is dictated by the granule saturation fraction, x^*. It can be said that at the initial time point, the amount of total liquid can be demarcated as internal and external based on the granule saturation fraction. Thus we can express the initial surface liquid, V_0 as

$$V_0(j) = l(j) \times x^* \qquad (4.1)$$

where $l(j)$ is the volume of the total liquid in the jth liquid bin. With the progression of time, the liquid on the surface of the particles vary due to the effect of liquid addition and consolidation. As consolidation occurs, liquid binder is squeezed on to the surface due to the compaction of the particles and reduction in pore volume. The partial derivative in terms of liquid volume, l takes care of defining the liquid content of the particles owing to the addition of external liquid. However, once particles have a certain liquid content and begin to appear in the corresponding higher liquid bins, surface liquid starts to appear based on the granule saturation coefficient. As particles start appearing in a certain bin, consolidation also progresses. Thus, at a certain time instant, the amount of surface liquid on the particle can be expressed as

$$V_{ext}(s,l,g,t) = \max\left(V_{ext}(s,l,g,t-1) + \frac{dg}{dt} \times x^*, 0\right)\Bigg|_{F(s,l,g)>0} \qquad (4.2)$$

In this study, a constant contact angle has been used, although in real scenario, the contact angle varies over time and is dynamic in nature following the Young-Dupre's equation. The dynamic contact angle could be expressed as a function of the surface tension and the friction coefficient (Seveno et al., 2002). The drop penetration time described in previous works by Hapgood et al. (2003) also gives an idea on the amount of time required by a droplet to completely sink into a particle pore. It is assumed that the liquid present on the surface is in the form of a single droplet. As time progresses, liquid begins to get squeezed out to the surface (for a particular bin) owing to consolidation. It is assumed to occur in the form of a single big droplet whose radius and thickness increases as more liquid keeps accumulating on the surface. This can be represented as a function of a constant contact angle, θ and has been shown in Equation (4.3)

$$R_{wet} = \frac{3V}{\pi}\Phi(\theta) \tag{4.3}$$

where,

$$\Phi(\theta) = \frac{sin^3(\theta)}{2 - 3cos(\theta) + cos^3(\theta)} \tag{4.4}$$

The area of the particle surface wetted by the liquid can be calculated by evaluating the area of a circle having a radius of R_{wet} (assuming the surface to be flat and ignoring the curvature).

With the progression of time, the total and surface liquid in case of wet particles keep increasing. In case of a dry particle without enough liquid content, the liquid hitting the particle sinks into the particles as long as the pores are not filled. Once the pores get filled to its saturation point, the excess liquid remains on the surface and contribute to higher aggregation of particles. The depth of the surface liquid, h_0 present can be expressed as a function of the volume and the wetted area (based on the dimensionless spray flux principle (Litster et al., 2001)) as

$$h_0(s, l, g) = 1.5 \times \frac{V(t, s, l, g)}{A_{wet}(s, l, g)} \tag{4.5}$$

The surface asperity, h_a is considered to be 2 % of the particle diameter upto a

maximum value of 3 μm. Using these information, the aggregation kernel is considered to be a product of a size dependant part and a size independent part. The aggregation kernel can be represented as

$$K_{agg}(s, l, g, s - s', l - l', g - g') = B_0 \Psi(s, l, g, s - s', l - l', g - g') \times A(s, l, g, s - s', l - l', g - g') \tag{4.6}$$

Where, $\Psi(s, l, g, s - s', l - l', g - g')$ is a binary variable depicting the Stoke's criterion and can be written as expressed in Equation (4.7) while $A(s, l, g, s - s', l - l', g - g')$ is obtained from the fractional wetted area of the two aggregating particles. $\Psi(s, l, g, s - s', l - l', g - g')$ can be calculated from the Stoke's criterion as

$$\Psi(s, l, g, s - s', l - l', g - g') = \begin{cases} 1, & \text{if } St \leq St^* \\ 0, & \text{if } St \geq St^* \end{cases} \tag{4.7}$$

where, the Stokes number, St and the critical Stokes number, St^* can be written as

$$St = \frac{8\tilde{m}u_0}{3\pi\mu\tilde{d}^2}$$
$$St^* = 2ln\frac{\lambda_{12}}{h_a} \tag{4.8}$$

where, $\tilde{m}$ is the harmonic mean of the mass of the two particles, u_0 is the velocity of the particles, μ is the viscosity of the binder, $\tilde{d}$ is the harmonic mean of the diameter of the aggregating particles and λ_{12} is the depth of the surface liquid on the particle. The factor $A(s, l, g, s - s', l - l', g - g')$ represents the product of the fractional wetted area of the two aggregating particles and can be written as

$$A(s, l, g, s - s', l - l', g - g') = \frac{A_{wet}(s, l, g)}{A_{total}(s, l, g)} \times \frac{A_{wet}(s - s', l - l', g - g')}{A_{total}(s - s', l - l', g - g')} \qquad (4.9)$$

The final aggregation kernel is taken to be a product of all these variables (Equation (4.6)) which focus on the various aspects that influence the possibility of a successful collision.

4.2   Results and discussions

Intuitively we have identified a few parameters that could be easily manipulated while running experiments in order to see the variations in the output properties of the proposed integrated model that is expressed as a function of the key operating parameters. This study will enable us to have a more vivid idea of which quantities are needed to be manipulated and to what extent, in order to define the final granule properties (e.g particle size and porosity)). The integrated model relates the various mechanisms to the fundamental operating parameters in a way such that the model is not completely decoupled, yet the solution technique is not very complicated. Some of the crucial operating parameters that affect the final outcome of the process are the number of rotations per minute of the impeller (rpm), the viscosity of the binder (μ), the contact angle (θ) of the binder liquid onto the surface of the particle and the liquid spray rate. The aggregation kernel proposed in this work is also novel and takes into consideration the various crucial operating parameters such as the viscosity of binder, contact angle and impeller speed.

4.2.1 Comparison between the semi-mechanistic aggregation kernel and the empirical kernels from literature

(a) Semi-mechanistic kernel   (b) Empirical kernel
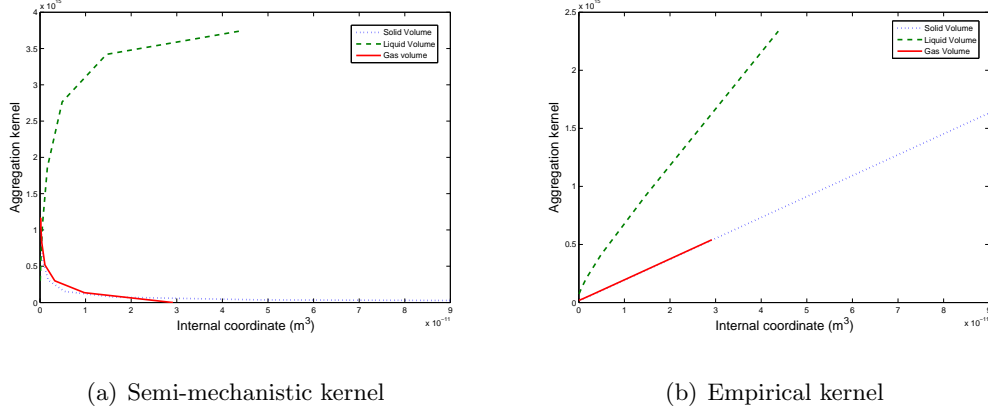
Figure 4.2: Comparison of the behavior of the semi-mechanistic kernel and the empirical kernels with respect to the individual volumes ($\beta(1,1,1,1,1,:)$ for gas, $\beta(1,1,1,1,:,5)$ for liquid and $\beta(1,1,1,:,1,1)$ for solid in both cases)

The aggregation kernel proposed in this paper is dynamic in nature and accounts for the changes in the system behavior as granulation progresses. The aggregation kernel takes into account the appearance of surface liquid for porous particles as liquid is sprayed over the particles and also attributes the occurrence of consolidation with the progress of the granulation process. The overall aggregation kernel is expressed as a product of the fractional wetted area, the factor owing to the Stoke's criterion and the constant value for scaling the kernel. In contrast to the empirical kernels more commonly used, this kernel shows remarkable variations with respect to the different internal coordinates, such as solid, liquid and gas volumes. Also, at the initial time, the particles that are more porous and dry are considered to not have any aggregation tendency. These trends cannot be captured using the empirical kernels. Figure 4.2 shows a comparison between the empirical kernels and the kernel proposed in this work.

From Fig 4.2, we can see that for the empirical kernel, the individual volumes are just lumped as the size and hence there is no realistic variation with respect to the individual volumes. The semi-mechanistic kernel instead, shows more realistic variation with

respect to the solid, liquid and gas volumes. For a constant solid and gas volume, as the liquid increases, the fractional wetted area also increases suggesting higher aggregation, which is in agreement with the figure. On the other hand, for a constant solid and liquid volume, the wetted area decreases as the porosity increases. As the porosity increases, a significant amount of liquid is used up to fill in the pores of the particle and after a certain point, surface liquid seems to emerge. Thus the amount of surface liquid and thus the wetted area is reduced for highly porous particles. For a constant liquid and gas volume, the fractional wetted area decreases as the solid volume increases. Due to increased solid volume, the overall size of the particle increases, but the liquid amount is still constant hence the amount of wetted area is same, but the total surface area present in the denominator is increased and hence the fractional wetted area is reduced. These physical events can be well captured in the proposed aggregation kernel.

4.2.2   Effect of the various model inputs/operating parameters on the final granulation outcome

The integrated model which takes into account the various fundamental operating parameters, can capture the steady growth and induction behavior under the conditions as also mentioned in the works of Walker (2007). The impeller speed affects both the aggregation and the consolidation of the particles, the viscosity and contact angle affects the aggregation mechanism, the liquid added affects the aggregation and the liquid distribution. The DOE used for this analysis was adopted from Pandey et al. (2011).

Effect of aggregation only

The aggregation kernel proposed in this work is a function of the liquid viscosity, impeller speed and the contact angle. This case involves studying the dynamics of the the aggregation mechanism (with no consolidation) on the final granule properties. It can be seen that for the highly porous particles, the overall porosity increases as aggregation occurs, however for less porous initial particles, the granule porosity reduces over time suggesting the resulting system to be more densely packed (Gluba et al., 2004). As anticipated, the average diameter of the particles increases with increasing

liquid spray rate due to higher availability of surface liquid (as also shown in Figure 4.3). With increasing binder viscosity, the liquid bridges formed between the particles are stronger thus indicating the formation of larger granules. The binder viscosity can be manipulated by changing the concentration of the binder solid in the liquid. Traditionally the empirical kernel is unable to address such effects, however the semi mechanistic kernel is capable of capturing such trends, as also shown in Figure 4.4. In case of the highly porous particles, there is a reduction in the availability of surface liquid (as consolidation is not considered), hence aggregation does not predominantly occur. However in the case of less porous particles, there is a steady growth pattern with a higher increase in the particle size owing to the stronger liquid bridges formed by more viscous fluid. In case of less porous particles, there is availability of surface liquid which aids in the occurrence of aggregation, thus the effect of viscosity is more pronounced. The change in binder liquid viscosity can be brought about by changing the concentration of solid binder in the liquid/water. For this work, we have assumed the three variations in the viscosity to be representative of binder concentrations of 0.5 %, 2.5 % and 5 % as was used in the work of Poon et al. (2009). The case showing the effect of impeller speed (Figure 4.5, no significant impact could be observed for the highly porous particles. This is also due to the unavailability of surface liquid which discourages the occurrence of aggregation. In case of less porous initial particles, there is enough surface liquid thus enabling the agglomeration of powder. With an increase in the velocity, the kinetic energy of the particles increases. Thus the agglomeration tendency of the particles reduces. This effect is controlled by the binary coefficient representing the Stoke's criterion that comprises of an integral part of the aggregation constant.
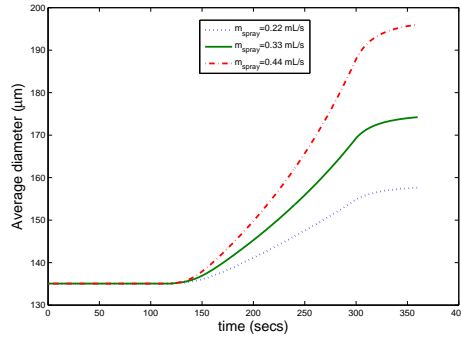
(a) Average diameter for highly porous particles
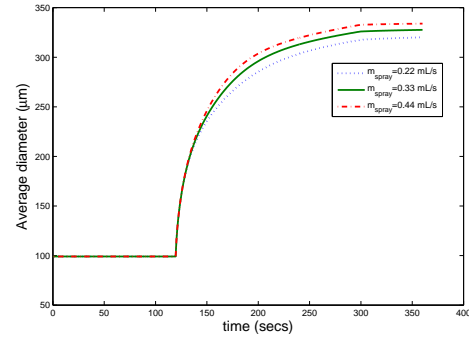
(b) Average diameter for less porous particles
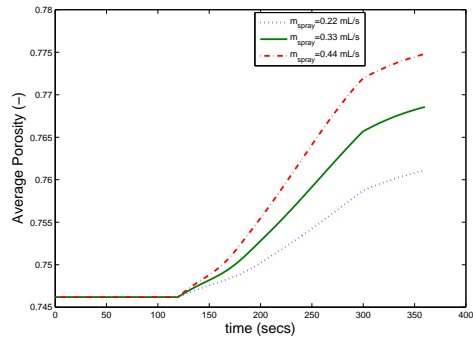
(c) Average porosity for highly porous particles
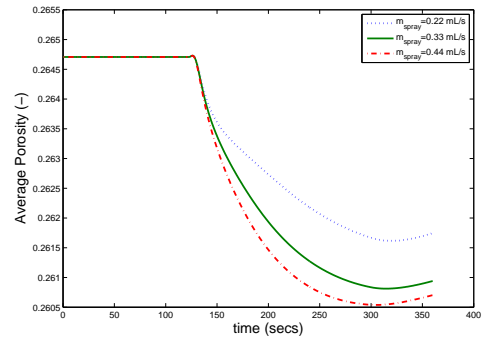
(d) Average porosity for less porous particles

(e) PSD at the end of the wet massing time for highly porous particles

(f) PSD at the end of the wet massing time for less porous particles

Figure 4.3: Comparative study showing the variation of liquid spray rate for the aggregation only case for highly porous and less porous particles

(a) Average diameter for highly porous particles

(b) Average diameter for less porous particles

(c) Particle size distribution at the end of wet massing for highly porous particles
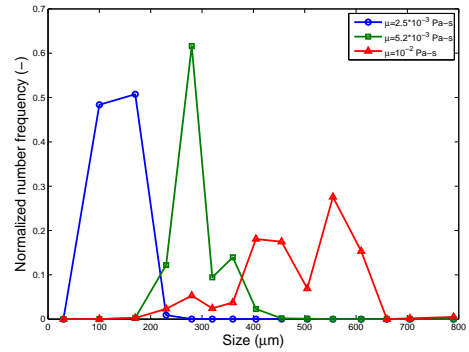
(d) Particle size distribution at the end of wet massing for less porous particles

Figure 4.4: Comparative study showing the variation of binder liquid viscosity for the aggregation only case for highly porous and less porous particles

Figure 4.6 shows the effect of the contact angle/wettability of the particle and the binder liquid on the bulk and distributed properties. The contact angle depicts the wettability of the particle for a certain binder liquid. The aggregation kernel is a function of the fractional surface area and the Stoke's criterion takes the depth of surface liquid into consideration. Thus, the effect of the contact angle is not monotonic. In the case of a lower contact angle (hydrophilic), the fractional surface area is higher, however due to the reduced depth of surface liquid, many aggregation events are not possible due to the violation of the Stoke's criterion. However, for higher contact angles (depicting hydrophobic), the available surface area for aggregation is less. This also reduces the chances of agglomeration to occur. Therefore, as also shown in the figure,

an intermediate contact angle is best suited for increased aggregation of particles.
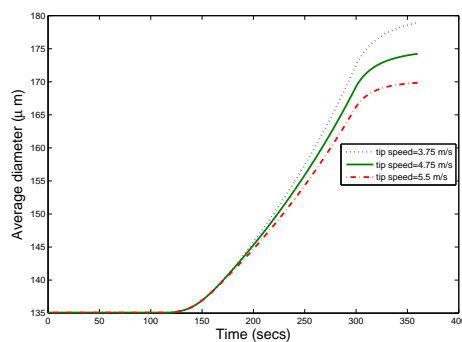
(a) Average diameter for highly porous particles
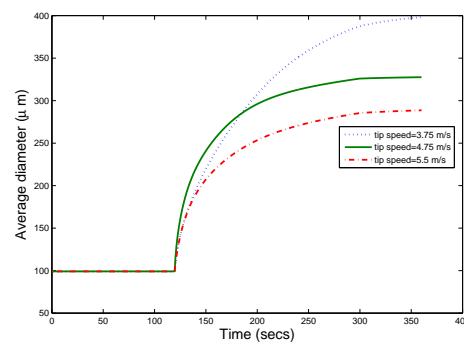
(b) Average diameter for less porous particles
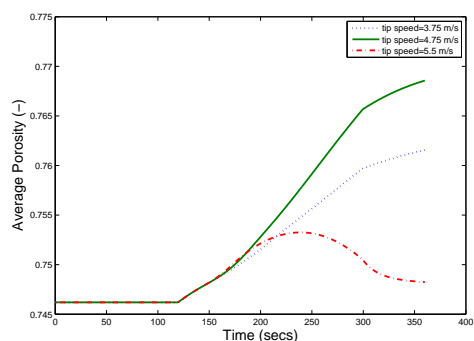
(c) Average porosity for highly porous particles
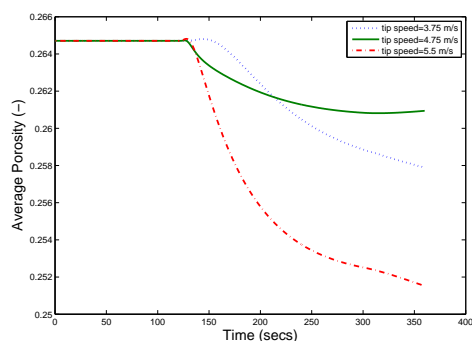
(d) Average porosity for less porous particles
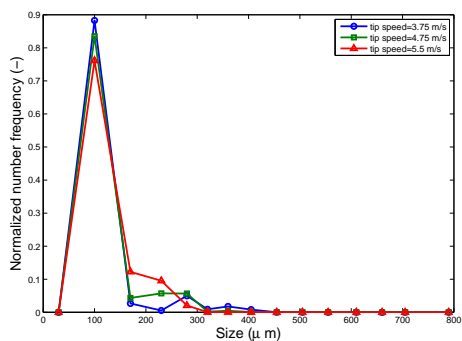
(e) PSD at the end of the wet massing time for highly porous particles
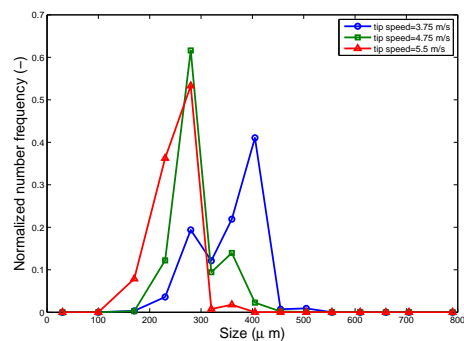
(f) PSD at the end of the wet massing time for less porous particles

Figure 4.5: Comparative study showing the variation of impeller speed for the aggregation only case for highly porous and less porous particles
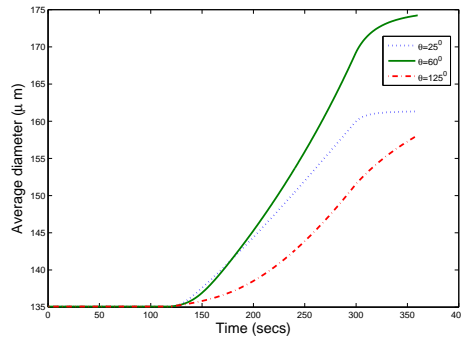
(a) Average diameter for highly porous particles
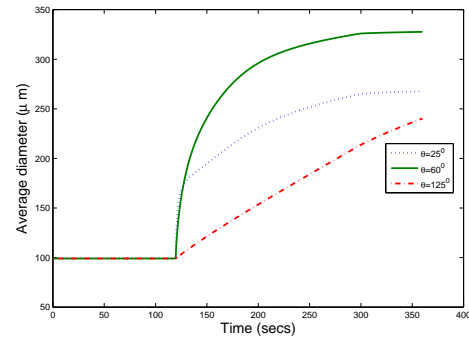
(b) Average diameter for less porous particles
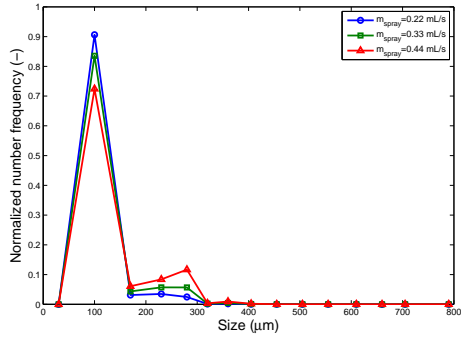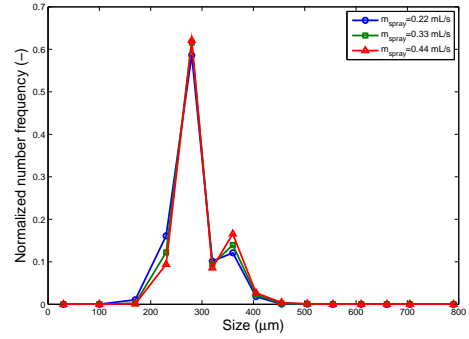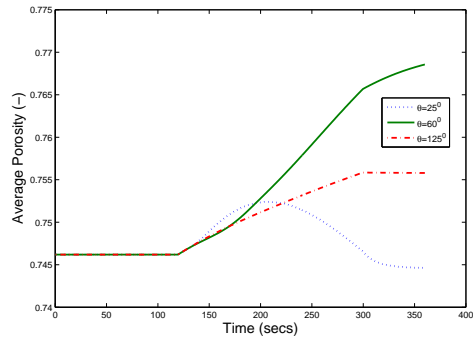
(c) Average porosity for highly porous particles
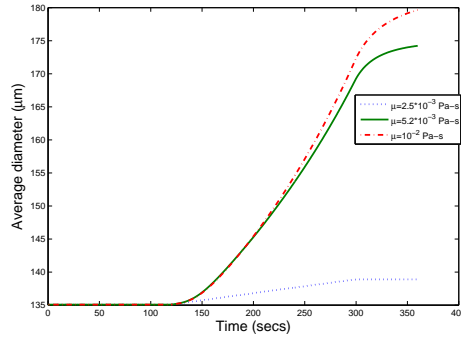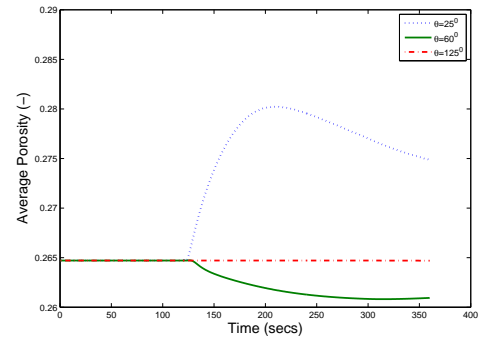
(d) Average porosity for less porous particles
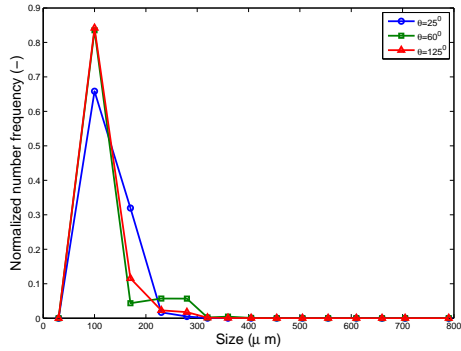
(e) PSD at the end of the wet massing time for highly porous particles
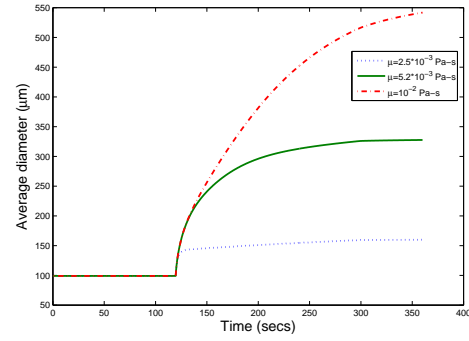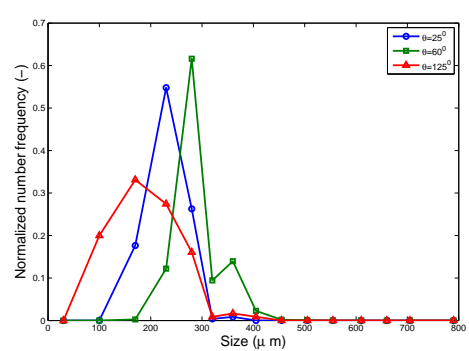
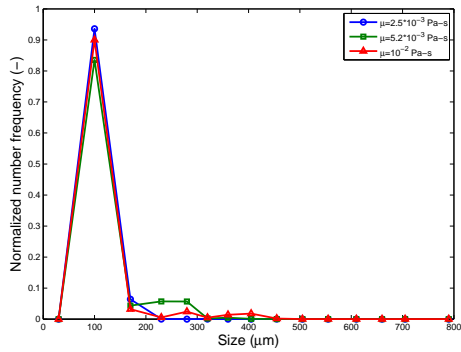(f) PSD at the end of the wet massing time for less porous particles

Figure 4.6: Comparative study showing the variation of contact angle for the aggregation only case for highly porous and less porous particles

Effect of the operating and formulation parameters on the final granule properties for the overall model

Two cases have been considered wherein the system is differentiated based on the porosity of the particles subjected to granulation. The initial porosity of the highly porous particles is 0.74 while that for the less porous particles is 0.263. Initially the particles are relatively dry, but as liquid is added, an increased amount of aggregation begins to occur thus resulting in the average diameter to increase. Consolidation plays a significant role in case of the highly porous particles. In case of highly porous initial particles, a prominent induction behavior can be captured owing to the lag in the availability of surface liquid aiding in aggregation. Therefore, the aggregation of particles is inhibited initially, however with the appearance of surface liquid, the growth is promoted rapidly. In the case of less porous particles, the growth observed is steady in nature due to the presence of liquid on the surface from the start.

Liquid amount variation

From Figures 4.7 and 4.8, the effect of liquid to solid ratio (brought about by adding liquid at different rates for a fixed time) on the various bulk and distributed properties can be noted. It can be seen that with increasing liquid spray rate, the particle diameter increases (Figures 4.7a, 4.8a). In the case of highly porous particles, an induction behavior is observed. With increasing liquid to solid ratio (liquid spray rate), the porosity of granules increases as the liquid occupies more space in the pores. With increasing liquid to solid ratio the porosity decreases in reality and that is driven by the increase in the consolidation of particles (Iveson and Litster, 1998; Hagrasy et al., 2013). The consolidation rate used in this work is not expressed as a function of the liquid to solid ratio (due to the lack of mechanistic knowledge) and hence the decrease in the porosity with increasing liquid spray rate cannot be observed. The effects of liquid spray rate are well established in the scientific community and can be very well captured using this model proposed in this work. The additional benefit is the ability to capture the steady and induction growth behavior, which are key abilities to capture

the observations as noted by Hapgood et al. (2003) in their regime-map analysis of the granulation process.
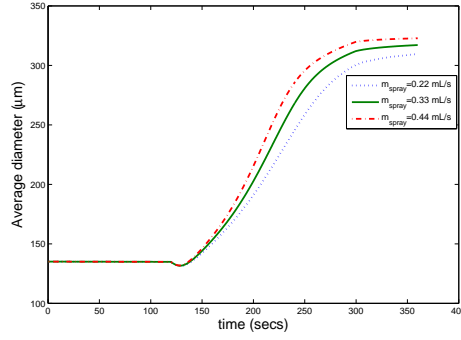
(a) Average particle diameter
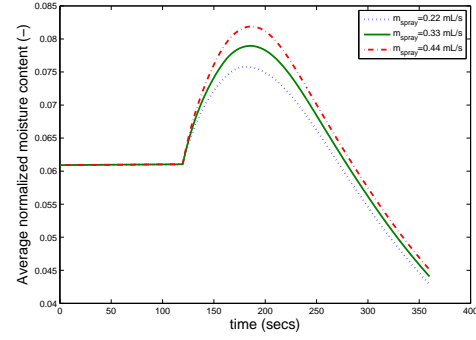
(b) Average particle porosity
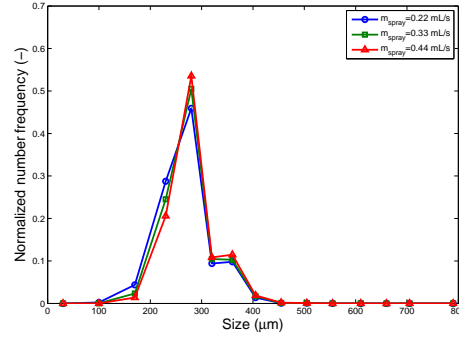
(c) PSD at the end of the wet massing time

Figure 4.7: Variation of liquid spray rate for highly porous particles showing the effect on the bulk and distributed properties

(a) Average diameter

(b) PSD at the end of the wet massing time
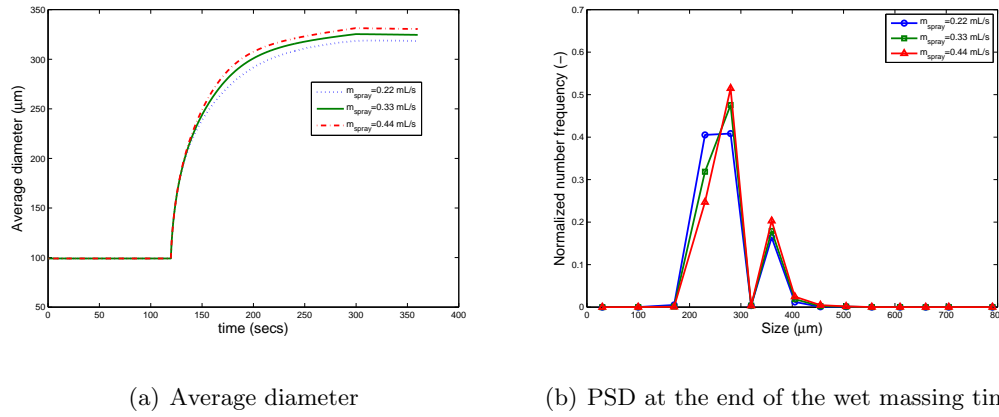
Figure 4.8: Variation of liquid spray rate for less porous particles showing the effect on the bulk and distributed properties

Viscosity variation

It can be seen that with increasing binder viscosity, the agglomeration of particles increases due to the stronger liquid bridge formed between the particles (Liu et al., 2000). However, the empirical aggregation kernels are unable to track such an effect as a function of the viscosity as they typically are not a function of liquid binder viscosity. Figures 4.9a and 4.10a clearly reveal the increase in the particle size as a function of the binder viscosity. It was also seen in the works of Iveson and Litster (1998), that as binder viscosity increases, the consolidation decreases. This suggests a reduced decrease in the granule porosity. The observations from Figures 4.9b and 4.10b are in accordance with the results expected in theory and experimentation. The aggregation kernel proposed in this work is thus capable of capturing the expected trends in the granule properties as a function of the binder viscosity (Figures 4.9 and 4.10).
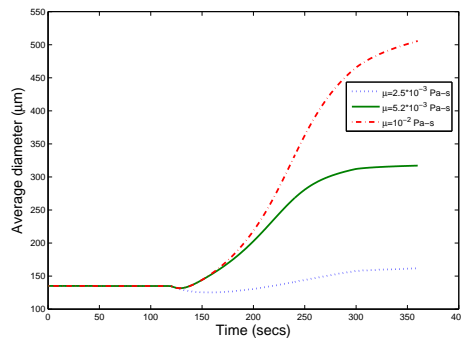
(a) Average diameter
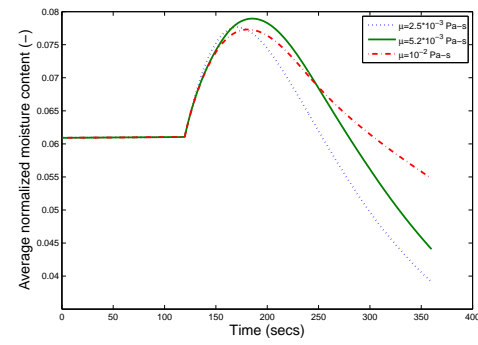
(b) Average porosity
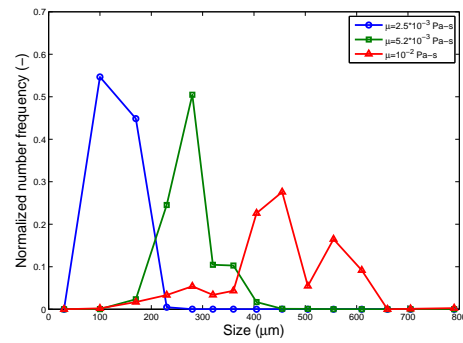
(c) PSD at the end of the wet massing time

Figure 4.9: Variation of binder viscosity for highly porous particles showing the effect on the bulk and distributed properties

(a) Average diameter

(b) Average porosity

(c) PSD at the end of the wet massing time
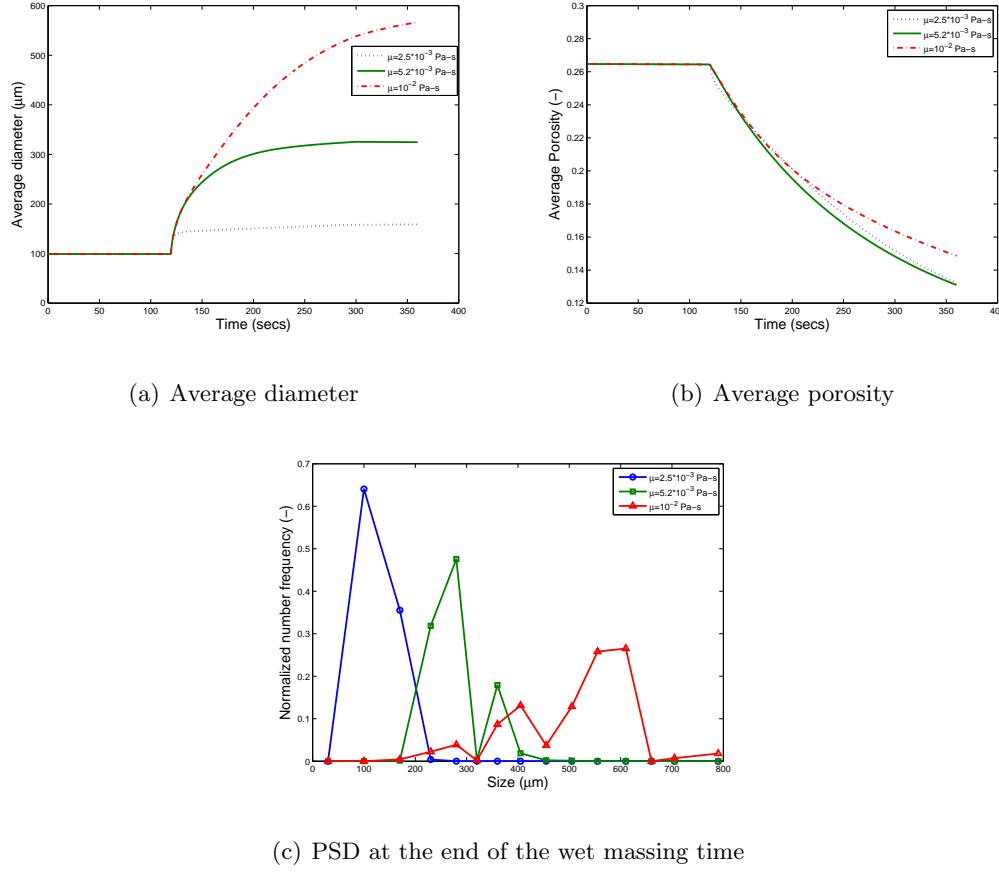
Figure 4.10: Variation of binder viscosity for less porous particles showing the effect on the bulk and distributed properties

Impeller speed variation

In this work, we have used a simplified expression to quantify the effect of the impeller speed on the consolidation by expressing it as a linear function of the rpm. The speed of the impeller directly affects the Stoke's criterion as shown in Equation (4.7) and (4.8). This suggests that for higher impeller speed, many aggregation instances are not viable, thus the aggregation is reduced. Physically, this can also be explained by the increased kinetic energy of the particles which is not dissipated by the collision forces for aggregation to occur. The impeller speed also affects the consolidation of particles and speeds the appearance of liquid on the surface. In case of highly porous particles it can be seen that the increase in the particle size is delayed for lower impeller speed. However, once there is sufficient liquid for aggregation to occur, the particle size increases and is

higher for lower impeller speed. The average porosity of the granules is also lower for higher impeller speed. This is brought about by the increased consolidation of particles resulting in a lower final porosity of the granules. Figures 4.11 and 4.12 shows the effect of the impeller speed on the bulk and distributed properties of the particles.

(a) Average diameter

(b) PSD at the end of the wet massing time

(c) PSD at the end of the wet massing time
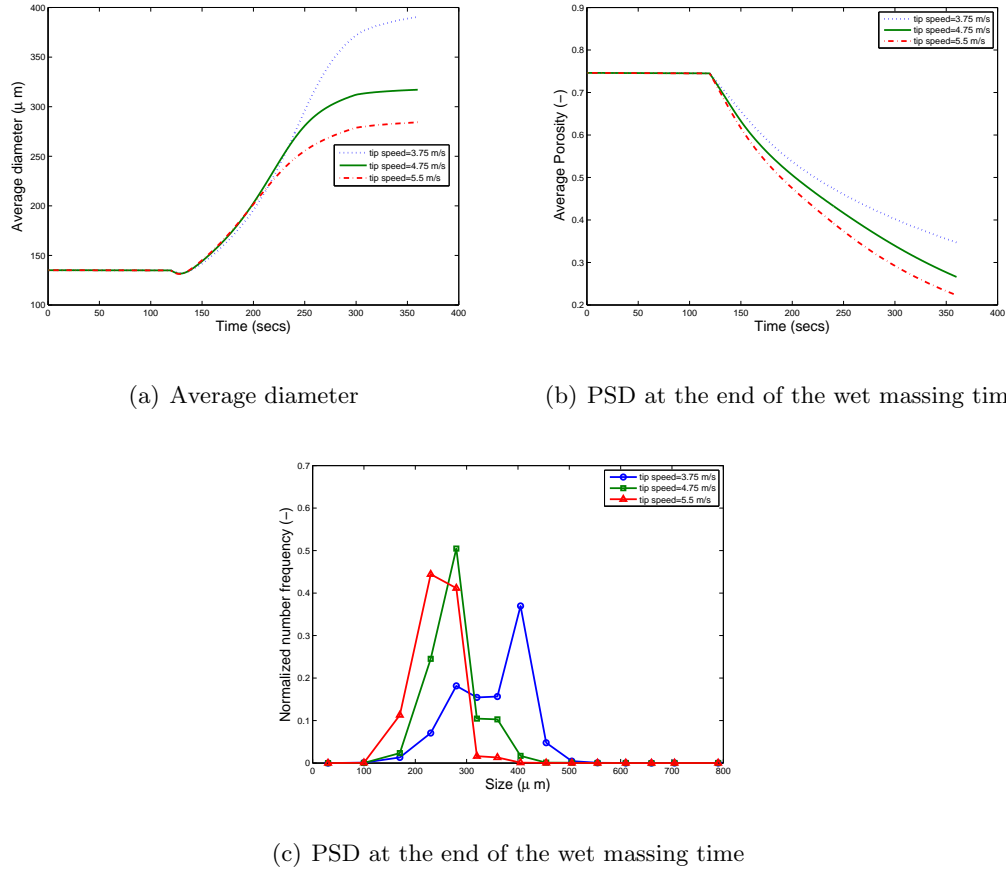
Figure 4.11: Variation of impeller speed for highly porous particles showing the effect on the bulk and distributed properties

(a) Average diameter

(b) Average porosity

(c) PSD at the end of the wet massing time
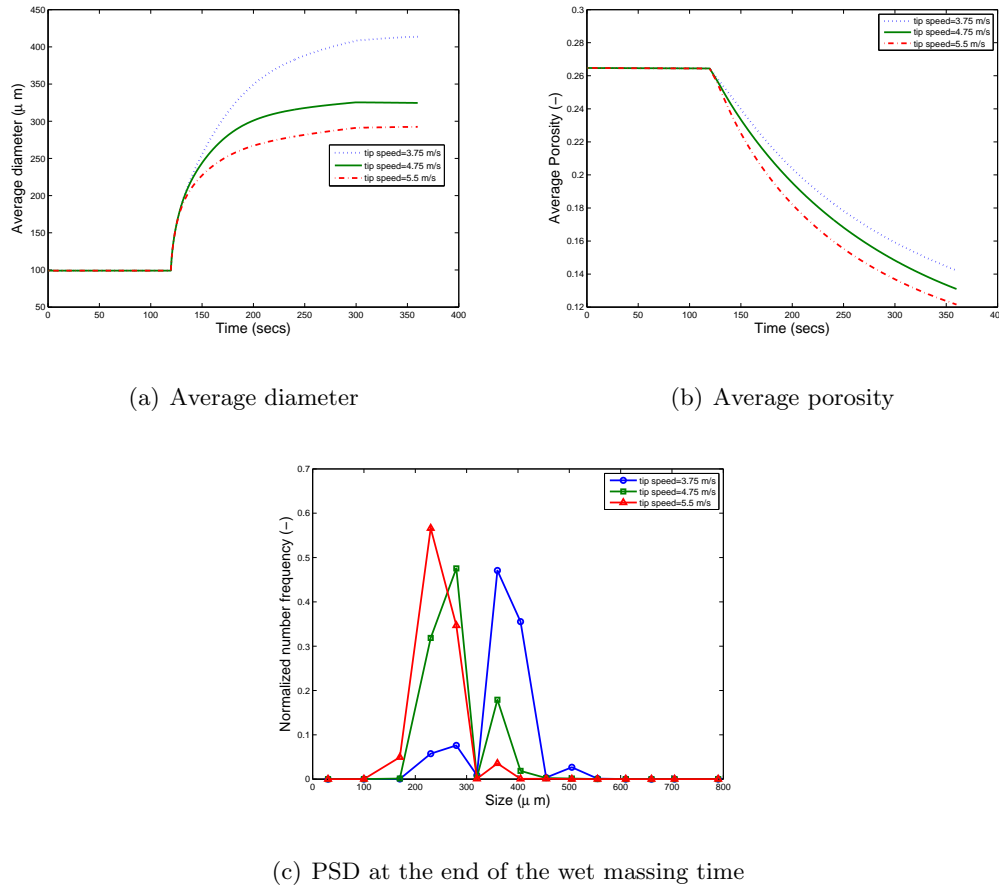
Figure 4.12: Variation of impeller speed for less porous particles showing the effect on the bulk and distributed properties

Contact angle variation

A major influence of the contact angle is on the fractional wetted area of the particles and the Stoke's criterion (indirectly). A contact angle of less than 90^0 indicates a more hydrophilic binder liquid on the surface whereas a contact angle of greater than 90^0 suggests a more hydrophobic binder liquid on the particle surface. The contact angle of the liquid on the solid surface determines the wettability of the particle with the binder liquid used. A smaller contact angles suggest higher wettability and the converse is true for higher contact angles. In our study, we have considered the contact angle to be such that the entire range of low and high wettability can be covered (hydrophilic as well as hydrophobic binder). For low contact angles, the wetted surface area of the

particles is larger which also suggests a fractional wetted area of the particle closer to 1. However, in this case, the depth of surface liquid is less, which does not allow enough thickness of liquid for the formation of a liquid bridge which could enable the coalescence mechanism to occur. This explains the increase in the particle size with an intermediate contact angle between the binder liquid and the particle surface as also seen in Figure 4.13 and 4.14. The PSD of the granules at the end of the wet massing period show good agreement with the expected qualitative bulk property plots. The average particle size plots also suggest a reduced delay with the onset of the aggregation mechanism for the more hydrophilic case compared to the hydrophobic case.

(a) Average diameter

(b) Average porosity

(c) PSD at the end of the wet massing time
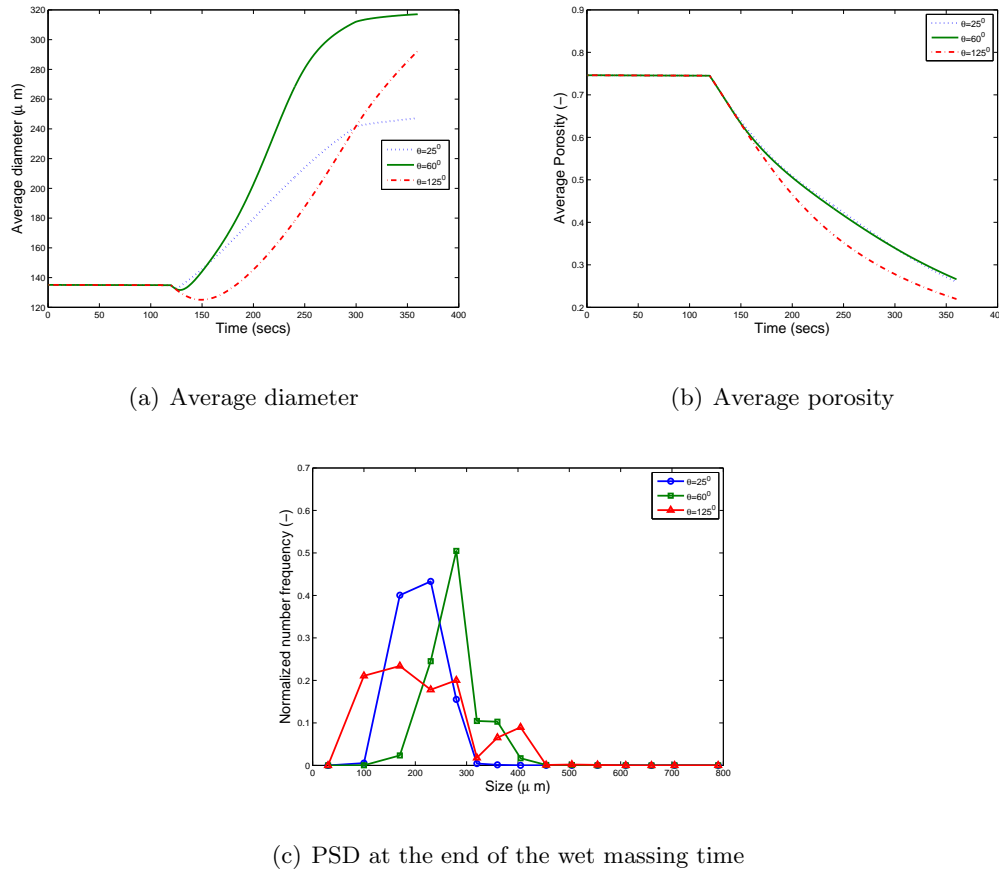
Figure 4.13: Variation of contact angle for highly porous particles showing the effect on the bulk and distributed properties

(a) Average diameter (b) PSD at the end of the wet massing time
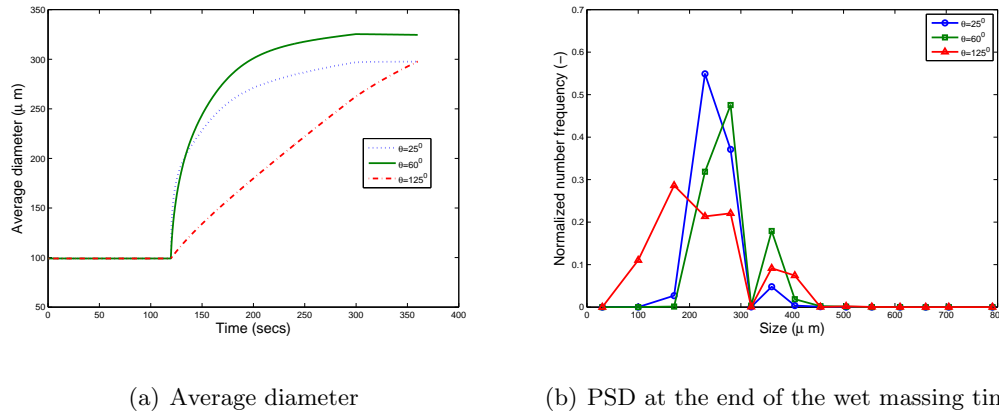
Figure 4.14: Variation of contact angle for less porous particles showing the effect on the bulk and distributed properties

The final time upto which the granulation process is ran or the wet massing time is yet another crucial variable that can affect the final granule properties. It is however quite straightforward and would not involve making significant changes in the model itself. Thus, detailed discussions in the granule properties with respect to changing wet massing time has not been provided in this work.

4.3 Chapter conclusions

This work deals with developing a semi-mechanistic aggregation kernel that is representative of the influence of the input parameters on the output quantities for a high-shear wet granulation process. The model can effectively capture the steady and induction growth behaviors as expected in experimental observations. Due to the capability to track real scenarios with minimal computational complexity, this model can be considered ideal to be furthered for control, optimization or process scheduling work. The ability of the model to be able to capture the intricate behavioral attributes observed during the practical granulation process makes this work novel and this model different from the pre-existing models noticed in literature. This model can be effectively utilized for open loop control and optimization of the granulation process. As the aggregation kernel can relate the final granule properties with the operating parameters, based on a sensitivity analysis, the contribution of the variation of each operating parameter to

the granule property can be realized. Therefore, this work provides an example how to utilize mechanistic modeling approach to reduce the uncertainty surrounding the high-shear wet granulation process design space development. Furthermore, it will significantly aid in optimally scheduling the granulation process such that the operating conditions are predetermined based on the final needs of the operator. Another significant benefit of this kernel is the reduced number of empirical parameters involved in the formulation which suggests reduced reliance on the estimation of multiple empirical parameters. The ability of this kernel to be able to capture the steady state and induction growth behaviors makes it a more practical kernel for modeling the complex particulate process such as granulation.

Chapter 5

Specific Aim IV: Compartment based model identification and open loop optimization of granulation processes

The details of the discussions provided in this section can be obtained in the publication:

- Chaudhury, A., Armenante, M., Ramachandran, R., 2014, Compartment based population balance modeling of a high shear wet granulation process using data analytics, Chemical Engineering Research & Design, Accepted for publication

Granulation is a not so well understood process that is commonly carried out in the industry with high recycle ratios. This chapter aims at obtaining a more systematic approach for optimally scheduling a granulation process in order to obtain the desirable final granule properties. This approach involves utilizing a detailed and mechanistic model, which can not only relate the process outcome to the operating conditions, but can also adequately account for the inhomogeneities existent within the system. The model can further be used to optimize the process and obtain operating parameters that can result in a desired output CQA.

5.1 Development of a compartment-based model for high-shear granulation process

A high-shear granulator is commonly assumed as a well-mixed system, with a single equation describing the overall vessel. However, there are various heterogeneities (particle velocity, liquid distribution) existent within the high-shear granulator and a single PBM might be inadequate to represent the overall system accurately. As discussed in the previous chapters, a lot of work observed in the literature has been aimed at investigating the system behavior based on regime-map analysis (Iveson et al., 2001a; Litster,

2003; Emady et al., 2011). Hapgood (2000) proposed the granulation process to fall into the droplet controlled regime, the intermediate regime or the mechanical dispersion regime. The droplet control regime is a more ideal scenario, wherein a droplet wets a single particle. This system is typically devoid of inhomogeneities (in terms of liquid) and is considered more uniform. The other asymptote-mechanical dispersion regime is however accompanied by a single droplet wetting multiple particles. This is associated with a lot of inhomogeneities within the process and also indicates limitations with respect to mixing. For a droplet controlled regime, the inhomogeneities are not very prominent, however, in reality, a system seldom corresponds to the droplet-controlled regime. A compartment-based model is expected to capture these heterogeneities within the system in terms of binder distribution and velocity.

A compartment based approach has been used for various particulate process in order to address the inhomogeneities. Maronga and Wnukowski (1997) used a compartment based approach for modeling a fluid bed coating process where they differentiated the coater into three distinct compartments (active spray zone, active drying zone and non-active domain). These observations (within a coater) were extended for a PBM based approach by Freireich et al. (2011); Li et al. (2011) where discrete element modeling (DEM) simulations were used to identify the particle flow information and residence time distribution (RTD) within each compartment. A compartment based approach has also been implemented to account for the inhomogeneities within a crystallization process (Kulikov et al., 2006; Ma et al., 2002). Börner et al. (2013) have also modeled a Wurster fluid bed granulator using a bi-compartment based model. Ramachandran and Chaudhury (2012) have previously modeled a continuous drum granulator using separate compartments. The high-shear granulator is conventionally treated as *well mixed* and is modeled using a single PBM, however this assumption could lead to oversimplification. Bouffard et al. (2012, 2013) have used DEM simulations to identify the various compartments existing within a rotor-based equipment. The information about the various compartments are then extended to develop a PBM along with a Markov-chain approach in order to quantify the motion of particles in each compartment. This approach however does not address the variations in the velocity of the particles as

result of the impeller rotating within the granulator. The approach adopted in the works of Bouffard et al. is stochastic in nature and has been tackled using Monte Carlo simulations.

The development of the compartments tracking the heterogeneity within the granulator requires multiple steps. The experiment is mimicked using Discrete Element Modeling (DEM) simulations that are operated under the same experimental conditions. The data extracted from the DEM simulations are further analyzed to demarcate the regions of homogeneity within the heterogeneous system. In the following subsections, details are provided regarding the step-by-step approach adopted for this exercise.

5.1.1   Model Calibration of a PBM to generate intermediate data

Experimental data was obtained for the high-shear granulation process, and the measurements included the final particle size distributions (PSDs) from the experiments described in our previous works (Pandey et al., 2013; Chaudhury et al., 2014a). In order to account for the change in the number and size of the particles, obtaining the PSDs at intermediate time points was required which lead to the need to calibrate the PBM in order to generate additional data. Thus, the model has been calibrated using the data for the final PSD presented in Chaudhury et al. (2014a). However, the model utilized in this work differs from that used in Chaudhury et al. (2014). The aggregation kernel used in this work (as described in the previous chapter) takes into account the semi-mechanistic kernel which is capable of tracking the steady and induction growth behavior and is also a function of process parameters such as liquid content and impeller speed. The objective function (Φ) for the optimization problem was then formulated as

$$\Phi(\theta) = \min_{\theta} \sum_{k=1}^{N} (O_k - E_k(\theta))^2 \tag{5.1}$$

$$\theta = [\beta_0 \ B \ k_{con} \ x_{sat} \ \varepsilon_{min}] \tag{5.2}$$

where, θ is the set of adjustable parameters, O_k is the kth measurement value, and $E_k(\theta)$

is the simulated value of that measurement. N is the total number of measurements across all experiments used in parameter estimation.
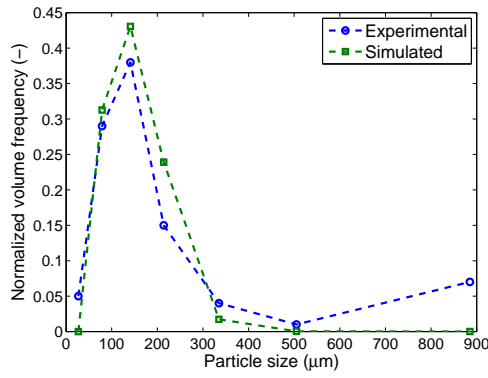
(a) Batch 2
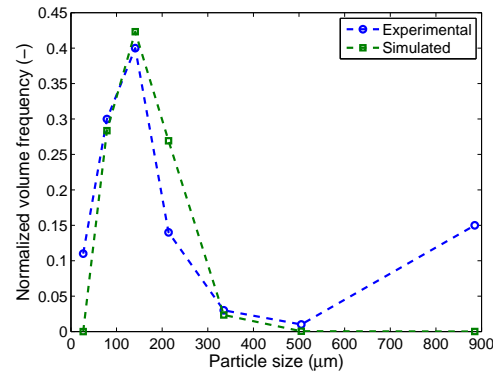
(b) Batch 3
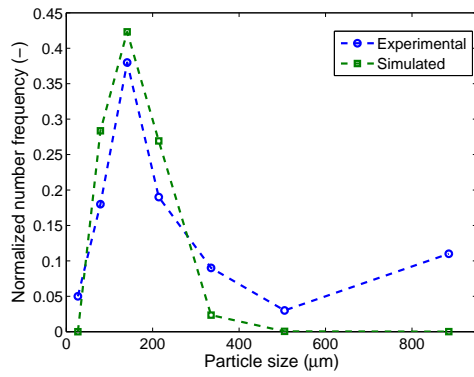
(c) Batch 7
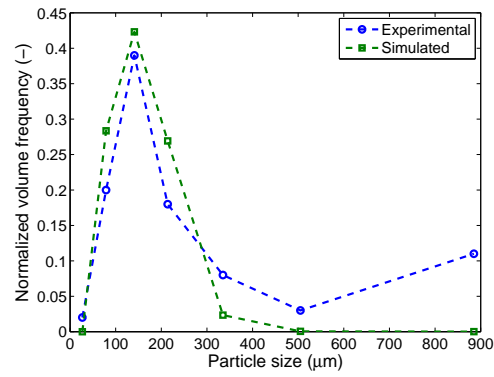
(d) Batch 8
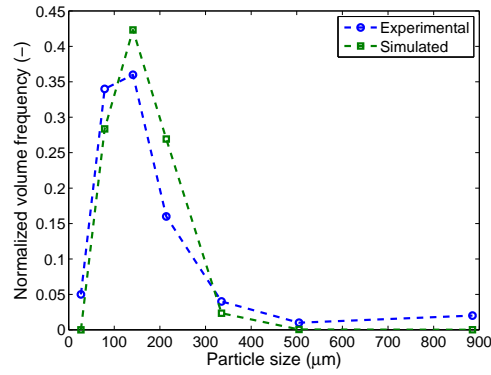
(e) Batch 11

Figure 5.1: Experimental and simulated end point particle size distributions from high shear granulator using parameter estimation

The measurements encompass the end point particle size distribution (PSD) from the granulation experiments. The simulated PSD is unable to capture the bimodal distribution as exhibited by the experimental results. A primary reason behind this discrepancy can be justified by the utilization of a single PBM for the process description. This also necessitates the need for a compartment based model that can better capture multimodal distributions. The variables estimated through this approach include the empirical coefficient for the aggregation kernel (β_0) as expressed in our previous works (Chaudhury et al., 2014b), the empirical coefficient for the breakage kernel (B) as expressed by Ramachandran et al. (2009), the empirical constant for consolidation (k_{con}), the granule saturation (x_{sat}) and the minimum porosity (ε_{min}).

Table 5.1: Set of estimated parameters obtained from model calibration

Parameter name	β_0	B	k_{con}	ε_{min}	x_{sat}
Estimated value	$7.8434e^{14}$	$5.2e^{-3}$	$6.2893e^{-8}$	0.1877	0.0314

The model was calibrated using the non-linear simplex method or the Nelder-Mead approach which is embedded in the $fminsearch$ function found in MATLAB$^{\circledR}$. Typical granulation experiments involve characterization of the system at the end time, thus leading to a lack of intermediate particle size data. However, the flow patterns within a granulator (within DEM) is a strong function of the number and size of the particles. Thus, it is important to run multiple DEM simulations using different PSDs. Using the model, intermediate PSDs were generated for the granulating system. This information is later used for setting up the DEM simulations. The results from the model calibration are shown in Figure 5.1 demonstrating good agreement between experimental and simulated data. The simulated results, however, show a unimodal size distribution whereas the experimental results suggest a bimodal distribution with a significant fraction of large particles. Typically, in the industrial granulation processes, while calibrating the model, it is essential to fit the model to the product range in the experimental data (which is well matched in this case). The mismatch with capturing the bimodal distribution is an artifact of the incapability of a single compartment

to capture the mechanical-dispersion regime (which is generally responsible for such multimodal distributions).

5.1.2   DEM simulations
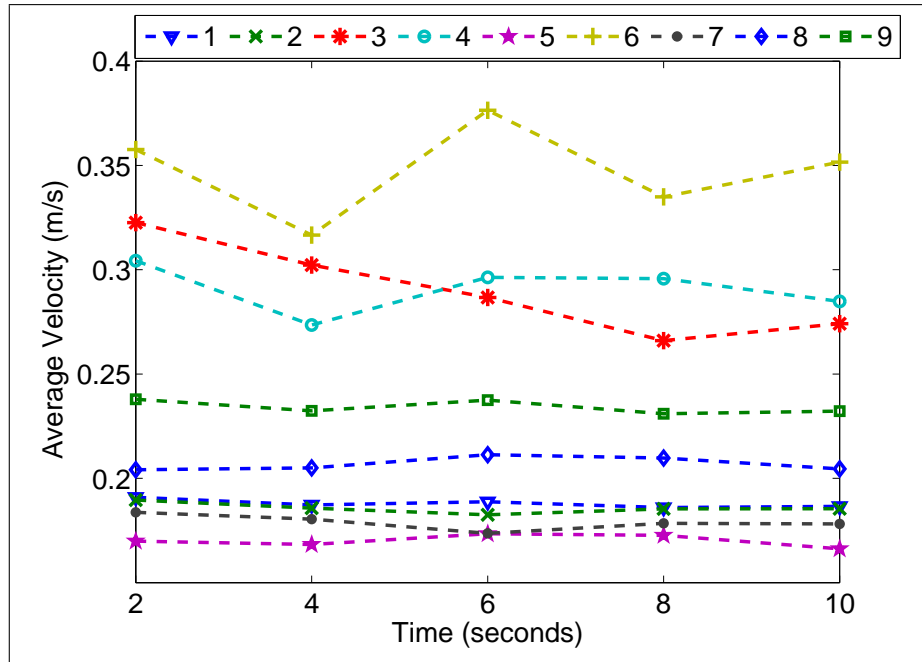
Figure 5.2: Evolution of average velocity over time for varying conditions described by the DOE for the test runs (the runs 1-9 are described in Table 5.3)

In order to better represent the experimental observations, DEM simulations (EDEM®, DEM solutions) were run to enable better particle-scale analysis of the data. DEM simulations are very efficient with mechanistically modeling the motion of particles in a system based on a force-balance approach. The forces acting on a particle are of two types, namely contact forces and body forces. The contact forces arise from particle-particle or particle-boundary collisions. The overall force can be shown as

$$\overrightarrow{F} = \overrightarrow{F_c} + \overrightarrow{F_b} \tag{5.3}$$

where, $\overrightarrow{F}$ is the overall force exerted on a particle due to all its interactions with

other solid entities (particles and boundaries), $\overrightarrow{F_c}$ represents all the normal and tangential contact forces and $\overrightarrow{F_b}$ denotes all the body forces acting on the particle. Newton's laws of motion are solved along with the Euler's equations for rotational motion in order to numerically obtain the new position of the particles over a small time-step (in the order of 10^{-6}). The default body force component within DEM (i.e. gravity) has been considered for the simulations while the damped Hertzian normal contact force and the Mindlin-Deresiewicz/Coulomb friction tangential force model comprise the contact forces acting on the particle (Dubey et al., 2011). Liquid addition has been captured in EDEM® by creating particles which get deleted from the system upon contact (Sen et al., 2014; Barrasso and Ramachandran, 2014). A separate factory of particles (representing the liquid particles) is created within the DEM simulations which are dropped on the solid particles within the granulator using a nozzle at the top. As the liquid particles hit the solid particles, they are deleted, however they impart a change in the liquid content property of the particle (as it gets deleted). This liquid content property is calculated based on the volume of the particle and the volume of the *liquid* particle that hit the particle and eventually gets deleted. The parametric settings used for setting up and running the DEM simulations are shown in Table 5.2.

Table 5.2: Settings used for the DEM simulations

	Parameter name	Value	Units
Particle properties	Shear modulus	2×10^6	Pa
	Poisson's ratio	0.25	$-$
	Density	1500	kg/m^{-3}
Particle-Particle interactions	Coefficient of static friction	0.5	$-$
	Coefficient of rolling friction	0.01	$-$
	Coefficient of restitution	0.1	$-$
Granulator vessel and blades	Material	*Steel*	
	Shear Modulus	80	GPa
	Poisson's ratio	0.29	$-$
	Density	7800	kg/m^{-3}
Particle-blade/ particle-wall interactions	Coefficient of static friction	0.5	$-$
	Coefficient of rolling friction	0.01	$-$
	Coefficient of restitution	0.1	$-$

A study was performed to identify the crucial quantities that affect the velocity and

position of the particles. The study involved keeping the total particle volume constant while varying the 1) size of each particle, 2) number of particles, 3) density of particles, and 4) fill level within the granulator. Monodisperse distributions were used for these test simulations. Table 5.3 shows the DOE used for the test runs. The simulations were run for 10 seconds and the average velocity of particles within the vessel was extracted every 2 seconds for the purpose of comparison. Figure 5.2 shows the variation in the average velocity over time and aids with the identification of the crucial conditions within the DEM framework that affect the output properties (e.g. velocity). It reveals that the number of particles (comparing run 2 to 3 where the number of particles are significantly different) and the size of the particles (considering runs 3, 4, 6 which utilize large particles) influences the average velocity of particles most. Also, it confirms the minimal effect of density variation of particles (as they get wetted or agglomerated) on the flow pattern (comparing the average velocity results in Figure 5.2 for experiment 1 and 2 in Table 5.3). This result enabled us to ignore the variation in the density of particles during the granulation process. Hence, it is necessary to account for the change in the number of particles and their size with the progression of time. This test study performed a sensitivity analysis for identifying the crucial operating parameters that affect the flow pattern of the particles within the granulator.

From the above test study, it is clear that the change in the number and size of particles within the granulator have to be taken into account. DEM lacks the ability to accommodate the change in particle number and size automatically within the simulation. This is overcome by spanning the entire time domain through short DEM simulations which start with the intermediate PSDs and run for a short period of time. The lack of intermediate PSD data is fulfilled by obtaining the intermediate PSDs from the calibrated model (as described in section 5.1.1) using the end point PSD. It can be assumed that the dynamic trajectory of particle agglomeration and growth can be tracked by fitting the end point PSD. Multiple DEM simulations were run with varying set of polydisperse particles (based on the intermediate PSD information obtained from the model) and varying total number of particles. Since DEM has limitations in terms of the number of particles it can accommodate, the number of particles have been scaled

Table 5.3: DOE for the test simulations

Run	Particle Dia (mm)	Particle Density (kg/m^3)	Total number	Total vol (m^3)	Total mass (kg)	Mass/particle (kg)	Geometry scale (Volume)	Geometry scale (Length)
1	2	1500	20000	8.37×10^{-5}	0.12567	6.28×10^{-6}	1	1
2	2	3000	20000	8.37×10^{-5}	0.2513	1.256×10^{-5}	1	1
3	5	1500	1280	8.37×10^{-5}	0.12567	9.817×10^{-5}	1	1
4	5	3000	1280	8.37×10^{-5}	0.2513	0.0001963	1	1
5	2	1500	30000	0.0001256	0.1885	6.28×10^{-6}	1	1
6	5	96	1280	8.37×10^{-5}	0.00804	6.28×10^{-6}	1	1
7	2.5	1500	20000	0.0001636	0.2454	1.227×10^{-5}	1	1
8	2.5	1500	10240	8.37×10^{-5}	0.12567	1.227×10^{-5}	1	1
9	2	1500	20000	8.37×10^{-5}	0.12567	6.28×10^{-6}	0.512	0.8

(such that the starting number of particles is 20000 and the rest follow the scaling factor accordingly) in order to run the simulation reasonably. The purpose of running the multiple discrete simulations is to address the variation in the system behavior as a function of the varying particle properties (and number). Each DEM simulation was run for a time segment of 6 seconds over the liquid addition period and for 12 seconds during the wet massing period. The DEM simulations allow the detailed analysis of data and capture the occurrences within the granulator from a mechanistic point of view.

5.1.3   Clustering for compartment identification
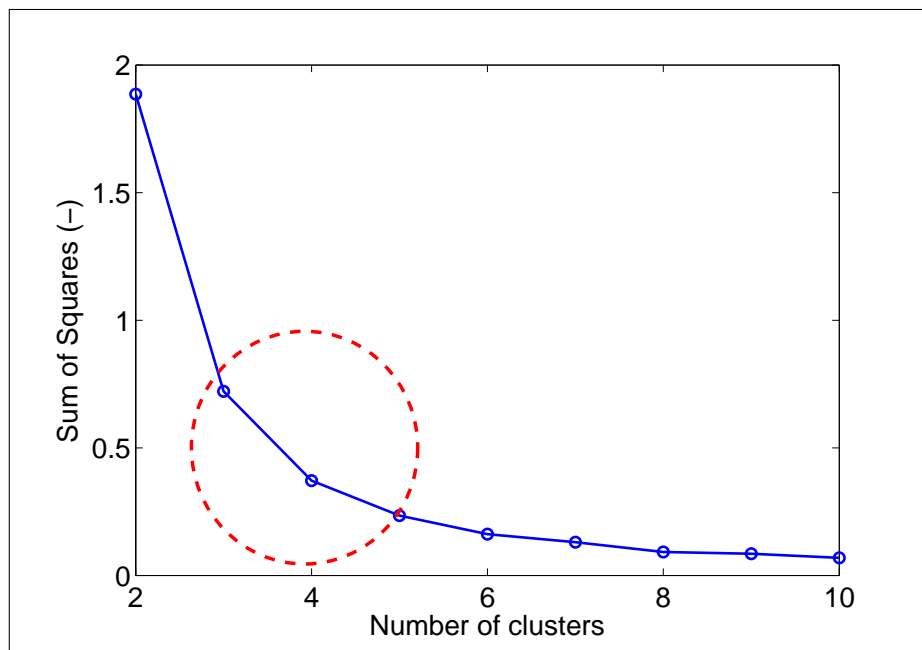
Figure 5.3: Sum-of-squares of variance for the clustering algorithm applied to experiment 11

Clustering methods are a set of popular tools using for data mining and machine learning purposes. It enables the grouping of datapoints that have similar attributes and also demarcates the group of points/clusters that behave differently. It can be successfully used to identify the compartments, which tend to group the points that behave similarly while isolating those groups from each other. For this purpose a simple unsupervised

learning technique-k means clustering algorithm has been utilized (Hartigan and Wong, 1979). It involves defining k centroids (each representing a cluster) that are placed in a systematic way within the dataset with the common choice being its placement farthest from each other. The next step involves associating all the points within the dataset to the nearest centroid that is a representative of the cluster. This leads to the formation of an initial set of clusters. The centroids (and hence the clusters) thus obtained are further revised and the step involving the association of the datapoints to the centroids is repeated. This happens iteratively until there is no change in the revised values of the centroids. The association step for identifying a cluster grouping for each points can be carried out using various criteria. The identification of the clusters is done based on the minimization of the sum of square error within the cluster (objective) function given by

$$SSE = \sum_{j=1}^{k} \sum_{i=1}^{n} ||x_i^{(j)} - c_j||_2^2 \tag{5.4}$$

where, $x_i^{(j)}$ represent the ith point within the dataset belonging to the jth cluster and c_j represents the centroid of the jth cluster. The distance between the points and the centroids are minimized in order to identify the clusters and the points lying within it. In this study, the euclidean distance has been considered as the criterion for obtaining the distance between the points and the centroids. Choosing an optimal value for k is also a crucial task. A lower value of k might lead to inadequacy with the clustering while a larger value of k can lead to overfitting. There are various approaches available for determining the optimal value of k e.g. Bayesian information criteria (BIC) (Kass and Wasserman, 1995) and various other well-established techniques. In this work, plotting the sum-of-squares of the variance as a function of the value of k followed by identifying the "elbow" of the plot (Yu et al., 2011) is utilized for fixing the value of k (compartments) within the framework. The partitioned dataset using the optimal k groups is then taken for further analysis of the data in order to obtain information about the isolated well-mixed compartments (clusters).

5.1.4   Data analysis and Analysis of Variance (ANOVA)

Regression analysis is performed on the *grouped* dataset obtained from the clustering analysis in order to obtain the relationship between the output properties as a function of the operating parameters. The clustering algorithm provides information about the number of clusters, the size of the clusters and the value of the centroids. This information is then taken to obtain the variation in the size of the clusters and the value of the centroids as a function of time, impeller speed and liquid to solids ratio. It is later discussed in the results section, how the number of clusters is found to be constant overall. The analysis of variance provides information with obtaining the significant operating conditions that affect the variation in the parameters for generating the compartments. This analysis leads to a compartment based model which is further utilized for the open-loop control as discussed in the following section.

5.2   Open loop control

Open loop control has been previously explored for certain particulate processes such as emulsion polymerization (Immanuel and Doyle III, 2003; Immanuel, 2002; Immanuel et al., 2007, 2008), however there has been no related work for improvement of the granulation process. Optimal control approach can lead to obtaining an optimal schedule for granulation operation such that the final granule properties match the desirable outcome. For implementing open loop control on the granulation process, a mechanistic model is required with detailed first principle based understanding of the effect of each operating parameter on the output properties. This kind of a study would enable us to identify the extent of manipulation needed for each operating condition such that the output properties would tend to match the desired value. The approach implemented in the works of Immanuel and Doyle III (2003) has been extended for a granulation process. One of the biggest gaps preventing this kind of a study from materializing is the lack of kernels that are not solely empirical, are a function of measurable operating parameters and are computationally inexpensive. The first two criteria for the kernels were satisfied, however the mechanistic kernel proposed by Immanuel and

Doyle III (2005) was associated with high computational overheads. This gap could be significantly bridged with the proposition of the semi-empirical, computationally inexpensive aggregation kernel (described in previous chapter) that takes into account the key parameters affecting the granulation outcome.

The problem statement involves obtaining an optimal recipe for operation of the granulation process based on detailed mechanistic knowledge and utilizing a compartment-based model. The crucial output quantities to be controlled during a granulation process are the particle size distribution and the particle porosity (Pandey et al., 2013). It should be noted that these multiple output quantities need to be simultaneously controlled for improved operation of the process. The overall optimization problem involving multiple objective functions can be solved using various gradient-based or metaheuristic optimization techniques. Immanuel (2002) had solved a similar problem for the emulsion polymerization process using a non-dominated sorting genetic algorithm (NSGA). This evolutionary algorithm was initially presented in the works of Deb et al. (2000) and was successfully implemented for obtaining the pareto optimal solutions of multi-objective optimization problems. The implementation of the NSGA method is however not strict and can be substituted by other equivalent algorithms that would serve the same purpose. It is however not a rigid choice for the optimization algorithm and can be substituted by various other optimization algorithm observed in the literature.

The multiple objectives involved in the optimization problem can also be dealt with in various ways. The optimization problem can be solved by formulating the objective function as a sum of the individual errors (weighted or non-weighted) in the quantities as shown in Equation (5.5)-(5.6). Another approach that can be used for developing the objective function could be considering the maximum of the multiple errors and then minimizing the maximum of those. This is also known as the min-max approach and has been shown in Equation (5.7). Yet another approach that can be used for the multiple objective functions is formulating the problem in an $\varepsilon - constraint$ form which involves minimizing a primary error/objective function and treating the other errors/objective functions as constraint applied to the system. This involves solving a multi-objective

system with a feasibility check based on the constraints applied to the system. The net result provides an optimal solution to the optimization problem which represents the best tradeoff solution considering both the objectives simultaneously (Equation (5.9).

$$Minimize \; \theta = \theta_1 + \theta_2 \tag{5.5}$$

$$Minimize \; \theta = w_1\theta_1 + (1 - w_1)\theta_2 \tag{5.6}$$

$$Minimize \; \theta = max(\theta_1, \theta_2) \tag{5.7}$$

$$Minimize \; \theta = \theta_1 \tag{5.8}$$

$$s.t \; \theta_2 < \varepsilon$$

where, ε is the tolerance value for the optimizer. The individual θ's can be given by

$$\theta_1 = \Sigma(PSD_{desired} - PSD_{computed})^2 \tag{5.9}$$

$$\theta_2 = (Porosity_{desired} - Porosity_{computed})^2 \tag{5.10}$$

Here, PSD represents the particle size distribution for the granules and porosity represents the porosity of the product class. A similar investigation can be found in the work by Bianco (2008), where multiple representations for the multi-objective optimization have been analysed along with the utilization of various optimization algorithms. This approach for obtaining an optimal schedule for running a granulation process can also be termed as a hierarchical control approach, where, the measurable quantities/process parameters influence the various mechanisms which in turn affect the final granule attributes (PSD, porosity). A schematic for this approach can be shown in Figure 5.4.
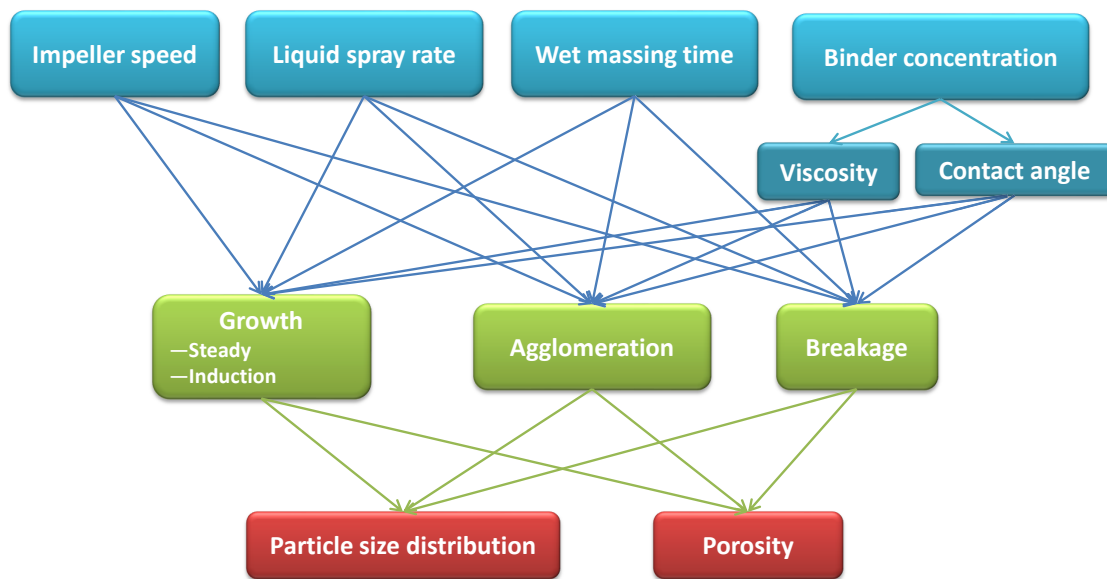
Figure 5.4: Schematic showing the hierarchy to be controlled while obtaining the optimal recipe for granulation

5.2.1 Model utilized for the open-loop control approach

The modeling framework utilized for the open-loop control approach involves considering a compartment based model along with various rate processes described using mechanistic information. The compartment model as described above has been utilized for this work. In addition to the mechanistic submodels as described above, the consolidation rate has also been expressed as a function of process parameters. Gantt et al. (2006) had earlier utilized the model proposed by Litster and Ennis (2004) which expressed the consolidation rate as a function of the impeller speed and the yield strength, Y_d. Similarly, the consolidation rate utilized in this work can be written as

$$\frac{dg}{dt} = a_1 exp^{(a_2 St_{def})} \frac{(s+l+g)(1-\epsilon_{min})}{s} \times [l - \frac{\epsilon_{min}s}{1-\epsilon_{min}} + g] \qquad (5.11)$$

where, a_1 represents the rate of collision (considered an empirical quanitity in this case), a_2 is an empirical constant and St_{def} is the Stoke's deformation number ($St_{def} = \frac{mu_0^2}{2D^3Y_d}$). It is a function of the particle mass, m, particle velocity, u_0, particle diameter, D and yield strength, Y_d. The yield strength of granules is a function of the moisture content, however there is no concrete information relating the moisture content of particles to the yield strength. Thus, we have considered the yield strength to be constant (irrespective of the moisture content or porosity of granules). The crucial operation conditions affecting the final granule attributes include the liquid to solid ratio, impeller speed, wet massing time, viscosity of the binder and the contact angle. The liquid to solid ratio can be manipulated by changing the flowrate of the liquid to the system. Changing the impeller speed for the high-shear granulator is also quite straight-forward. The viscosity and contact angle of the binder can be manipulated by changing the concentration of the dissolved solid in the binder. Considering the system to consist of microcrystalline cellulose (MCC) granulated using polyvinylpyrrolidone (PVP), the information relating the concentration to the viscosity and contact angle of the binder solution is obtained from literature (Benali et al., 2009). Based on the data for pure water, 2 %, 3 % and 5 % solutions of PVP, a regression approach is used to obtain an expression describing the variation in the viscosity and contact angle as a function of the binder solid concentration in the solution. These correlations have been fed into the model in order to accommodate the variation in the viscosity and contact angle of the binder as a function of its concentration in the solution.
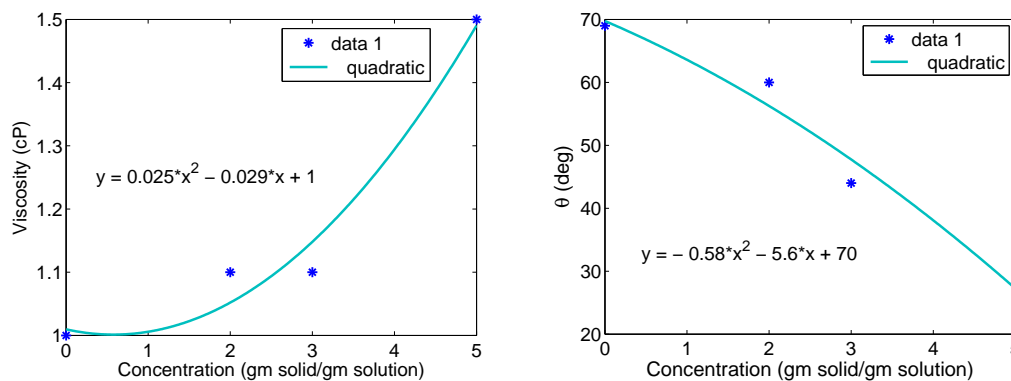
(a) Variation of viscosity with binder concentration

(b) Variation of contact angle with binder concentration

Figure 5.5: Regression for relating the contact angle and viscosity with the binder concentration

As discussed before, various optimization algorithms can be used to solve this problem in order to decide on the operating conditions to get a target distribution. However, since there are multiple CQAs involved, the optimization algorithm is expected to yield solutions belonging to the pareto front. The optimal solutions can be obtained by treating the multiple objective functions in various ways (Equations (5.5)-(5.9)). The ε-constraint approach can be accommodated using a metaheuristic technique or by scripting the optimization algorithm. However, the metaheuristic techniques are more computationally expensive and thus the best choice would be to utilize a gradient-based or simplex approach for the optimization. The objective function can be treated as a weighted sum of the multiple objective functions. It should be ensured that an optimal solution is existent for a specific pair of weighting factors and the model is also capable. The detailed analysis for the existence of optimal solution is discussed in section 5.3.

5.3 Results and discussions

5.3.1 Data analysis results for compartment model formulation
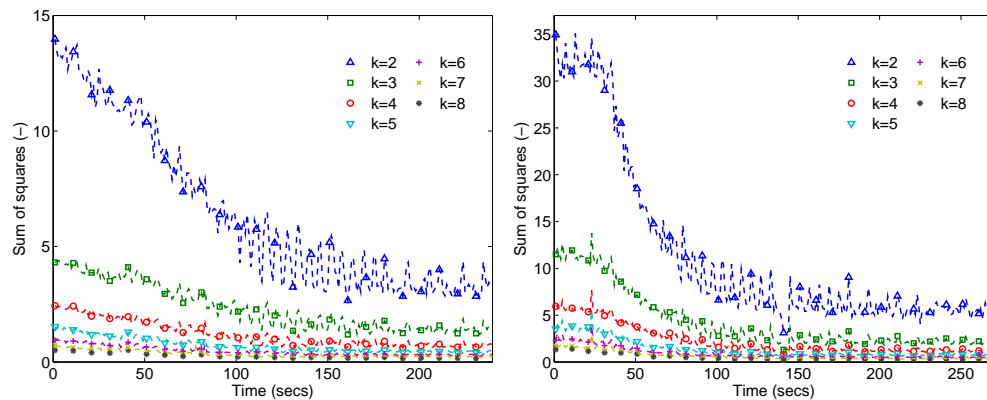
(a) Batch 2

(b) Batch 3
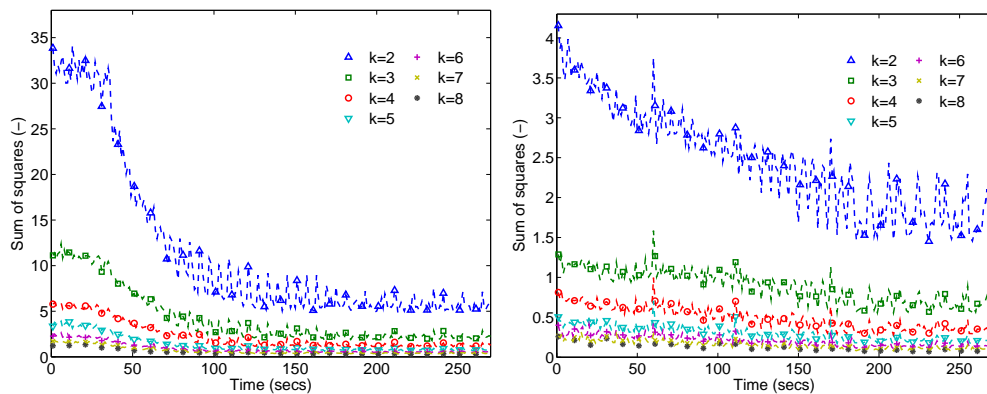
(c) Batch 7

(d) Batch 8
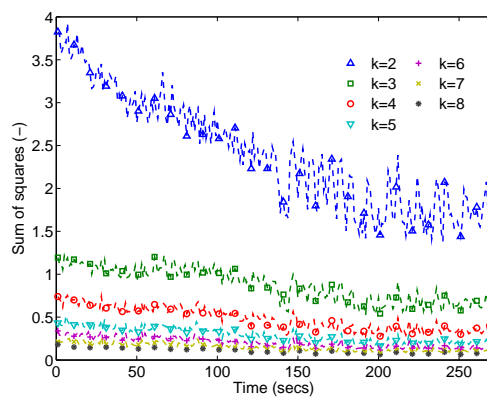
(e) Batch 11

Figure 5.6: Time evolution of the sum-of-squares of variance for varying choice of k

(a) t = 1

(b) t = 30

(c) t = 100

(d) t = 180
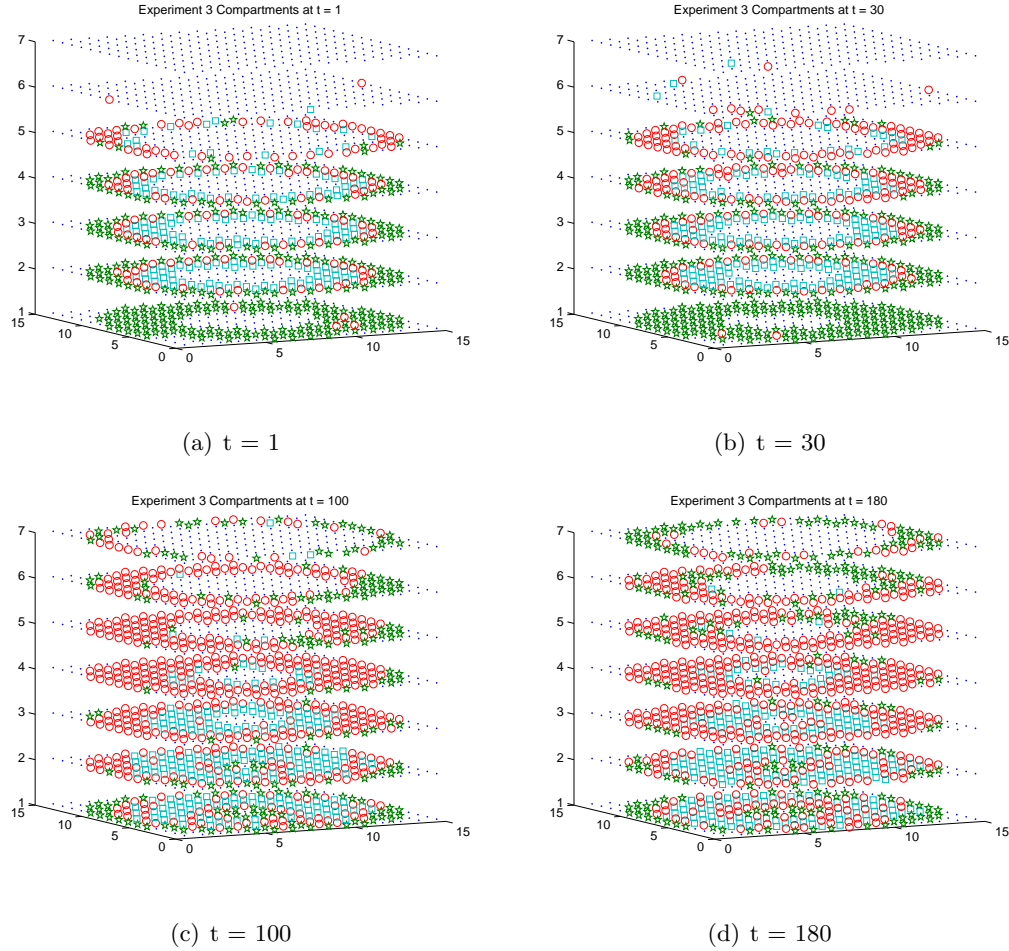
Figure 5.7: Clusters within the granulator at different time instances ($\cdot$ − compartment 1, $\circ$−compartment 2, $\square$−compartment 3, $\star$−compartment 4). The X, Y and Z axis depicts the *gridbingroup*s in the DEM simulation replicating the granulator

The analysis of the data has been performed in multiple steps and involved the utilization of various statistical tools. The intermediate PSDs for running the DEM simulations have been obtained from model calibration using experimental data. Table 5.1 lists the estimated values of the empirical parameters obtained from the model calibration study. From there on, the results have been analyzed statistically to gain more insight towards the occurrences within a high-shear granulator operating in batch mode. The granulator geometry within the DEM framework has been discretized into 15, 7 and 15 grids (*gridbingroup*) in the x, y and z directions respectively in order to accommodate enough particles within a *gridbingroup* while not considering excess

number of particles such that the resolution gets bad. This choice of the number of grids is used to ensure stability of the results. The average velocity values have been exported from the DEM simulations at each second (averaged over a time period of 0.2 seconds) for each of the grids and have been utilized further for the analysis. The k-means clustering algorithm was run on the exported velocity data and based on identifying the elbow of the sum-of-squares of variance, the optimal number of clusters was 4. This is also shown in Figure 5.3.
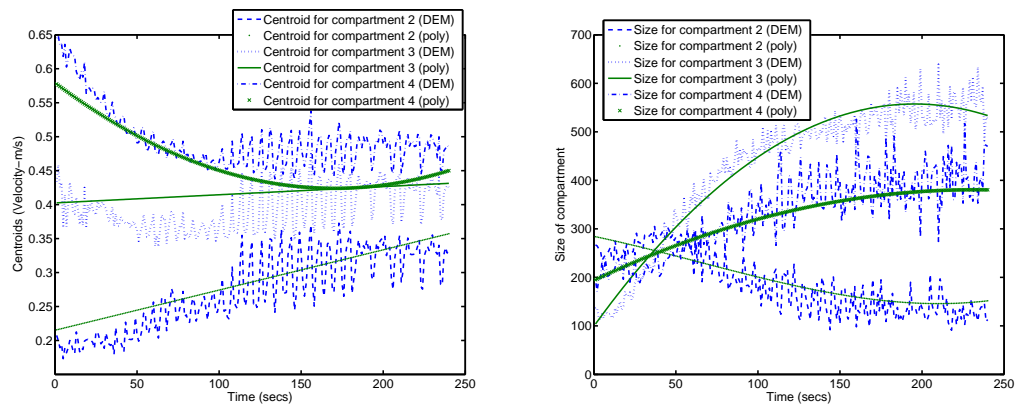
(a) Centroid values for L/S=25%, Impeller speed=4.75 m/s

(b) Cluster sizes (number of *gridbingroup* belonging to a cluster) for L/S=25%, Impeller speed=4.75 m/s
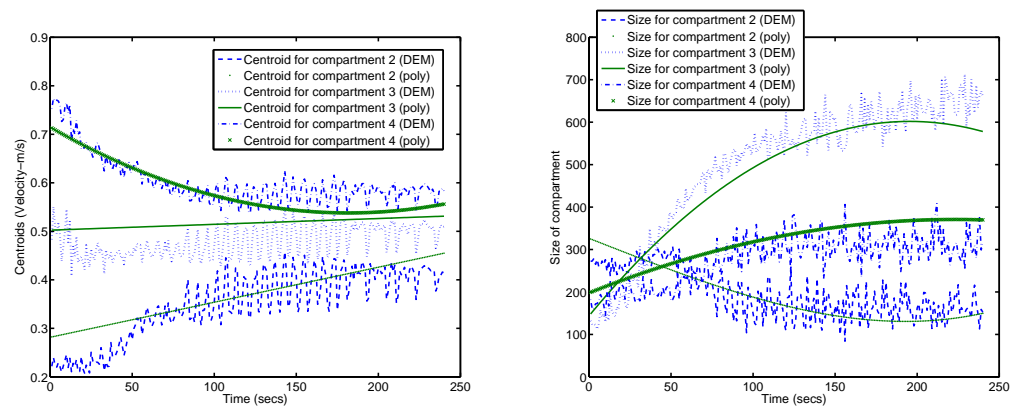
(c) Centroid values for L/S=30%, Impeller speed=5.05 m/s

(d) Cluster sizes (number of *gridbingroup* belonging to a cluster) for L/S=30%, Impeller speed=5.05 m/s

Figure 5.8: Validation results from the regression analysis

The time evolution of the sum-of-squares was also performed from the clustering algorithm applied to the different experimental datasets. The time evolution of the sum-of-squares is shown in Figure 5.6. It should be noted that for all the experiments, the distance between the time evolution for $k = 4$ onwards gets significantly densified. This confirms the choice of $k = 4$ for the optimal number of clusters to adequately address the inhomogeneities within the granulator in terms of the average velocity. The four clusters/compartments within the granulator indicate-the region of zero velocities (due to absence of particles), the region of high velocity, region of low velocity and the shear zone. Figure 5.7 reveals the variation in the cluster sizes as a function of time for experiment 3. The clustered datapoints comprise of the grids which have similar average velocity values within the granulator. Also each cluster is assigned with a representative average velocity value (centroid). The size of a cluster indicates the number of grids within the DEM discretization of the granulator that have similar velocity characteristics. The size of the cluster can thus enable to depict the volume fraction within the granulator volume that have a certain average velocity. This information is needed for the formulation of the compartment model.

The results from identifying the compartments with respect to velocity have been further analyzed using ANOVA and regression analysis in order to obtain the relationship between the output quantities (centroids and sizes of each compartment) as a function of time, impeller speed and liquid to solid ratio. The software Design-Expert$^{®}$ (by Stat-Ease, Inc) was used for obtaining the ANOVA results from the data. To begin the analysis, the initial models were assumed to have a quadratic form for the centroid output and a cubic form for the size output. Insignificant terms not needed for preserving the hierarchy of the model were then dropped from the regression equations. Tables 5.4 and 5.5 summarize the results from the analysis of variance study. It can be seen that time and the impeller speed have a prominent influence on the variation in the size (volume boundary) and centroids of the various compartments. The liquid to solid ratio does not affect the compartments (across experiments) with respect to velocity variation due to the fact that the contact model used within the DEM simulation did

not take cohesion into account. Thus, the change in the velocity patterns (across experiments) due to cohesion within the system could not be identified. However, it is expected that a contact model that takes into account the cohesion within the system, should be able to account for the variation in the size and centroids of the compartments (across experiments when the operating conditions are varied) as a function of the liquid to solid ratio. It should be noted that the first cluster within the granulator represents the empty space that is devoid of particles and hence is neglected in this study.

Table 5.4: Summary of the centroid and size fits developed with ANOVA

Property	DF	Mean	SD	F Value	R-Squared
Centroid for Shear Zone	3	0.30 m/s	0.036 m/s	8745.44	0.9522
Centroid for Low Velocity Bulk	2	0.40 m/s	0.026 m/s	32649.43	0.9802
Centroid for High Velocity Bulk	5	0.51 m/s	0.025 m/s	21881.67	0.9881
Size for Shear Zone	10	526.5 grids	133.55 grids	82.68	0.3871
Size for Low Velocity Bulk Zone	5	1125.3 grids	137.85 grids	2213.76	0.8939
Size for High Velocity Bulk Zone	6	739.1 grids	93.5 grids	701.20	0.7621

In order to address the heterogeneity in terms of liquid, a unique spray zone has been identified within the granulator which is depicted by the volume which contain wet particles as soon as the liquid drop hits the particle bed. In order to avoid complexity, the number of clusters with respect to the liquid distribution is considered to be 2 which can differentiate between the bulk and the spray zone. For each discrete (6 second of simulation) simulation, the liquid content of the particles is exported at the time value when the liquid particles just hit the particle bed and wets a particles lying in the spray zone. The number of cells within the granulator is identified from the clustering algorithm and was found to lie between a value of 1-4. The variation in the number of cells was observed to be randomly oscillating between the above-mentioned range, hence an average value for the number of volume grids and centroids have been adopted for each experimental dataset.

The polynomial expressions (Table 5.5) obtained from the regression analysis have been validated using DEM results for experiments modeled under different operating

Table 5.5: Polynomials for centroids and sizes developed from ANOVA (where A is Time, B is Liquid Content, C is Impeller Speed)

Property	Significant Terms	Polynomial
Centroid for Shear Zone	A,C	$-0.64 - 1.08 \times 10^{-3}A + 0.18C + 3.52 \times 10^{-4}AC$
Centroid for Low Velocity Bulk Zone	A,C	$-0.88 + 1.20 \times 10^{-4}A + 0.27C$
Centroid for High Velocity Bulk Zone	A,C	$-0.43 - 2.58 \times 10^{-4}A + 0.07C - 3.30 \times 10^{-4}AC + 5.36 \times 10^{-6}A^2 + 0.03C^2$
Size for Shear Zone	A,B,C	$-366.2 + 11.77A + 11.69B + 101.4C - 0.222AB - 1.95AC - 0.036A^2 - 0.197B^2$ $+7.02 \times 10^{-3}A^2C + 3.73 \times 10^{-3}AB^2 + 1.38 \times 10^{-5}A^3$
Size for Low Velocity Bulk Zone	A,B,C	$-390.0 + 4.69A - 9.80B + 133.5C - 0.012A^2 + 0.16B^2$
Size for High Velocity Bulk Zone	A,B,C	$-115.6 + 2.39A + 29.0B - 24.37C - 0.164AC - 3.47 \times 10^{-3}A^2 - 0.48B^2$
Size of Spray Zone	B,C	$1.585 - 0.022B + 0.11C - 2.45 \times 10^{-3}BC + 3.79 \times 10^{-4}B^2$

conditions. Two sets of DEM simulations were run for L/S content of 25 %, impeller speed of 4.75 m/s and LS content 30 % and impeller speed of 5.05 m/s which were used for validation purposes. The cluster sizes and centroids were identified from the DEM simulations for these two sets of operating conditions and were validated against the values obtained from the regression polynomials. Figure 5.8 reveals that the regression analysis lead to predictive results and can thus be extended for further interpolation.

5.3.2   Formulation of the compartment model
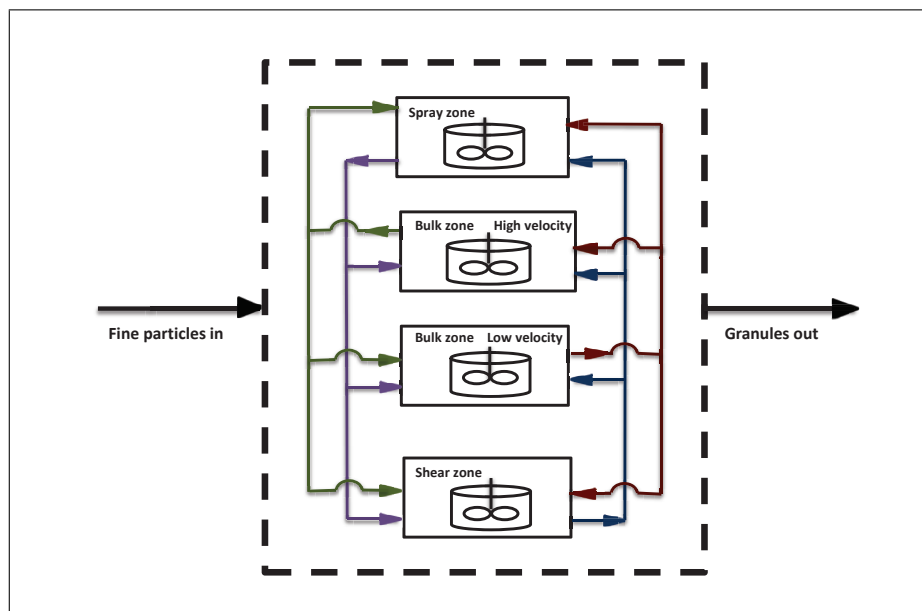
Figure 5.9: Schematic showing the formulation of the compartments within the granulator
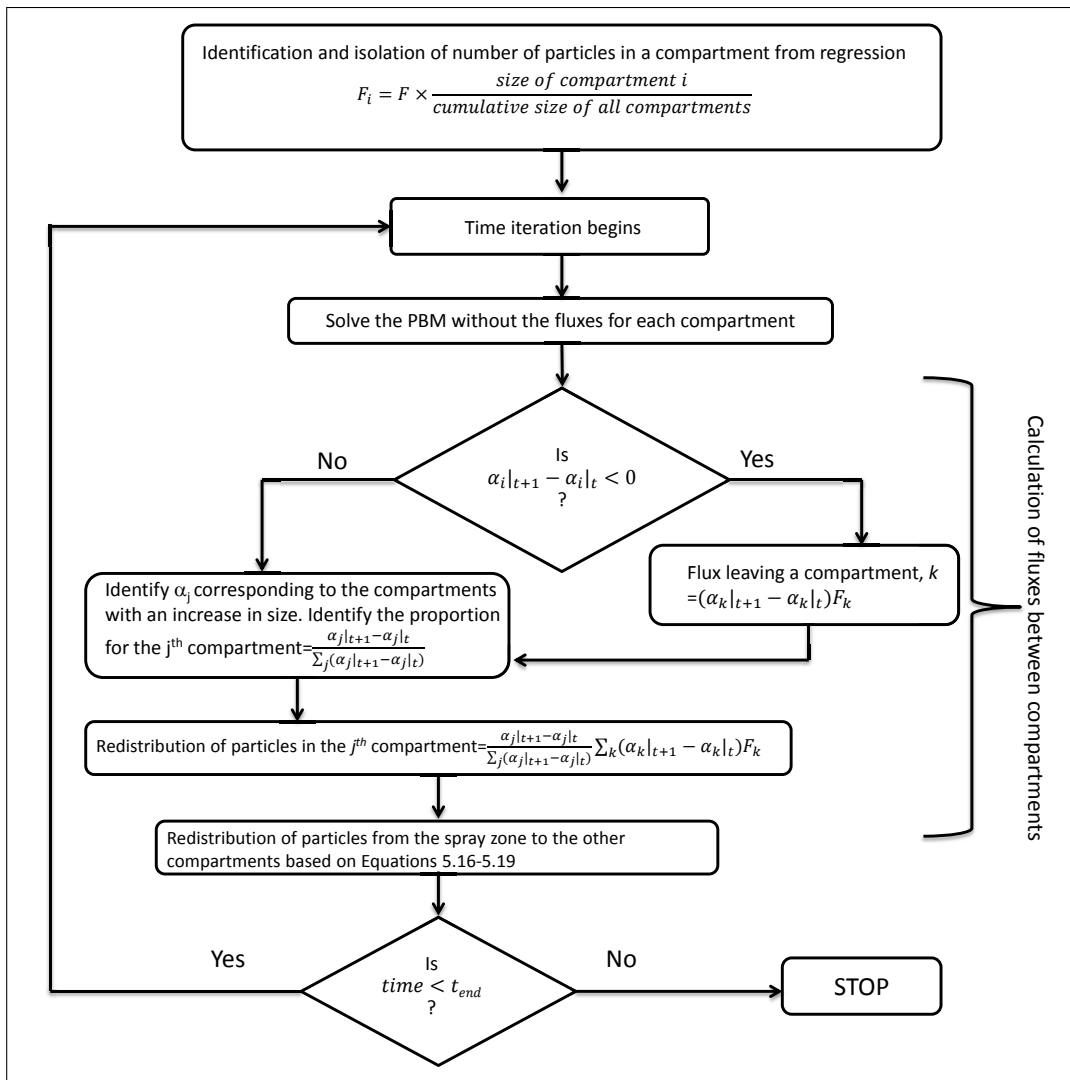
Figure 5.10: Algorithm used for formulating and solving the compartment model

The compartment model is expected to sufficiently track the inhomogeneities within the granulator. The various compartments that have been identified from the above analysis leads to the demarcation of four distinct regions within the granulator in terms of velocity and liquid distribution. The spray region, the shear region, and high and low velocity region within the bulk can address the heterogeneities in a lumped manner. The spray region is characterized by the wetting mechanism, the shear zone comprises of breakage while the bulk (high and low velocity) comprise of primarily aggregation and consolidation along with some breakage. The overall granulator can be modeled using four compartments that contribute to a particular mechanism and which also

exchange particles between each other in an arrangement similar to parallel electrical circuits. Figure 5.9 shows a schematic describing the formulation used for the compartment based framework. The various compartments within the granulator are marked by a specific mechanism that is dominant in that region. The spray compartment is characteristic of the wetting of particles while the bulk region (both high and low velocity region) comprises of the consolidation, aggregation and breakage mechanisms. The shear compartment is marked by the dominance of the breakage mechanism due to the high amount of shear within the region because of the large velocity gradient. This framework can be represented in the form of a system of partial differential equations as shown in Equation (5.12)-(5.15).

$$\frac{\partial}{\partial t}F_1(s,l,g,t) + \frac{\partial}{\partial l}\left[F_1(s,l,g,t)\frac{dl}{dt}\right] = Flux_{1,\Delta\alpha}(s,l,g,t) + Flux_{1,wet}(s,l,g,t) \quad (5.12)$$

$$\frac{\partial}{\partial t}F_2(s,l,g,t) + \frac{\partial}{\partial g}\left[F_2(s,l,g,t)\frac{dg}{dt}\right] = \Re_{agg,2}(s,l,g,t) + \Re_{break,2}(s,l,g,t) \quad (5.13)$$

$$+ Flux_{2,\Delta\alpha} + Flux_{2,wet}(s,l,g,t)$$

$$\frac{\partial}{\partial t}F_3(s,l,g,t) + \frac{\partial}{\partial g}\left[F_3(s,l,g,t)\frac{dg}{dt}\right] = \Re_{agg,3}(s,l,g,t) + \Re_{break,3}(s,l,g,t) \quad (5.14)$$

$$+ Flux_{3,\Delta\alpha}(s,l,g,t) + Flux_{3,wet}(s,l,g,t)$$

$$\frac{\partial}{\partial t}F_4(s,l,g,t) = \Re_{break,4}(s,l,g,t) + Flux_{4,\Delta\alpha}(s,l,g,t) + Flux_{4,wet}(s,l,g,t) \quad (5.15)$$

where, F_i represents the number of particles enclosed within the ith compartment. The number of particles in the ith compartment is obtained by multiplying the initial size fraction of the ith compartment (size of the ith compartment/sum of sizes of all compartments) to the total number of particles present within the granulator. For the granulation process, since there is an overall change in the particle size and the number of particles involved, mechanistically tracking the fluxes ($Flux_{i,\Delta\alpha}$ and $Flux_{i,wet}$) between the particles becomes complicated. The compartment model presented in this section first isolates the number of particles enclosed within each compartment followed by updating the PBM for the particular compartment which modifies the evolution of a particular property amongst a number of particles that are present in the compartment.

The fluxes ($Flux_{i,\Delta\alpha}$) entering or leaving a compartment is calculated based on the size change of each compartment while $Flux_{i,wet}$ enables the distribution of wet particles from the spray zone to the various compartments and vice-versa. The variable α_i represents the normalized size of the compartment or the size fraction of a compartment ($\alpha_i = size\ of\ compartment\ i/cumulative\ size\ of\ all\ compartments = V_i/\Sigma_i V_i$). The fluxes between the compartments are a function of the change in their respective α's over time and also due to the distribution of wet particles from the spray zone. In order to conserve the total volume of the spray compartment, the fluxes owing to the circulation of wet particles are calculated as

$$Flux_{1,wet} = -0.6 \times F_1(s,l,g,t) + 0.6 \times \tfrac{V_1}{3V_2}F_2(s,l,g,t) + 0.6 \times \tfrac{V_1}{3V_3}F_3(s,l,g,t) \quad (5.16)$$

$$+0.6 \times \tfrac{V_1}{3V_4}F_4(s,l,g,t)$$

$$Flux_{2,wet} = 0.6 \times \tfrac{F_1(s,l,g,t)}{3} - 0.6 \times \tfrac{V_1}{3V_2}F_2(s,l,g,t) \quad (5.17)$$

$$Flux_{3,wet} = 0.6 \times \tfrac{F_1(s,l,g,t)}{3} - 0.6 \times \tfrac{V_1}{3V_3}F_3(s,l,g,t) \quad (5.18)$$

$$Flux_{4,wet} = 0.6 \times \tfrac{F_1(s,l,g,t)}{3} - 0.6 \times \tfrac{V_1}{3V_4}F_4(s,l,g,t) \quad (5.19)$$

It is assumed that when the size of a compartment at the $t + 1^{th}$ time instant is less than the tth time instant, particles leave that compartment. This way the F arrays are accumulated for each compartment where the size of the compartment shrinks. This F distribution is then redistributed amongst the particles which have an increase in the size of the compartment at the $t + 1^{th}$ time instant compared to the tth instant. The redistribution of the particles leaving certain compartments into other compartments are done in proportion to the increase in their sizes. The fluxes ($Flux_{i,wet}$) is however calculated based on the the circulation of the wet particles from the spray zone into the other compartments. A schematic of the compartment model formulation and solution is shown in Figure 5.10. The identification of the compartment sizes and then isolating the mechanisms on particles belonging to a certain number of particles and thereby introducing the fluxes between compartments can represent the inhomogeneities observed in the granulator. The semi-mechanistic aggregation kernel utilized to represent

the aggregation mechanism within compartments 2 and 3 is a function of the velocity and liquid content. Thus the agglomeration behavior in compartments 2 and 3 will be different owing to their difference in liquid content (due to the fluxes) and their velocity (imparted by the agitation). The breakage mechanism considered in compartments 2, 3, and 4 are also a function of the shear present within the compartment (and hence an artifact of the velocity variation). Thus the breakage pattern within these compartments vary based on the velocity variation in these compartments. This work does not consider the mechanistic breakage kernel proposed by Ramachandran et al. (2009), however including the mechanistic breakage kernel within the model can also enable to account for the breakage behavior as a function of the liquid content present within the compartment. This suggests the ability of the compartment model to capture the varied behavior of the various mechanisms within each compartment as a function of its velocity and liquid attributes.

It should be noted that for this modeling framework, an accurate model for the surface renewal theory based approach has not been implemented for the spray zone. All particles are added or removed from a compartment based on the net change in their α's. The implementation of a surface renewal based approach to the spray zone is expected to be a more accurate representation, however it is beyond the current scope of the model presented in this thesis. However, in order to account for the renewal of the wet surface in the spray zone, 60 % of particles within the spray zone are circulated to other compartments in order to allow distribution of the liquid. Another assumption with the distribution of particles amongst compartments involve reassigning same volume (based on 60% of the particles in the spray zone) of wet particles within each of the other three compartments. This is however an arbitrary choice for circulating the wet particles and a more accurate modeling approach would be to implement the principles of surface renewal theory (Sherony, 1981).

The primary objective behind formulating a compartment-based model is to be able to successfully track the inhomogeneities within the "well-mixed" high-shear granulator. Some consequences of considering a well mixed homogeneous model includes the incapability in tracking the mechanical-dispersion regime (Hapgood et al., 2003). A wider

PSD is expected when the system is not well-mixed or the binder is not distributed properly across the granulator. Hapgood et al. (2003) correlated the mechanical-dispersion regime as a function of the spray flux. The spray flux can be attributed to the various process parameters such as the viscosity of the binder, the mode of binder addition, the amount of binder added. Using the compartment model presented in this work, not only can these conditions be effectively captured, but the variation in the mechanisms due to changing average velocity can also be accounted for. It is expected that the PSD would be wider for a more heterogeneous case. It can be seen in figure 5.11 that the evolution of the particle properties are different in each compartment owing to the mechanism that is predominant in the compartment. Thus, the liquid content is very different in each of those regions initially, however with time, the liquid homogenizes between the compartments and attain the same value. As expected, there is a larger amount of fines at earlier time points, however with the progress of time, the number of fines decrease while the number of coarse particles increase. Compartment 1 is dominated by the wetting mechanism (spray zone) and hence suggests large particles (or nuclei) that are also significantly moist compared to the particles in the other compartments. Compartment 4 (shear region) on the other hand is predominated by breakage and hence suggests the existence of a large amount of fines (as also shown in Figure 5.11). As a consequence of this approach, the overall PSD within the granulator is also wider in case of the compartment model (as shown in Figure 5.12). However, as time progresses, the system homogenizes and as expected intuitively, the PSD gets narrower. This suggests the capability of the compartment model to be able to capture the mechanical dispersion regime. The utilization of a compartment model can thus enable better representation of the granulation process taking place in a high-shear granulator.
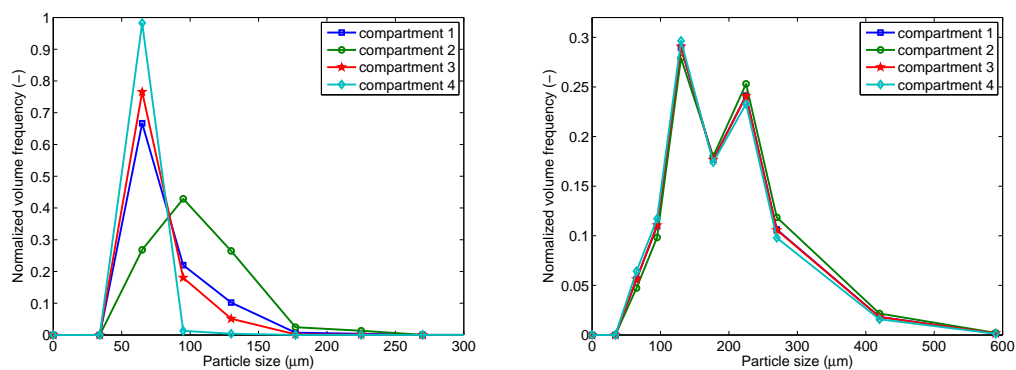
(a) PSD within each compartment at t=180 seconds

(b) PSD within each compartment at t=280 seconds
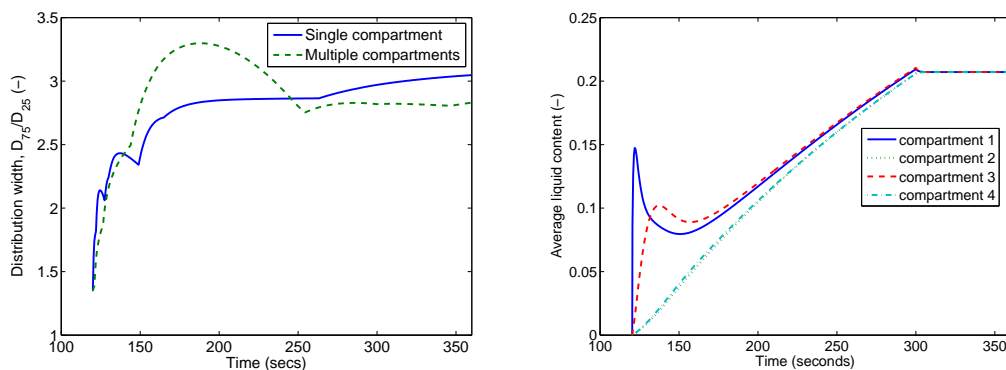
(c) Evolution of the distribution width over time

(d) Average liquid content within each compartment

Figure 5.11: Comparison of the evolution of size distribution within the single and multi-comparment model. Evolution of liquid content within each compartment (multi-compartment model) over time
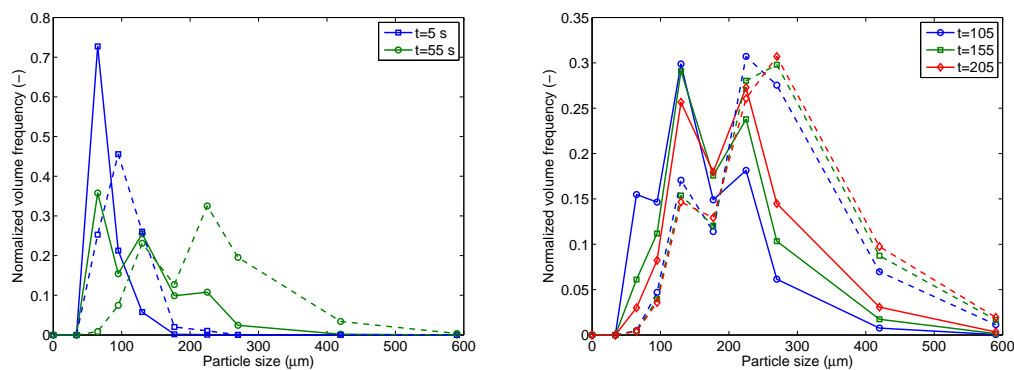
(a) PSD for the single and compartment model at initial time instances (single=dashed line, compartment=solid line)

(b) PSD for the single and compartment model at later time instances (single=dashed line, compartment=solid line)
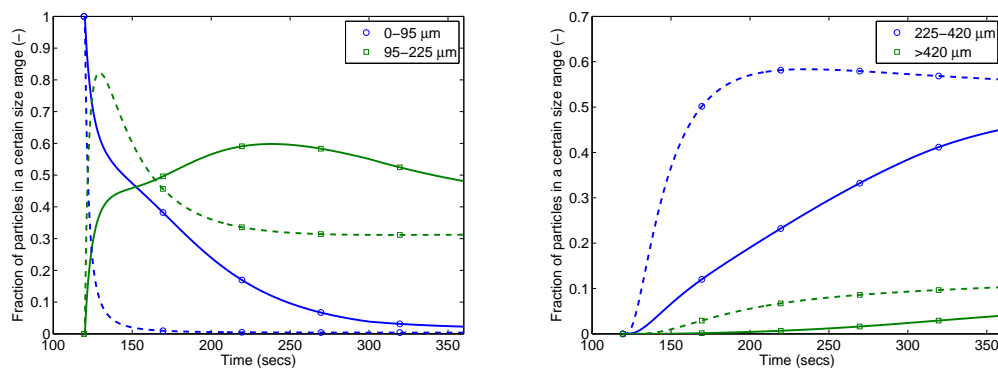
(c) Evolution of the PSD (for finer particles) over time (single=dashed line, compartment=solid line)

(d) Evolution of the PSD (for coarser particles) over time (single=dashed line, compartment=solid line)

Figure 5.12: Comparison between the single and multi-compartment model (time mentioned in the legend is after the onset of liquid addition)

5.3.3   Existence of optimal solutions for open loop control

It is crucial to check the possibility of obtaining an optimal solution for the open-loop control problem based on implementing the optimization as a weighted sum of the multiple objective functions. The granulation process that is represented using a compartment model (as discussed above) and considering mechanistic submodels for the various mechanisms is utilized for this analysis. The description of the model is

provided above. In order to test the applicability of a weighted sum for the multiple objectives, the model is run with varying values for the different variables that are optimized using the open-loop control approach. The different variables were varied at different levels and the individual errors (PSD and porosity) were plotted for a combination of these different variable values. From Figure 5.13 (a) it can be seen that for certain combination of variables, both the errors can be reasonably minimized. Thereafter, using varying levels of the weighting factor, w_1, the optimization was run (using the same initial guess). The optimization algorithm utilized for this purpose includes the Nelder-Mead simplex approach which is implemented using the $fminsearch$ solver provided by $MATLAB^{\circledR}$ 2013b. Figure 5.13 (b) shows the optimized solution based on varying weights for summing the multiple objective functions. It can be seen that for a few set of w_1 values, the overall error can be significantly minimized. These studies have been used to further the appropriate choice for the weighting factors for the objective functions. Based on this figure, a w_1 value of 0.65 has been chosen to weigh the error with respect to the PSD while $1 - w_1$ equaling 0.35 has been used to weigh the error with respect to the porosity.
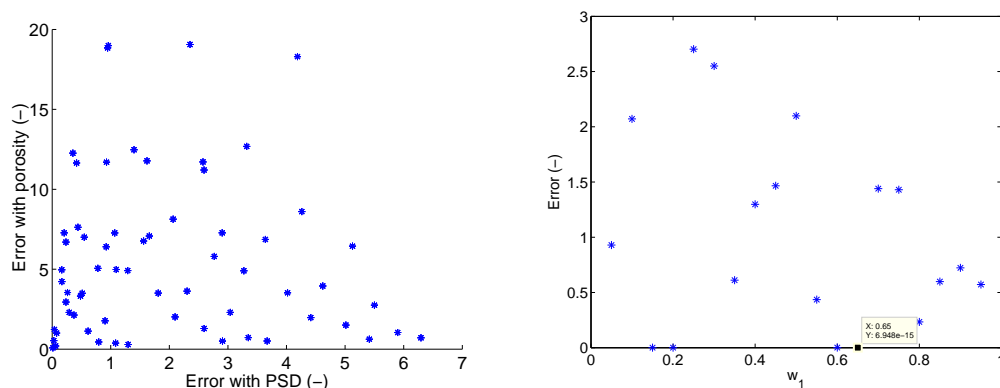
(a) Plotting the errors with respect to PSD vs that for porosity by varying the values for the operating variables

(b) Error minimization using varying w_1 and $(1 - w_1)$ combinations

Figure 5.13: Analysis for testing the existence of optimal solutions using a weighted sum of errors

5.3.4 Optimal solutions

Based on the discussion provided in the previous sub-section, the optimization problem thus posed and solved can be written as

$$Minimize\ \theta = 0.65\theta_1 + 0.35\theta_2 \tag{5.20}$$

where,

$$\theta_1 = \Sigma(PSD_{desired} - PSD_{computed})^2 \tag{5.21}$$

$$\theta_2 = (Porosity_{desired} - Porosity_{computed})^2 \tag{5.22}$$

The optimal values for the various operating parameters that are aimed to be obtained include the liquid amount/liquid flowrate/liquid to solid ratio, speed of the impeller, concentration of the binder and the end point for running the process. For this study, the liquid addition has been fixed, thus the end point of the granulation is decided based on the wet massing time. The desired PSD and porosity are obtained from the simulation itself, using certain values for the operating conditions. The study is formulated in the form of an inverse problem, whereby the optimal values for the variables in order to achieve a specific CQA is a known quantity. In order to mimic a more flexible process, the liquid addition has been varied as a piecewise constant function over time with the rate being fixed over four intervals. The simulated process spans over a time duration of 4 minutes plus the wet massing time. The wet massing time was fixed at 30 seconds in order to simulate the target distributions. The model has been run for a dry mixing time of 2 minutes, followed by the addition of liquid over 2 minutes. Within the 2 minute duration for adding liquid, the liquid rate was held constant over a period of 30 seconds (thus suggesting four varying flowrates held constant over 30 seconds). Intermediate distributions were also considered in the optimization in order to account for the dynamic parametric values. The initial settings used for generating the target distribution are shown in table 5.6

Table 5.6: Settings used for the operating conditions in order to obtain the desired distributions

Parameter name	Set value	time duration
Dry mixing time		120 seconds
Liquid rate	10 %	120-150 seconds
Liquid rate	15 %	150-180 seconds
Liquid rate	20 %	180-210 seconds
Liquid rate	40 %	210-240 seconds
Concentration of binder	2 %	entire time
Impeller speed	350 rpm	entire time
Wet massing time		30 seconds

The target distribution generated using these parametric settings are shown in Figure 5.14

(a) Target PSD used for the optimization

(b) Target porosity distribution for the optimization
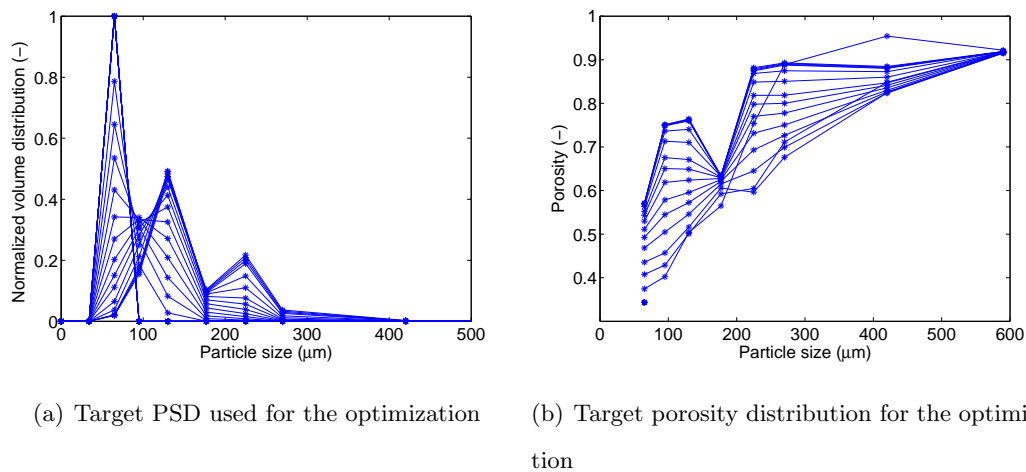
Figure 5.14: Target distributions used for the optimization over time

This data is fed into the Nelder-Mead simplex algorithm and the optimization is thus run. The optimal values and outcome distributions obtained from the optimization are shown in Figure 5.15.

(a) Optimized simulated PSD

(b) Optimized simulated porosity
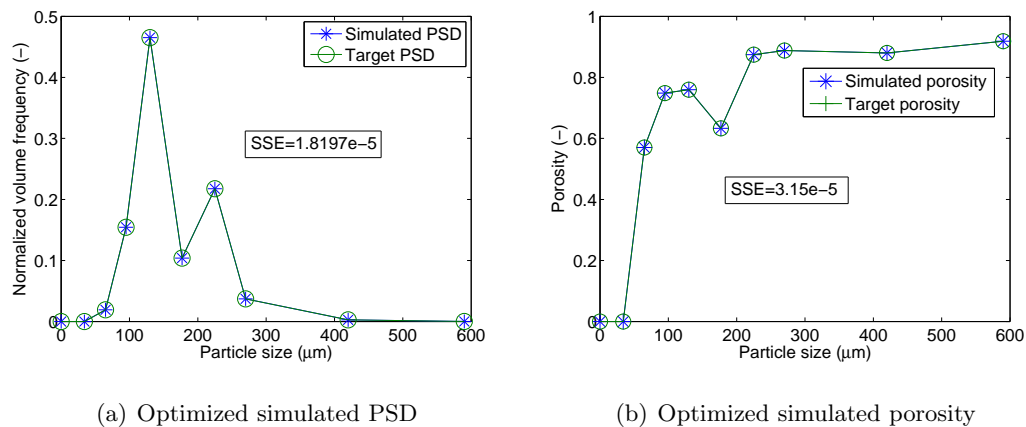
Figure 5.15: Comparison of the optimized results against the target distributions at final time instance

It should be noted that the results have also been plotted at intermediate time instances, and there is a good agreement between the experimental and simulated results. The operating settings obtained from the optimization is presented in Table 5.7. Additional analysis is also performed in order to gain insight on the extent of error from the optimization.

Table 5.7: Optimized values for the operating conditions and the error analysis

Parameter name	Optimization prediction	Relative error %
Liquid rate	10.0138 %	0.14
Liquid rate	15.0068 %	0.05
Liquid rate	19.9779 %	0.11
Liquid rate	40.072 %	0.18
Concentration of binder	1.98 %	0.04
Impeller speed	350.154 rpm	0.77
Wet massing time	16.106	46.33

The above table indicates the error between the target and the optimized operating conditions to be minimal. The optimal solutions can be obtained based on the approach suggested above. There is a significant mismatch between the wet massing time for granulation, however, the error between the simulated and target PSD are very low. A dynamic sensitivity analysis might facilitate the identification of the crucial parameters for efficient particle design of the granules.

5.4   Chapter Conclusions

A high-shear granulator is typically modeled as a single well-mixed compartment. However from this analysis it can be seen that there exists heterogeneities within the granulator with respect to liquid content and particle velocity. The high-shear granulator generally operates under the mechanical dispersion regime which is a heterogeneous system. Our hypothesis suggests that a single well mixed compartment representation of the high shear granulator is inaccurate. A multi-scale approach using a coupled model can provide an improved description of the granulation process, however, demarcating fewer compartments within the high-shear granulator and using the model presented in this work is less time consuming and can also address the variations within a granulation. The compartment model can account for these heterogeneities within the granulator and can successfully capture the mechanical dispersion regime. The results from this study can also be extended for different operating conditions within the design space in order to identify the number, size and centroid value of the compartments. A multi-compartment approach to model the high-shear granulator is better owing to its capabilities to address the inhomogeneities within the system. Another advantage of utilizing the compartment model is it capability of capturing the mechanical dispersion regime. The conventional approach of modeling a high-shear granulator is by assuming it to be a single well-mixed compartment, however the powerful statistical tools reveal the existence of heterogeneities within the vessel. Using the regression analysis, this compartment model can not only be developed for the present system, but can also be interpolated for different experimental systems by varying the impeller speed and the liquid content.

The figures suggest different distribution for the particle sizes and the liquid content within the different compartments. The aggregation and breakage kernel are a function of the velocity which imparts to the varied behavior of the particles within each compartment. This approach accounts for the heterogeneities within the granulator. This is the classical observation of the behavior under mechanical dispersion regime. With the progression of time, the compartments within the granulator homogenize thus

leading to the narrowing in the PSD over time. The compartment model is expected to make improved predictions to experimental observations due to its capability to capture the mechanical dispersion regime which is the more common observation in high-shear granulation processes.

The open loop control approach involves considering a mechanistic model which has also been compartmentalized in order to obtain the most accurate representation of the high-shear granulation system. The open loop control can make good predictions for the operating condition based on the simultaneous consideration of the PSD and porosity. The methodology presented in this dissertation focuses on a purely theoretical, inverse problem approach, however this methodology can also be extended for real, experimental systems. A mechanistic, compartment-based model can be calibrated against experimental results within a certain design space. Thereafter, the model can be utilized for generating estimates for the operating conditions for a different target distribution. This approach can provide deeper insights towards the efficient operation of a high-shear granulation process for obtaining target CQAs and can significantly alleviate the need for multiple experimental trials for process optimization.

Chapter 6

Thesis conclusions and future directions

This dissertation is primarily aimed at utilizing PBMs for improving the operation of wet granulation processes. For this purpose, a multi-dimensional PBM has been formulated, which is thereby used to study the behavior of the highly complex granulation process. Chapter 2 primarily focuses on the development of a multi-dimensional PBM describing the granulation process. A novel coupled mass and energy balance framework has also been proposed for the inclusion of drying into a fluid-bed granulation system. This framework can significantly improve the understanding of the effect of operating parameters on the outcome of a fluid-bed granulator. This can be used to optimize the process operation for fluid bed granulation. One of the biggest disadvantages of implementing PBMs for process understanding is the large number of empirical parameters that are associated with the framework. For this purpose, it is very crucial to be able to come up with mechanistic submodels/kernels for the various mechanisms, so that number of empirically fitted parameters can be minimized.

Due to the large number of empirical parameters within a PBM, the applicability of the PBM becomes obsolete beyond the design space within which the model has been calibrated. This urges the need for obtaining more mechanistic information introduced into the model, such that, the model is capable of making predictions beyond the design space. For model calibrations, parameter estimation has to be considered, which requires minimizing the error between the model output and the experimental results. Various optimization algorithms can be utilized for this purpose, however it is more desirable to use algorithms that suggest the global optima as opposed to the local optima. Another approach would involve convexification of the objective function, or tweaking

the objective function, such that the algorithm points towards a somewhat global optima. In this work, the metaheuristic algorithm-particle swarm optimization has been employed for the estimation, which is expected to provide a global minima. The results showed reasonable predictions, however the mismatches can be attributed to the modeling framework that was utilized for the process representation. This motivated the formulation for a mechanistic PBM which can capture the effect of process conditions.

A semi-mechanistic kernel has also been proposed in this work, which relates the input parameters (e.g. liquid to solid ratio, impeller speed, viscosity, contact angle) to the aggregation propensity. The biggest highlight of this aggregation kernel lies in the fact that it demarcates the internal vs external liquid and is also capable of capturing the steady and induction growth behavior. This kernel can be implemented in the PBM for getting deeper insights into the system dynamics. It is expected that this kernel will successfully make predictions beyond the design space used for model calibration. In order to efficiently and accurately solve the PBMs, development of sohpisticated numerical techniques is mandatory. In this work, various numerical techniques have been proposed that can solve the PBMs with minimal computational overheads and high accuracy. While the cell average technique enables the discretization of the spatial domain using nonlinear grids (fewer number of grids), the tensor decomposition approach involves developing a reduced order framework which can accommodate large number of grids for the linear discretization. In both cases, the accuracy of the solution has not been compromised. The biggest strength of developing an ROM using the tensor decomposition approach lies in the fact that it can not only break the "curse of dimensionality" but can also significantly reduce the discretization error that is associated with large grid widths. The most ideal situation would be to combine these two approaches and propose a numerical technique that can compress the data from the cell average approach using tensor decomposition. This is expected to significantly reduce the computational time and memory requirements. Research on the development of numerical techniques for solution of PBMs can be a very promising field, as it would facilitate the possibility of employing efficient parameter estimation techniques

for model calibration.

In the last specific aim of this dissertation, the focus has shifted to developing a compartment based model and implementing it for open loop control. The common assumption of the high-shear granulator as a well-mixed vessel is an over-simplification. For this purpose, it is crucial to identify the various compartments within a high-shear where inhomogeneities exist in terms of the particle velocity and the liquid content. Each compartment is however considered as a well-mixed zone that exchanges material/information with each other. This work exploits the power of data analytics to identify the size and centroid values for the velocity in each compartment. A regression approach is implemented which provides information regarding the varying sizes of each compartment and the representative centroid value of a quantity in that compartment. The regression yields polynomial expressions which are a function of time, liquid to solid ratio and impeller speed. A spray zone is additionally included into the compartment framework which addresses the inhomogeneities with respect to binder distribution. Since this is preliminary work, it has not included a very mechanistic representation for the depletion of the spray zone and the renewal of the wet surface. The implementation of surface renewal theory should provide better insights on the occurrences within the spray zone. The compartment based model can better represent the high-shear granulation system and is thus a strong framework that can be used for open-loop control.

The open-loop control approach can only work successfully when the model utilized for the systems approach is accurate and mechanistic in nature. Therefore, the modeling framework proposed in the initial chapters of this dissertation can form a solid foundation to implement the open-loop control approach. The analysis provided in Chapter 5 is crucial to understand the convergence of the optimization algorithm to yield pareto-optimal solutions. Using this, *optimal* weights were identified, that can minimize the error between the model output and the desired distribution, and provide insights about the optimal scheduling scheme for the granulation process. Although the open-loop control directs more emphasis to the optimization algorithm utilized for the work, considering a mechanistic model is equally important. It is very crucial to

relate the operating conditions to the various submodels within the PBM. For this reason, the consolidation rate has been related to the impeller speed using dimensionless numbers such as St_{def}. The Stoke's deformation number is however a function of the yield Stress as well. There is limited information available in literature that relates the yield Stress to the liquid content in the system. Obtaining a deeper understanding with regard to relating the various mechanisms to the different operating conditions would provide a great platform for utilizing the mechanistic models to gain insight about the improved operation of the process. This thesis does propose a few steps towards moving to first-principle driven approach, however there is still substantial work needed before the models are entirely predictive. There is a huge need to shift towards mechanistic models, such that the number of empirical parameters within the PBM can be significantly reduced and the model is capable of making predictions and other useful information beyond the design space. The tools developed as part of this dissertation is not specific to wet granulation processes. Similar concepts can be applied for various other unit operations such as mixing, crystallization and so on. With additional information regarding the powder properties, these approaches can be easily applicable to systems containing different solid materials. Overall, due to the discrete nature of PBMs, it can be easily utilized to describe various particulate processes and processes involving the handling of solids.

6.0.1 Future directions

Investigations involving efficient parameter estimation techniques for accommodating multiple objective functions for model calibration of PBM would significantly benefit the predictive ability of the framework. Additionally, the ROM as proposed in chapter 3 can be furthered in order to be applicable for the non-linear discretization of PBMs. It should significantly reduce the computational overheads associated with the solution to PBMs. Further mechanistic understanding of the granulation process can improve the predictive ability of the PBMs. It can successfully make predictions outside the design space used for the model calibration. The semi-mechanistic kernel proposed in chapter 4 utilizes the viscous Stoke's number, however incorporating the Stoke's

deformation number can provide a better representation of the wet granulation process. There is a lack of understanding on the effect of liquid to solid ratio on the yield stress of the granules. The liquid binder added to the system is also distributed uniformly across all particles, however incorporating the principles of surface renewal theory into the compartment-based model can provide a more fundamental representation of the process.

The work described in this dissertation is mostly focused on pharmaceutical applications, however these methods can be easily extended for other applications, e.g. detergents, food. The detergent industry primarily uses reactive granulation processes, whereby there is a simultaneous occurrence of reaction and granulation. In the wet granulation description provided in this thesis, there is no overall change in the chemical properties of the solid. The granulation process relevant to the detergent industry is however associated with a modification in the chemical properties of the powder as well. The PBM can be used for describing the granulation process, however additional kinetic equations are required for updating the physical and chemical behavior of the system as a function of the progress of reaction. Wet granulation processes can also be utilized in the food industry to granulate milk powder. The powder properties differ from that used in the pharmaceutical industry, however these models can be extended for varying applications by modifying the material properties of the system. This also re-emphasizes the need for predictive models, such that the models can be extrapolated for different systems with minimum effort.

This dissertation aims to answer a lot of questions that were posed in the past, however it also raises additional questions which can pave way for substantial future work. This dissertation addresses multiple issues that acted as obstacles for obtaining a predictive model, however due to the partial alleviation of the various obstacles, there is still some future work required in terms of mechanistic understanding of granulation processes and efficient numerical techniques for PBMs for formulating a predictive model for improving the inefficient operation of granulation processes.

Bibliography

Annapragada, A., Neilly, J., 1996. On the modelling of granulation processes: A short note. Powder Technology 89 (1), 83 – 84.

Attarakih, M. M., Bart, H.-J., Faqir, N. M., 2006. Solution of the population balance equation using the sectional quadrature method of moments (sqmom). In: 16th European Symposium on Computer Aided Process Engineering and 9th International Symposium on Process Systems Engineering. Vol. 21 of Computer Aided Chemical Engineering. pp. 209 – 214.

Bader, B. W., Kolda, T. G., 2007. Efficient matlab computations with sparse and factored tensors. SIAM Journal on Scientific Computing 30 (1), 205–231.

Barrasso, D., Ramachandran, R., 2012. A comparison of model order reduction techniques for a four-dimensional population balance model describing multi-component wet granulation processes. Chemical Engineering Science 80, 380 – 392.

Barrasso, D., Ramachandran, R., 2014. Multi-scale modeling of granulation processes: Bi-directional coupling of PBM with DEM via collision frequencies. Chemical Engineering Research and Design (http://dx.doi.org/10.1016/j.cherd.2014.04.016).

Batterham, R. J., Hall, J. S., Barton, G., 1981. Pelletizing kinetics and simulation of full scale balling circuits. In: Proceedings of the Third International Symposium on Agglomeration, Nuremberg, 1981.

Benali, M., Gerbaud, V., Hemati, M., 2009. Effect of operating conditions and physicochemical properties on the wet granulation kinetics in high shear mixer. Powder Technology 190 (12), 160 – 169.

Bianco, N., 2008. Optimal control of particle size distribution in semi-batch emulsion polymerisation. Ph.D. thesis, Imperial College, London, UK.

Boerefijn, R., Hounslow, M., 2005. Studies of fluid bed granulation in an industrial r&d context. Chemical Engineering Science 60 (14), 3879 – 3890.

Börner, M., Peglow, M., Tsotsas, E., 2013. Derivation of parameters for a two compartment population balance model of wurster fluidised bed granulation. Powder Technology 238 (0), 122 – 131.

Bouffard, J., Bertrand, F., Chaouki, J., 2012. A multiscale model for the simulation of granulation in rotor-based equipment. Chemical Engineering Science 81 (0), 106 – 117.

Bouffard, J., Bertrand, F., Chaouki, J., Dumont, H., 2013. Discrete element investigation of flow patterns and segregation in a spheronizer. Computers & Chemical Engineering 49 (0), 170 – 182.

Boukouvala, F., Muzzio, F. J., Ierapetritou, M. G., 2010. Predictive modeling of pharmaceutical processes with missing and noisy data. AIChE Journal 56 (11), 2860–2872.

Buccholz, S., 2010. Future manufacturing approaches in the chemical and the pharmaceutical industry. Chemical Engineering and Processing: Process Intensification 49, 993–995.

Cameron, I., Wang, F., Immanuel, C., Stepanek, F., 2005. Process systems modelling and applications in granulation: A review. Chemical Engineering Science 60 (14), 3723 – 3750.

Chakraborty, J., Kumar, S., 2007. A new framework for solution of multidimensional population balance equations. Chemical Engineering Science 62 (15), 4112 – 4125.

Chaudhury, A., Barrasso, D., Pandey, P., Wu, H., Ramachandran, R., 2014a. Population balance model development, validation, and prediction of cqas of a high-shear wet granulation process: Towards qbd in drug product pharmaceutical manufacturing. Journal of Pharmaceutical Innovation 9 (1), 53–64.

Chaudhury, A., Kapadia, A., Prakash, A. V., Barrasso, D., Ramachandran, R., 2013a. An extended cell-average technique for a multi-dimensional population balance of granulation describing aggregation and breakage. Advanced Powder Technology 24 (6), 962 – 971.

Chaudhury, A., Niziolek, A., Ramachandran, R., 2013b. Multi-dimensional mechanistic modeling of fluid bed granulation processes: An integrated approach. Advanced Powder Technology 24 (1), 113 – 131.

Chaudhury, A., Ramachandran, R., 2013. Integrated population balance model development and validation of a granulation process. Particulate Science and Technology 31 (4), 407–418.

Chaudhury, A., Wu, H., Khan, M., Ramachandran, R., 2014b. A mechanistic population balance model for granulation processes: Effect of process and formulation parameters. Chemical Engineering Science 107, 76 – 92.

Chen, J., Saad, Y., 2009. On the tensor svd and optimal low rank approximation of tensors. SIAM Journal on Matrix Analysis and Applications 30 (4), 1709–1734.

Davies, W. L., Gloor, W. T., 1971. Batch production of pharmaceutical granulations in a fluidized bed i: Effects of process variables on physical properties of final granulation. Journal of Pharmaceutical Sciences 60 (12), 1869–1874.

de Silva, V., Lim, L., 2008. Tensor rank and the ill-posedness of the best low-rank approximation problem. SIAM Journal on Matrix Analysis and Applications 30 (3), 1084–1127.

Deb, K., Pratap, A., Agarwal, S., Meyarivan, T., 2000. A fast elitist multi-objective genetic algorithm: Nsga-ii. IEEE Transactions on Evolutionary Computation 6, 182–197.

Dubey, A., Sarkar, A., Ierapetritou, M., Wassgren, C. R., Muzzio, F. J., 2011. Computational approaches for studying the granular dynamics of continuous blending

processes, 1 dem based methods. Macromolecular Materials and Engineering 296 (3-4), 290–307.

Emady, H. N., Kayrak-Talay, D., Litster, J. D., 2013. A regime map for granule formation by drop impact on powder beds. AIChE Journal 59 (1), 96–107.

Emady, H. N., Kayrak-Talay, D., Schwerin, W. C., Litster, J. D., 2011. Granule formation mechanisms and morphology from single drop impact on powder beds. Powder Technology 212 (1), 69 – 79.

Fichthom, K. A., Weinberg, W. H., 1991. Theoretical foundations of dynamical monte carlo simulations. Journal of Chemical Physics 95 (2), 1090–1096.

Freireich, B., Li, J., Litster, J., Wassgren, C., 2011. Incorporating particle flow information from discrete element simulations in population balance models of mixer-coaters. Chemical Engineering Science 66 (16), 3592 – 3604.

Gantt, J. A., Cameron, I. T., Litster, J. D., Gatzke, E. P., 2006. Determination of coalescence kernels for high-shear granulation using dem simulations. Powder Technology 170 (2), 53 – 63.

Garcia, A. L., van den Broeck, C., Aertsens, M., Serneels, R., 1987. A monte carlo simulation of coagulation. Physica A: Statistical and Theoretical Physics 143 (3), 535–546.

Gernaey, K. V., Gani, R., 2010. A model-based systems approach to pharmaceutical product-process design and analysis. Chemical Engineering Science 65, 5757–5769.

Glaser, T., Sanders, C. F. W., Wang, F. Y., Cameron, I. T., Ramachandran, R., Litster, J. D., Poon, J. M. H., Immanuel, C. D., Doyle III, F. J., 2009. Model predictive control of drum granulation. Journal of Process Control 19, 615–622.

Gluba, T., Obraniak, A., Gawot-Mlynarczyk, E., 2004. The effect of granulation conditions on bulk density of a product. Physicochemical Problems of Mineral Processing 38, 177–186.

Goreinov, S., 2008. On cross approximation of multi-index arrays. Doklady Mathematics 77, 404–406.

Hagrasy, A. E., Hennenkamp, J., Burke, M., Cartwright, J., Litster, J., 2013. Twin screw wet granulation: Influence of formulation parameters on granule properties and growth behavior. Powder Technology 238, 108 – 115.

Hapgood, K. P., 2000. Nucleation and binder dispersion in wet granulation. Ph.D. thesis, University of Queensland, Australia.

Hapgood, K. P., Litster, J. D., Smith, R., 2003. Nucleation regime map for liquid bound granules. AIChE Journal 49 (2), 350–361.

Hartigan, J. A., Wong, M. A., 1979. Algorithm as 136: A k-means clustering algorithm. Journal of the Royal Statistical Society. Series C (Applied Statistics) 28 (1), 100–108.

Hounslow, M., 1998. The population balance as a tool for understanding particle rate processes. KONA 16, 179–193.

Hounslow, M. J., Ryall, R. L., Marshall, V. R., 1988. A discretized population balance for nucleation, growth, and aggregation. AIChE Journal 34 (11), 1821–1832.

Hu, X., Cunningham, J., Winstead, D., 2008. Understanding and predicting bed humidity in fluidized bed granulation. Journal of Pharmaceutical Sciences 97 (4), 1564–1577.

Hulburt, H., Katz, S., 1964. Some problems in particle technology: A statistical mechanical formulation. Chemical Engineering Science 19 (8), 555 – 574.

Immanuel, C., 2002. Experimental analysis, mathematical modeling and control of particle size distribution in semi-batch emulsion polymerization. Ph.D. thesis, University of Delaware.

Immanuel, C. D., Doyle III, F. J., 2003. Computationally efficient solution of population balance models incorporating nucleation, growth and coagulation: application to emulsion polymerization. Chemical Engineering Science 58 (16), 3681 – 3698.

Immanuel, C. D., Doyle III, F. J., 2005. Solution technique for a multi-dimensional population balance model describing granulation processes. Powder Technology 156 (2-3), 213 – 225.

Immanuel, C. D., Wang, Y., Bianco, N., 2007. Iterative batch-to-batch control of particle size distribution in semi-batch emulsion polymerisation. In: 17th European Symposium on Computer Aided Process Engineering. Vol. 24 of Computer Aided Chemical Engineering. pp. 853 – 858.

Immanuel, C. D., Wang, Y., Bianco, N., 2008. Feedback controllability assessment and control of particle size distribution in emulsion polymerisation. Chemical Engineering Science 63 (5), 1205 – 1216.

Iveson, S., Litster, J., Ennis, B., 1996. Fundamental studies of granule consolidation part 1: Effects of binder content and binder viscosity. Powder Technology 88 (1), 15 – 20.

Iveson, S. M., 2002. Limitations of one-dimensional population balance models of wet granulation processes. Powder Technology 124, 219–229.

Iveson, S. M., Litster, J. D., 1998. Growth regime map for liquid-bound granules. AIChE Journal 44 (7), 1510–1518.

Iveson, S. M., Litster, J. D., Hapgood, K., Ennis, B. J., 2001a. Nucleation, growth and breakage phenomena in agitated wet granulation processes: a review. Powder Technology 117 (1-2), 3 – 39.

Iveson, S. M., Wauters, P. A., Forrest, S., Litster, J. D., Meesters, G. M., Scarlett, B., 2001b. Growth regime map for liquid-bound granules: further development and experimental validation. Powder Technology 117 (12), 83 – 97.

Kass, R. E., Wasserman, L., 1995. A reference bayesian test for nested hypotheses and its relationship to the schwarz criterion. Journal of the American Statistical Association 90 (431), 928–934.

Kennedy, J., Eberhart, R., 1995. Particle swarm optimization. In: Neural Networks, 1995. Proceedings., IEEE International Conference on. Vol. 4. pp. 1942–1948.

Klatt, K. U., Marquardt, W., 2009. Perspectives of process systems engineering-personal views from academia and industry. Computer and Chemical Engineering 33, 536–550.

Knight, P., Instone, T., Pearson, J. M., Hounslow, M., 1993. An investigation into the kinetics of granulation using a high shear mixer. Powder Technology 77, 159–169.

Kolda, T., Bader, B., 2009. Tensor decompositions and applications. SIAM Review 51 (3), 455–500.

Kulikov, V., Briesen, H., Marquardt, W., 2006. A framework for the simulation of mass crystallization considering the effect of fluid dynamics. Chemical Engineering and Processing: Process Intensification 45 (10), 886 – 899.

Kumar, J., 2006. Numerical approximations of population balance equations in particulate systems. Ph.D. thesis, Otto-von-Guericke University, Germany.

Kumar, J., Peglow, M., Warnecke, G., Heinrich, S., 2008. An efficient numerical technique for solving population balance equation involving aggregation, breakage, growth and nucleation. Powder Technology 182 (1), 81 – 104.

Kumar, R., Kumar, J., Warnecke, G., 2011. Numerical methods for solving two-dimensional aggregation population balance equations. Computers and Chemical Engineering 35 (6), 999 – 1009.

Kumar, S., Ramkrishna, D., 1996a. On the solution of population balance equations by discretization–i. a fixed pivot technique. Chemical Engineering Science 51 (8), 1311 – 1332.

Kumar, S., Ramkrishna, D., 1996b. On the solution of population balance equations by discretizationii. a moving pivot technique. Chemical Engineering Science 51 (8), 1333 – 1342.

Lee, K., 1983. Change of particle size distribution during brownian coagulation. Journal of Colloid and Interface Science 92 (2), 315 – 325.

Li, J., Freireich, B., Wassgren, C., Litster, J. D., 2011. A general compartment-based population balance model for particle coating and layered granulation. AIChE Journal.

Liffman, K., 1992. A direct simulation monte-carlo method for cluster coagulation. Journal of Computational Physics 100 (1), 116 – 127.

Lin, Y., Lee, K., Matsoukas, T., 2002. Solution of the population balance equation using constant-number monte carlo. Chemical Engineering Science 57 (12), 2241 – 2252.

Linniger, A. A., Chowdhry, S., Bahl, V., Krendl, H., Pinger, H., 2000. A systems approach to mathematical modeling of industrial processes. Computers and Chemical Engineering 24, 591–598.

Litster, J., 2003. Scaleup of wet granulation processes: science not art. Powder Technology 130 (1-3), 35 – 40.

Litster, J., Ennis, B., 2004. The Science and engineering of granulation processes. Kluwer Academic Publishers.

Litster, J., Hapgood, K., Michaels, J., Sims, A., Roberts, M., Kameneni, S., Hsu, T., 2001. Liquid distribution in wet granulation: dimensionless spray flux. Powder Technology 114 (13), 32 – 39.

Litster, J. D., Smit, D. J., Hounslow, M. J., 1995. Adjustable discretized population balance for growth and aggregation. AIChE Journal 41 (3), 591–603.

Liu, L. X., Litster, J. D., 2002. Population balance modelling of granulation with a physically based coalescence kernel. Chemical Engineering Science 57 (12), 2183 – 2191.

Liu, L. X., Litster, J. D., Iveson, S. M., Ennis, B. J., 2000. Coalescence of deformable granules in wet granulation processes. AIChE Journal 46 (3), 529–539.

Liu, Y., Cameron, I., 2001. A new wavelet-based method for the solution of the population balance equation. Chemical Engineering Science 56 (18), 5283 – 5294.

Liu, Y., Cameron, I., 2003. A new wavelet-based adaptive method for solving population balance equations. Powder Technology 130 (1-3), 181 – 188.

Long, C., Gantt, J., Gatzke, E., june 2005. Batch granulation control using a simplified population balance and nonlinear model predictive control. In: American Control Conference, 2005. Proceedings of the 2005. Vol. 2. pp. 949 – 954.

Ma, D. L., Tafti, D. K., Braatz, R. D., 2002. Optimal control and simulation of multidimensional crystallization processes. Computers and Chemical Engineering 26 (7-8), 1103 – 1116.

Madec, L., Falk, L., Plasari, E., 2003. Modelling of the agglomeration in suspension process with multidimensional kernels. Powder Technology 130 (1-3), 147 – 153.

Marchal, P., David, R., Klein, J. P., Villermaux, J., 1988. Crystallization and precipitation engineering-i. an efficient method for solving population balance in crystallization with agglomeration. Chemical Engineering Science 43, 59.

Marchisio, D. L., Pikturna, J. T., Fox, R. O., Vigil, R. D., Barresi, A. A., 2003a. Quadrature method of moments for population-balance equations. AIChE Journal 49 (5), 1266–1276.

Marchisio, D. L., Soos, M., Sefcik, J., Morbidelli, M., Barresi, A. A., Baldi, G., 2006. Effect of fluid dynamics on particle size distribution in particulate processes. Chemical Engineering and Technology 29 (2), 191–199.

Marchisio, D. L., Vigil, R. D., Fox, R. O., 2003b. Implementation of the quadrature method of moments in cfd codes for aggregation?breakage problems. Chemical Engineering Science 58 (15), 3337 – 3351.

Maronga, S., Wnukowski, P., 1997. Establishing temperature and humidity profiles in fluidized bed particulate coating. Powder Technology 94 (2), 181 – 185.

Marshall Jr., C. L., Rajniak, P., Matsoukas, T., 2011. Numerical simulations of two-component granulation: Comparison of three methods. Chemical Engineering Research and Design 89 (5), 545 – 552.

Marshall Jr., C. L., Rajniak, P., Matsoukas, T., 2013. Multi-component population balance modeling of granulation with continuous addition of binder. Powder Technology 236, 211 – 220.

Nursin, B., 2010. Mathematical modelling and optimisation of the formulation and manufacture of aggregate food products. Ph.D. thesis, National University of Ireland, Cork, Ireland.

Osborne, J. D., Sochon, R. P., Cartwright, J. J., Doughty, D. G., Hounslow, M. J., Salman, A. D., 2011. Binder addition methods and binder distribution in high shear and fluidised bed granulation. Chemical Engineering Research and Design 89 (5), 553 – 559.

Oseledets, I., 2011. Tensor-train decomposition. SIAM Journal of Scientific Computing 33 (5), 2295–2317.

Oseledets, I., Tyrtyshnikov, E., 2009. Breaking the curse of dimensionality, or how to use svd in many dimensions. SIAM Journal of Scientific computing 31 (5), 3744–3759.

Oseledets, I., Tyrtyshnikov, E., 2010. Tt-cross approximation for multidimensional arrays. Linear Algebra and its Applications 432 (1), 70 – 88.

Pandey, P., Tao, J., Chaudhury, A., Ramachandran, R., Gao, J. Z., Bindra, D. S., 2013. A combined experimental and modeling approach to study the effects of high-shear wet granulation process parameters on granule characteristics. Pharmaceutical Development and Technology 18 (1), 210–224.

Pandey, P., Tao, J., Gao, J. Z., Bindra, D., Narang, A., Ramachandran, R., Chaudhury, A., 2011. A combined experimental and computational approach to the scale-up of high-shear wet granulation. In: Proc. 2011 AIChe Annual Meeting (Minneapolis, USA, October 2011).

Pandya, J., Spielman, L., 1983. Floc breakage in agitated suspensions: Effect of agitation rate. Chemical Engineering Science 38 (12), 1983 – 1992.

Peglow, M., Kumar, J., Warnecke, G., Heinrich, S., Tsotsas, E., Mrl, L., Hounslow, M. J., 2006. An improved discretized tracer mass distribution of hounslow et al. AIChE Journal 52 (4), 1326–1332.

Pinto, M. A., Immanuel, C. D., Doyle III, F. J., 2007. A feasible solution technique for higher-dimensional population balance models. Computers and Chemical Engineering 31 (10), 1242 – 1256.

Poon, J. M.-H., Immanuel, C. D., Doyle III, F. J., Litster, J. D., 2008. A three-dimensional population balance model of granulation with a mechanistic representation of the nucleation and aggregation phenomena. Chemical Engineering Science 63 (5), 1315 – 1329.

Poon, J. M. H., Ramachandran, R., Sanders, C. F. W., Glaser, T., Immanuel, C. D., Doyle III, F. J., Litster, J. D., Stepanek, F., Wang, F. Y., Cameron, I. T., 2009. Experimental validation studies on a multi-scale and multi-dimensional population balance model of batch granulation. Chemical Engineering Science 64, 775–786.

Prakash, A. V., Chaudhury, A., Barrasso, D., Ramachandran, R., 2013a. Simulation of population balance model-based particulate processes via parallel and distributed computing. Chemical Engineering Research and Design 91 (7), 1259 – 1271.

Prakash, A. V., Chaudhury, A., Ramachandran, R., 2013b. Parallel simulation of population balance model-based particulate processes using multicore cpus and gpus. Modelling and Simulation in Engineering 10.1155/2013/475478.

Qamar, S., Warnecke, G., 2007. Solving population balance equations for two-component aggregation by a finite volume scheme. Chemical Engineering Science 62 (3), 679 – 693.

Rajniak, P., Mancinelli, C., Chern, R., Stepanek, F., Farber, L., Hill, B., 2007. Experimental study of wet granulation in fluidized bed: Impact of the binder properties on the granule morphology. International Journal of Pharmaceutics 334 (1-2), 92 – 102.

Rajniak, P., Stepanek, F., Dhanasekharan, K., Fan, R., Mancinelli, C., Chern, R. T., 2009. A combined experimental and computational study of wet granulation in a wurster fluid bed granulator. Powder Technology 189, 190–231.

Ramachandran, R., Ansari, M. A., Chaudhury, A., Kapadia, A., Prakash, A. V., Stepanek, F., 2011. A quantitative assessment of the influence of primary particle size distribution on granule inhomogeneity. Chemical Engineering Science 71, 104–110.

Ramachandran, R., Chaudhury, A., 2012. Model-based design and control of a continuous drum granulation process. Chemical Engineering Research and Design 90 (8), 1063 – 1073.

Ramachandran, R., Immanuel, C. D., Stepanek, F., Litster, J. D., Doyle III, F. J., 2009. A mechanistic model for breakage in population balances of granulation: Theoretical kernel development and experimental validation. Chemical Engineering Research and Design 87 (4), 598 – 614.

Ramachandran, R., Poon, J. M. H., Sanders, C. F. W., Glaser, T., Immanuel, C. D., Doyle III, F. J., Litster, J. D., Stepanek, F., Wang, F. Y., Cameron, I. T., 2008. Experimental studies on distributions on granule size, binder content and porosity in batch drum granulation: inferences on process modelling requirements and process sensitivities. Powder Technology 188, 89–101.

Rambali, B., Baert, L., Massart, D., 2001. Using experimental design to optimize the process parameters in fluidized bed granulation on a semi-full scale. International Journal of Pharmaceutics 220 (1-2), 149 – 160.

Reklaitis, G. V., Khinast, J., Muzzio, F., 2010. Pharmaceutical engineering science - new approaches to pharmaceutical development and manufacturing. Chemical Engineering Science 65, iv–vii.

Reynolds, G., Fu, J., Cheong, Y., Hounslow, M., Salman, A., 2005. Breakage in granulation: A review. Chemical Engineering Science 60 (14), 3969 – 3992.

Salman, A. D., Hounslow, M. J., Seville, J. P. K., 2007. Granulation. Elsevier.

Sen, M., Barrasso, D., Singh, R., Ramachandran, R., 2014. A multi-scale hybrid cfd-dem-pbm description of a fluid-bed granulation process. Processes 2 (1), 89–111.

Seveno, D., Ledauphin, V., Martic, G., Voue, M., De Coninck, J., 2002. Spreading drop dynamics on porous surfaces. Langmuir 18 (20), 7496–7502.

Sherony, D. F., 1981. A model of surface renewal with application to fluid bed coating of particles. Chemical Engineering Science 36 (5), 845 – 848.

Shi, Y., Eberhart, R., 1998. A modified particle swarm optimizer. In: Evolutionary Computation Proceedings, 1998. IEEE World Congress on Computational Intelligence., The 1998 IEEE International Conference on. pp. 69–73.

Smith, M., Matsoukas, T., 1998. Constant-number monte carlo simulation of population balances. Chemical Engineering Science 53 (9), 1777 – 1786.

Sochon, R. P. J., Zomer, S., Cartwright, J. J., Hounslow, M. J., Salman, A. D., 2010. The variability of pharmaceutical granulation. Chemical Engineering Journal 164, 285–291.

Soos, M., Sefcik, J., Morbidelli, M., 2006. Investigation of aggregation, breakage and restructuring kinetics of colloidal dispersions in turbulent flows by population balance modeling and static light scattering. Chemical Engineering Science 61 (8), 2349 – 2363.

Stepanek, F., Rajniak, P., 2006. Droplet morphologies on particles with macroscopic surface roughness. Langmuir 22 (3), 917–923.

Stepanek, F., Rajniak, P., Mancinelli, C., Chern, R., Ramachandran, R., 2009. Distribution and accessibility of binder in wet granules. Powder Technology 189 (2), 376 – 384.

Su, J., Gu, Z., Li, Y., Feng, S., Xu, X. Y., 2007. Solution of population balance equation using quadrature method of moments with an adjustable factor. Chemical Engineering Science 62 (21), 5897 – 5911.

Su, J., Gu, Z., Li, Y., Feng, S., Xu, X. Y., 2008. An adaptive direct quadrature method of moment for population balance equations. AIChE Journal 54 (11), 2872–2887.

Su, J., Gu, Z., Xu, X., 2009. Advances in numerical methods for the solution of population balance equations for disperse phase systems. Science in China Series B: Chemistry 52, 1063–1079.

Tan, M. X. L., Hapgood, K. P., 2011. Foam granulation: Binder dispersion and nucleation in mixer-granulators. Chemical Engineering Research and Design 89, 526–536.

Vanni, M., 2000. Approximate population balance equations for aggregation?breakage processes. Journal of Colloid and Interface Science 221 (2), 143 – 160.

Verkoeijen, D., Pouw, G. A., Meesters, G. M. H., Scarlett, B., 2002. Population balances for particulate processes–a volume approach. Chemical Engineering Science 57 (12), 2287 – 2303.

Walker, G. M., 2007. Chapter 4 drum granulation processes. In: A.D. Salman, M. H., Seville, J. (Eds.), Granulation. Vol. 11 of Handbook of Powder Technology. pp. 219 – 254.

Wang, F., Cameron, I., 2007. A multi-form modelling approach to the dynamics and control of drum granulation processes. Powder Technology 179 (12), 2 – 11.

Wang, F., Ge, X., Balliu, N., Cameron, I., 2006. Optimal control and operation of drum granulation processes. Chemical Engineering Science 61 (1), 257 – 267.

Wright, D. L., McGraw, R., Rosner, D. E., 2001. Bivariate extension of the quadrature method of moments for modeling simultaneous coagulation and sintering of particle populations. Journal of Colloid and Interface Science 236 (2), 242 – 251.

Wynn, E. J. W., 2004. Simulating aggregation and reaction: New Hounslow DPB and four-parameter summary. AIChE Journal 50 (3), 578–588.

Yu, S., Liu, X., Tranchevent, L.-C., Glnzel, W., Suykens, J. A. K., De Moor, B., Moreau, Y., 2011. Optimized data fusion for k-means laplacian clustering. Bioinformatics 27 (1), 118–126.